Galactic diffuse gamma-rays

Masaki Mori

Department of Physics,

College of Science & Engineering,

Ritsumeikan University

July 31, 2009, Dept. Astronomy, Kyoto University

GeV gamma-ray sky by EGRET

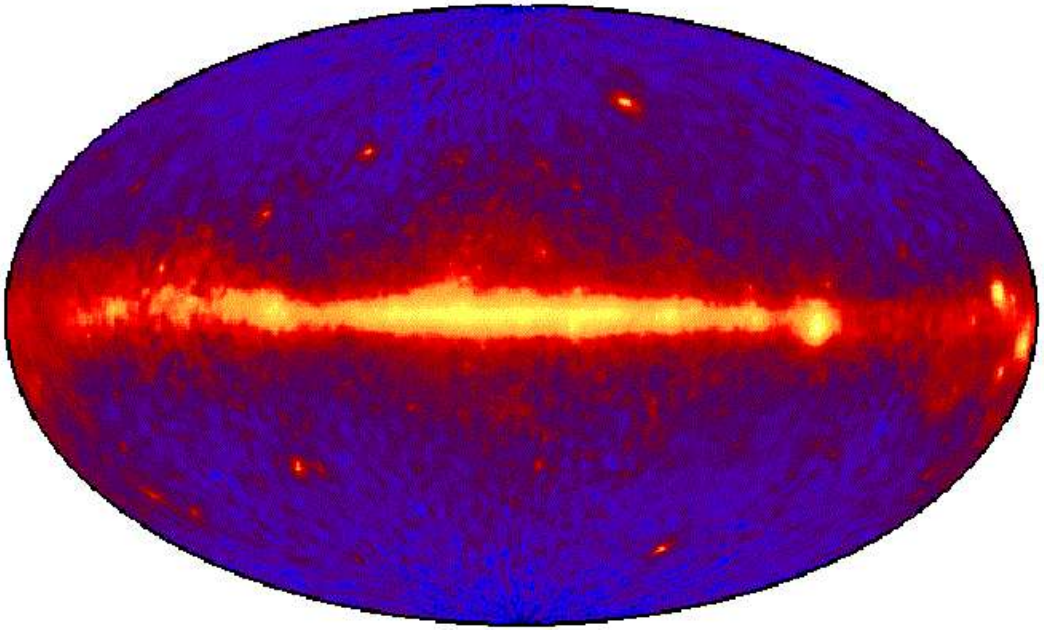

Compton Gamma-ray Observatory (1991-2000)

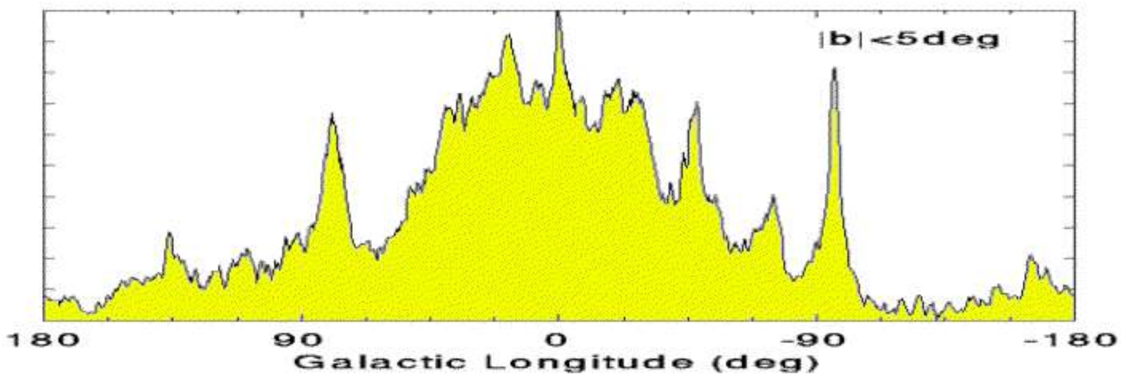

Diffuse emission: ~80% of total gamma-ray flux!

Gamma-ray detection

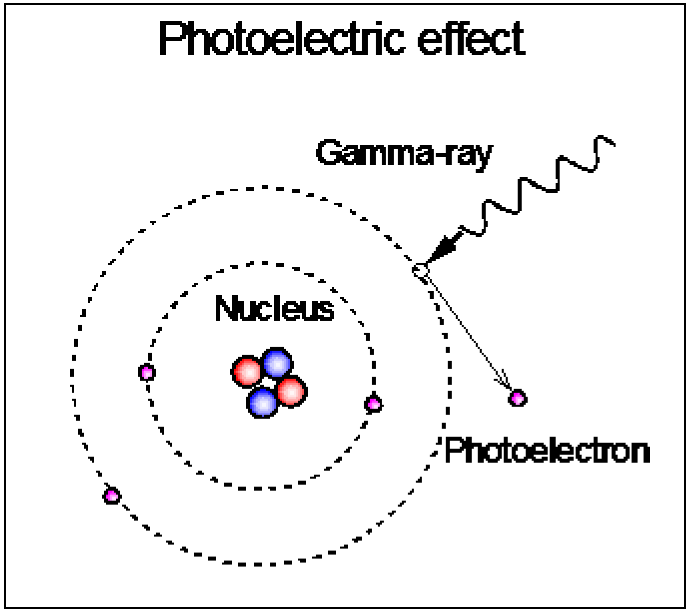

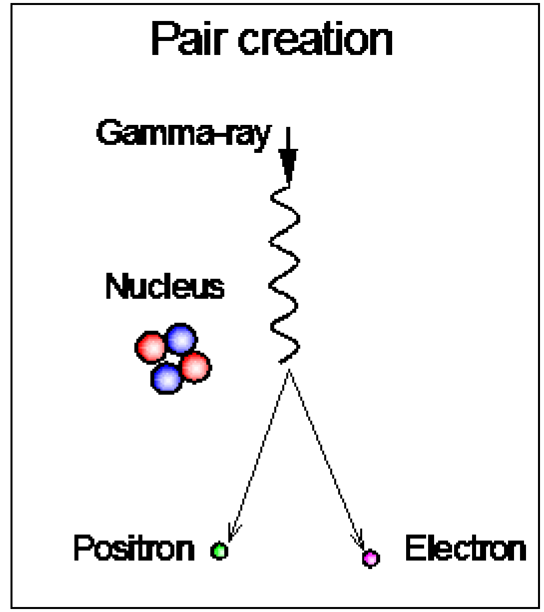

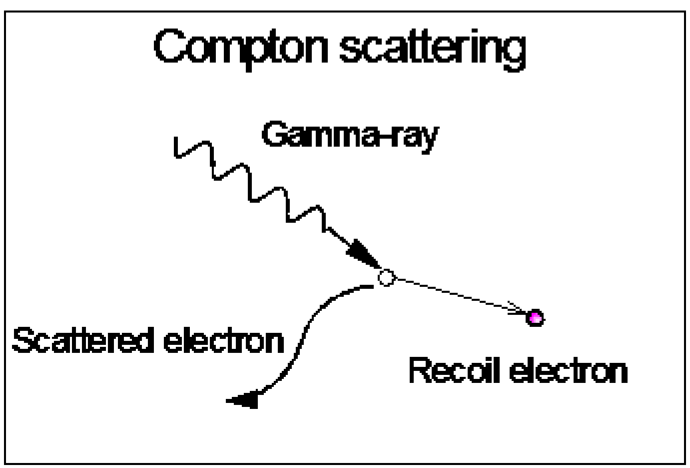

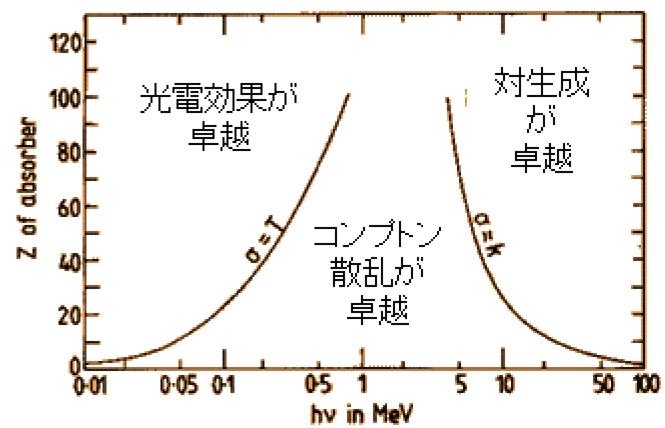

Evans 1955

Gamma-ray detector

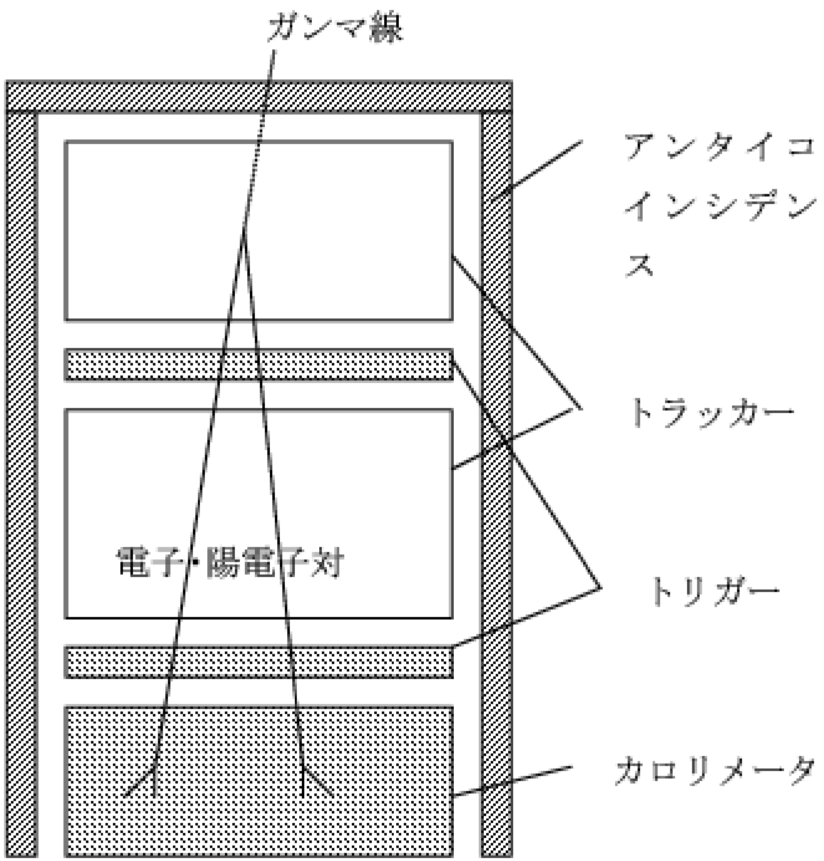

EGRET (Energetic Gamma Ray Experiment Telescope

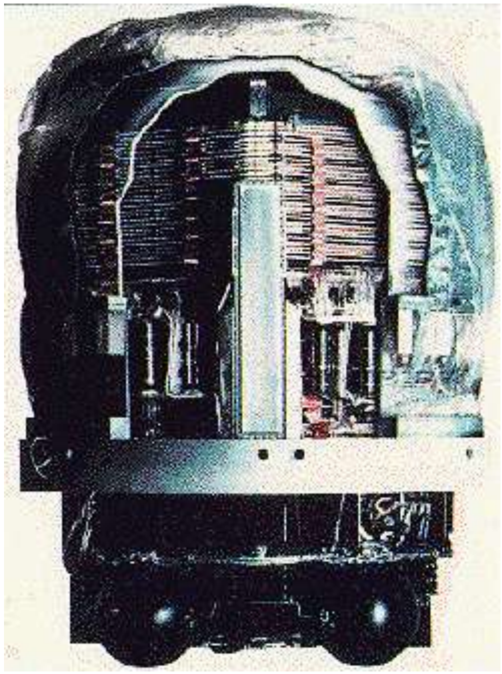

SAS-2 & COS-B Profile

SAS-2 (Thompson et al. 1976)

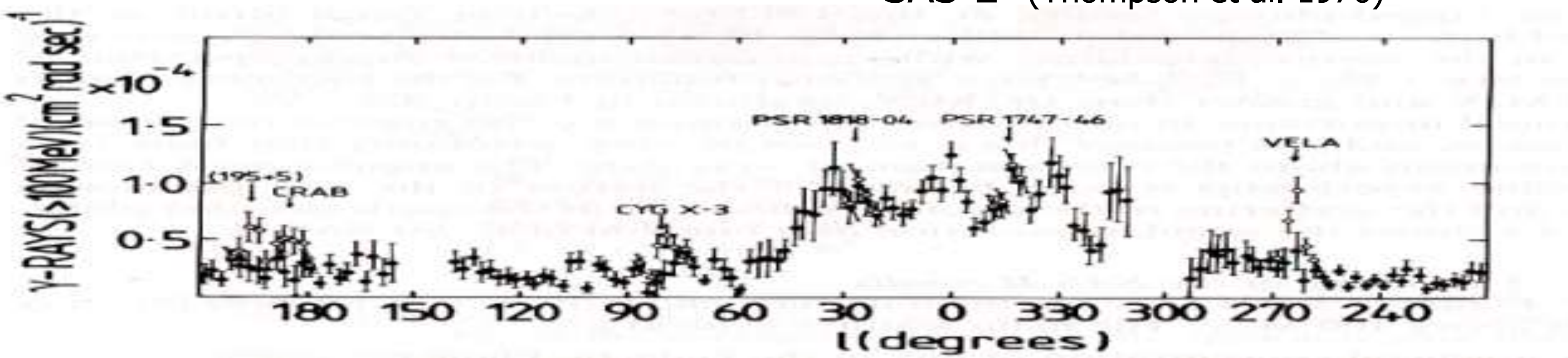

COS-B (Mayer-Hasselwander et al. 1982)

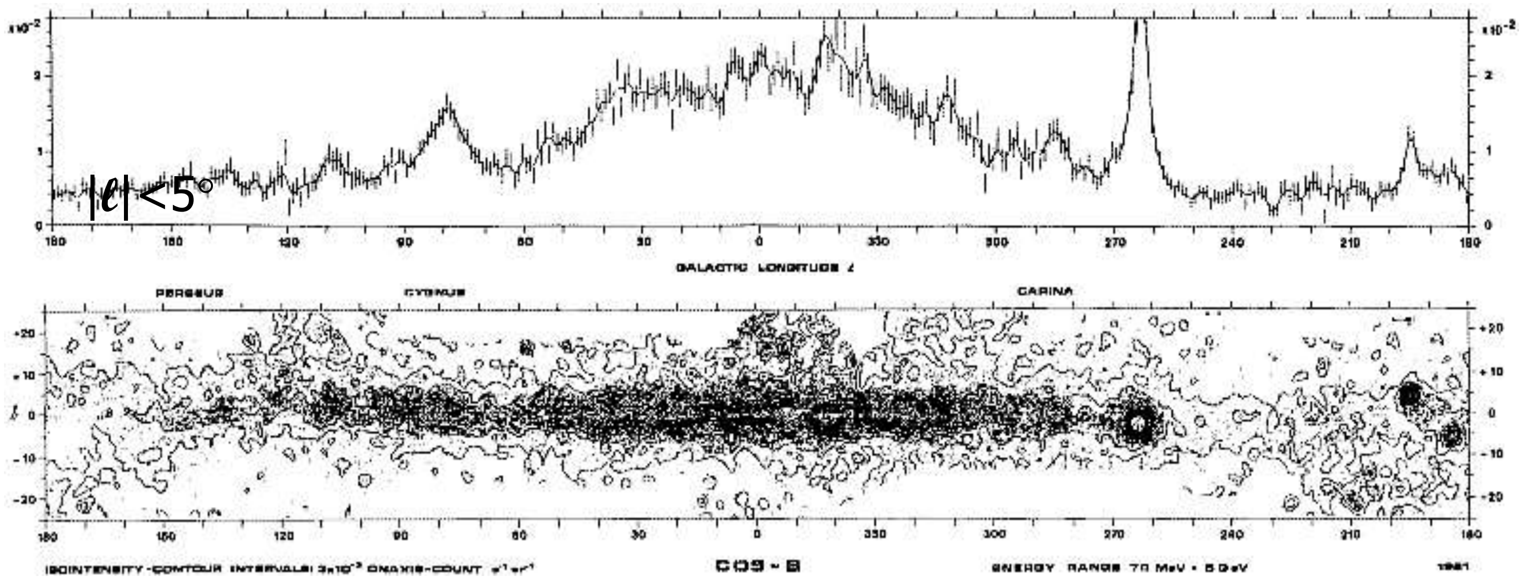

SAS-2 & COS-B Spectrum

Stecker 1979

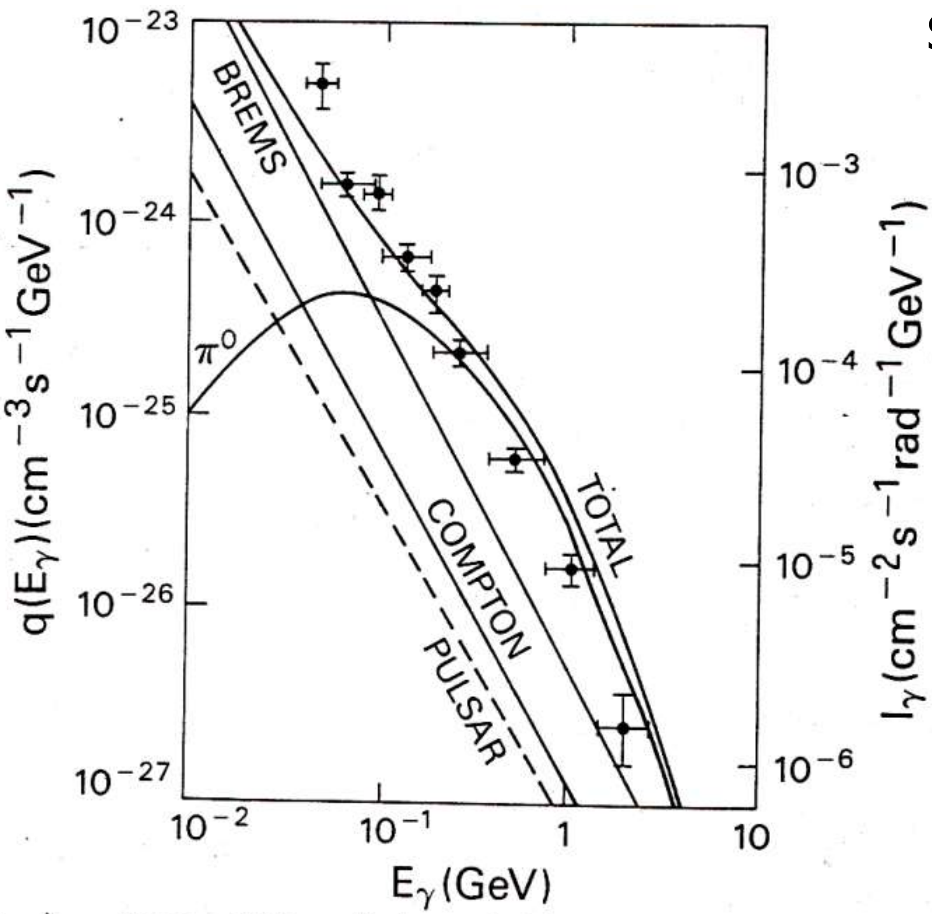

Fig. 4. Local differential production spectra for major diffuse production processes and the pulsar component as discussed in the text (left hand scale). The right hand scale and data points are from the COS-B and SAS-2 data in the longitude range around the galactic center and are shown in comparison to the predicted shape of the total spectrum.

EGRET Intensity Map

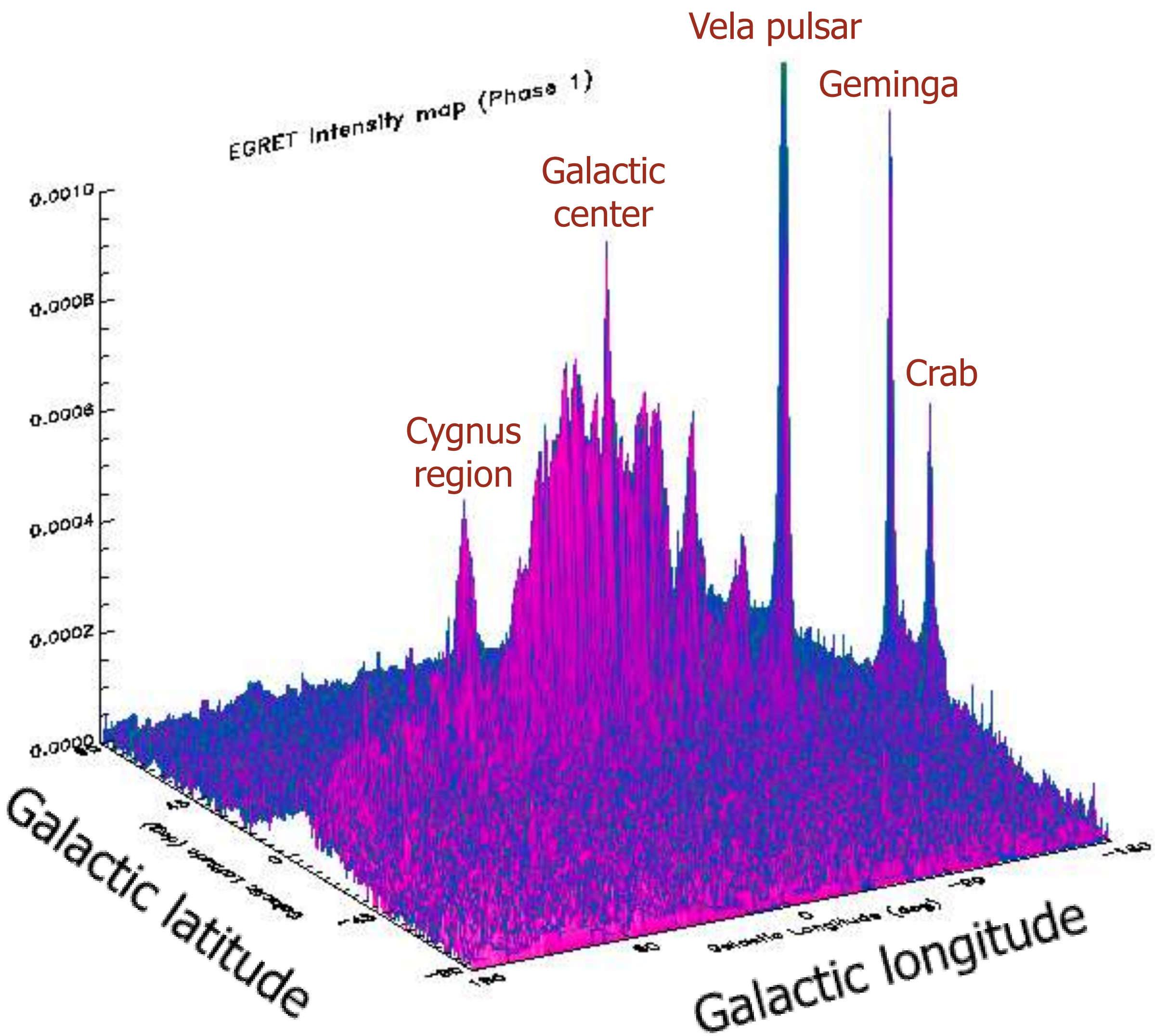

Point sources = Observed intensity – Diffuse model

EGRET observed intensity

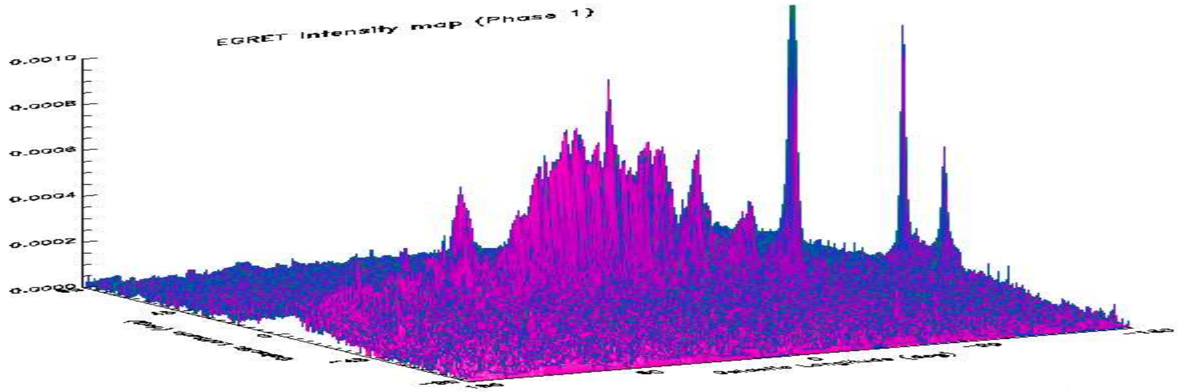

Diffuse model

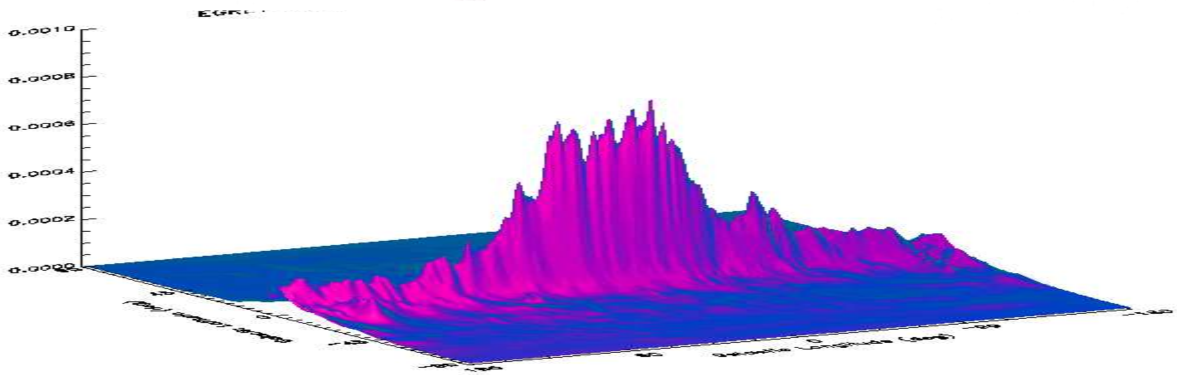

Intensity – model

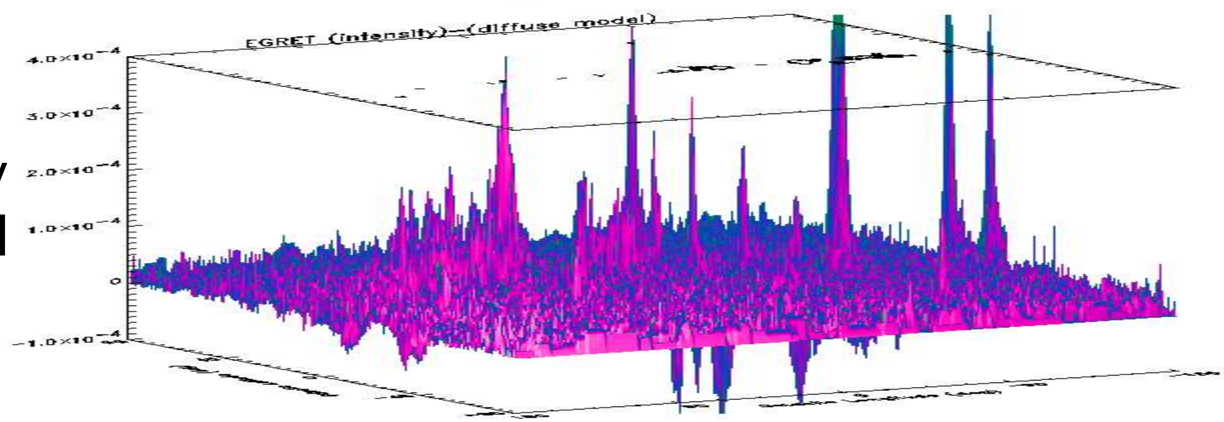

Depends on diffuse model!

Mattox et al., ApJ 461, 396 (1996)

Likelihood analysis

Maximize L to get best fit:

The likelihood is the probability of the observed EGRET data for a specific model of high-energy γ-ray emission. It is the product of the probability for each pixel:

$$L = \prod_{ij} p_{ij} , \qquad (3)$$

where

$$p_{ij} = \frac{\theta_{ij}^{n_{ij}} e^{-\theta_{ij}}}{n_{ij}!} \qquad (4)$$

is the Poisson probability of observing n_{ij} counts in pixel ij when the number of counts predicted by the model is θ_{ij}. The logarithm of the likelihood is more conveniently calculated

$$\ln L = \sum_{ij} n_{ij} \ln(\theta_{ij}) - \sum_{ij} \theta_{ij} - \sum \ln(n_{ij}!) . \qquad (5)$$

Because the last term is model independent, it is not useful for estimation or for the likelihood ratio test. Neglecting the last term,

$$\ln L = \sum_{ij} n_{ij} \ln(\theta_{ij}) - \sum_{ij} \theta_{ij} . \qquad (6)$$

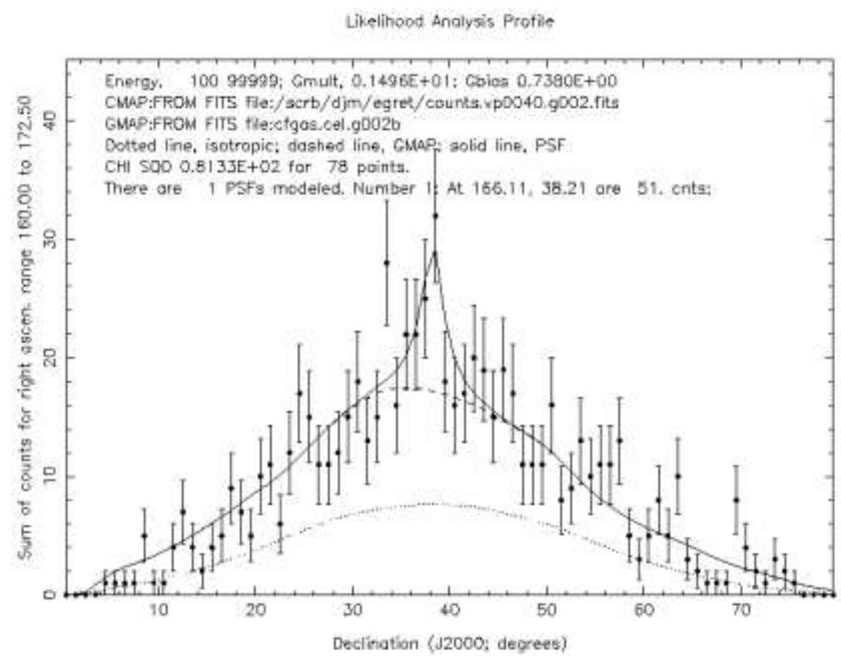

Model = $K_1 \times$(diffuse model)
$+ K_2 \times$(isotropic)
$+\Sigma_i F_i \times$(PSF)$_i$

Adjust K_1&K_2 and seek for best fit with F_i

Diffuse Emission Model

- Three main components:

➢ Bremsstrahlung: electron + matter $\rightarrow \gamma$ + X

➢ Inverse Compton: electron + photons $\rightarrow \gamma$ + X

➢ Nuclear interaction: proton(nuclei) + matter $\Rightarrow \pi^0 \rightarrow 2\gamma$

Matter = HI + HII + H_2

Photon = 2.7K BB + FIR + NIR + Optical + UV

Two approaches

Mainly for cosmic-ray propagation

- GALDIF (Hunter et al.)

EGRET/GLAST Diffuse Emission Model

- Inputs to model:
  - Gamma-ray production processes in the ISM
    - Pion production, Bremsstrahlung, inverse Compton scattering
  - Tracers of the ISM (matter and radiation)
    + Galactic rotation curve → 3-D ISM distribution
    - HI (21 cm), H_2 (115 GHz CO), HII (pulsar dispersion), low-energy photon density
  - Physical parameters:
    - N(HI)/W_{HI} conversion factor, CR spectrum, e/p ratio, interaction cross-sections, Galactic rotation curve, etc.
  - Model assumptions:
    - Assume the CRs are in *dynamic balance* with ISM
- *There are only two adjustable parameters in this calculation!*
  - Molecular mass ratio, X=N(H_2)/W_{CO}, CR coupling scale
- *Discrepancies between model and observation are directly interpretable in terms of model inputs and parameters.*

More on the ISM ...

More on dynamic balance ...

July 23, 2004

- GALPROP (Strong et al.)

Transport Equation

$$\frac{\partial \psi(\vec{r},p,t)}{\partial t} = q(\vec{r},p) \quad \text{sources (SNR, nuclear reactions...)}$$

$$\text{diffusion} \quad + \vec{\nabla}\cdot[D_{xx}\vec{\nabla}\psi - \vec{V}\psi] \quad \text{convection}$$

$$\text{diffusive reacceleration} \quad + \frac{\partial}{\partial p}\left[p^2 D_{pp}\frac{\partial}{\partial p}\frac{\psi}{p^2}\right]$$

$$\text{E-loss} \quad - \frac{\partial}{\partial p}\left[\frac{dp}{dt}\psi - \frac{1}{3}p\vec{\nabla}\cdot\vec{V}\psi\right] \quad \text{convection}$$

$$\text{fragmentation} \quad - \frac{\psi}{\tau_f} - \frac{\psi}{\tau_d} \quad \text{radioactive decay}$$

$\psi(\mathbf{r},p,t)$ – *density per total momentum*

Igor V. Moskalenko/NASA-GSFC 2 GLAST meeting/SLAC 2004/09/27-30

Bertsch et al. ApJ 416, 587 (1993)

Galactic Matter Distribution (GALDIF)

- HI : 21cm surveys
  Weaver & Williams (1973)
  Maryland-Parkes (1986)
  Leiden-Green Bank (1985)
- H_2 : $N(H_2) = X\ W_{CO}$
  CO: Columbia CO survey at 2.6mm (1987)
- HII : Taylor & Cordes (1993)
  (pulsar dispersion / interstellar scattering measure)
- Interstellar radiation field : 2.7K BB + FIR + NIR + Optical + UV
- Local Electron spectrum : Skibo (1993) [$E^{-2.42}$ injection]
- Local Proton spectrum : Stecker (1970) [$E^{-2.7}$]
- Cosmic-ray enhancement factor $\rho \propto N(\mathrm{HI})+N(\mathrm{H_2})+N(\mathrm{HII})$
  Gaussian along the Galactic axis (scaling parameter r_0)

Only two parameters in this model :
$X = (1.5\pm0.2)\times10^{20}$ H-mol cm^{-2}(K km s^{-1})$^{-1}$
$r_0 = (2.0\pm0.5)$ kpc

Hunter et al. ApJ 481, 205 (1997)

Cosmic-ray Enhancement Factor (GALDIF)

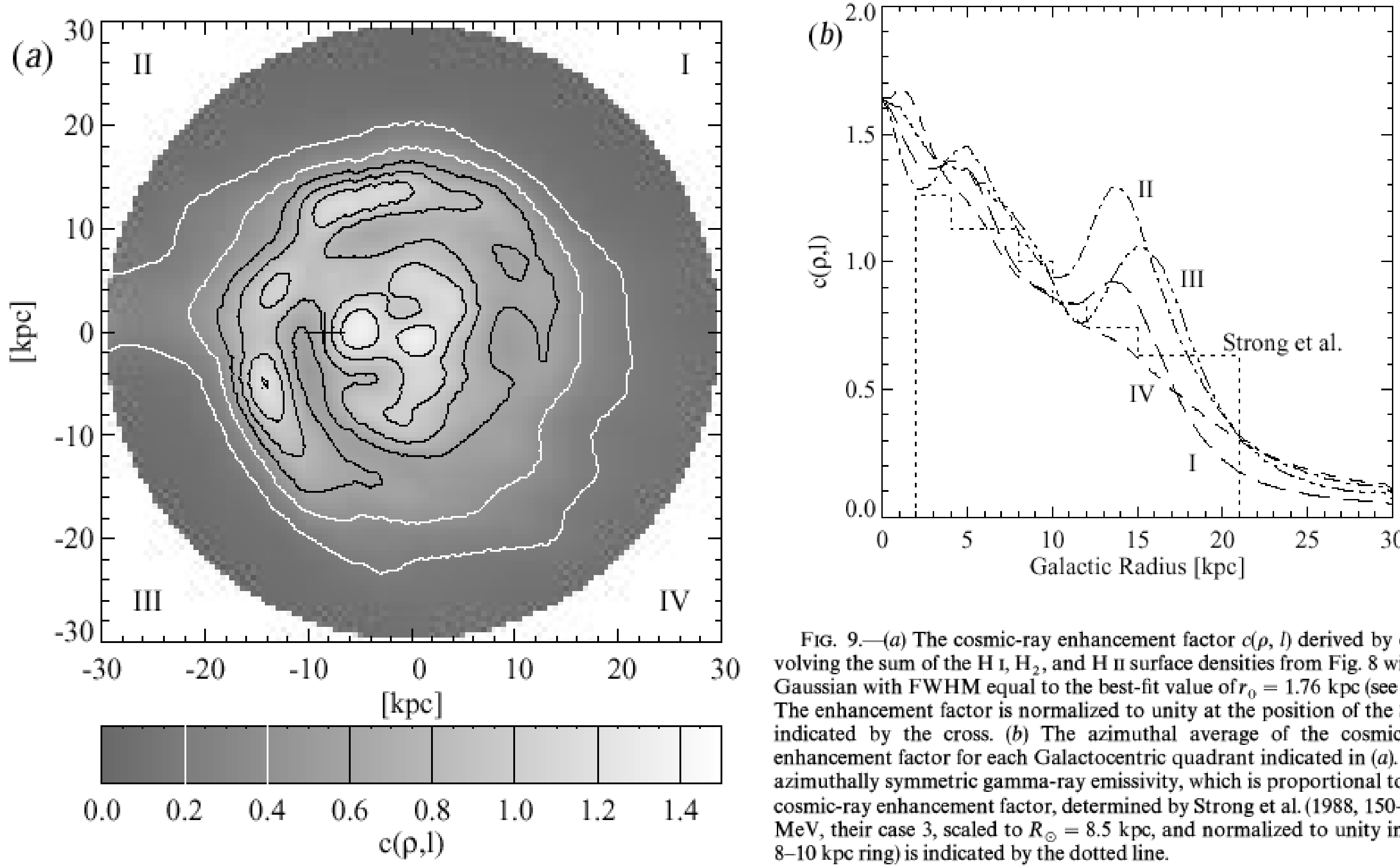

FIG. 9.—(*a*) The cosmic-ray enhancement factor $c(\rho, l)$ derived by convolving the sum of the H I, H_2, and H II surface densities from Fig. 8 with a Gaussian with FWHM equal to the best-fit value of $r_0 = 1.76$ kpc (see § 5). The enhancement factor is normalized to unity at the position of the Sun, indicated by the cross. (*b*) The azimuthal average of the cosmic-ray enhancement factor for each Galactocentric quadrant indicated in (*a*). The azimuthally symmetric gamma-ray emissivity, which is proportional to the cosmic-ray enhancement factor, determined by Strong et al. (1988, 150–300 MeV, their case 3, scaled to $R_\odot = 8.5$ kpc, and normalized to unity in the 8–10 kpc ring) is indicated by the dotted line.

Hunter et al. ApJ 481, 205 (1997)

GALDIF: Longitudinal Profile

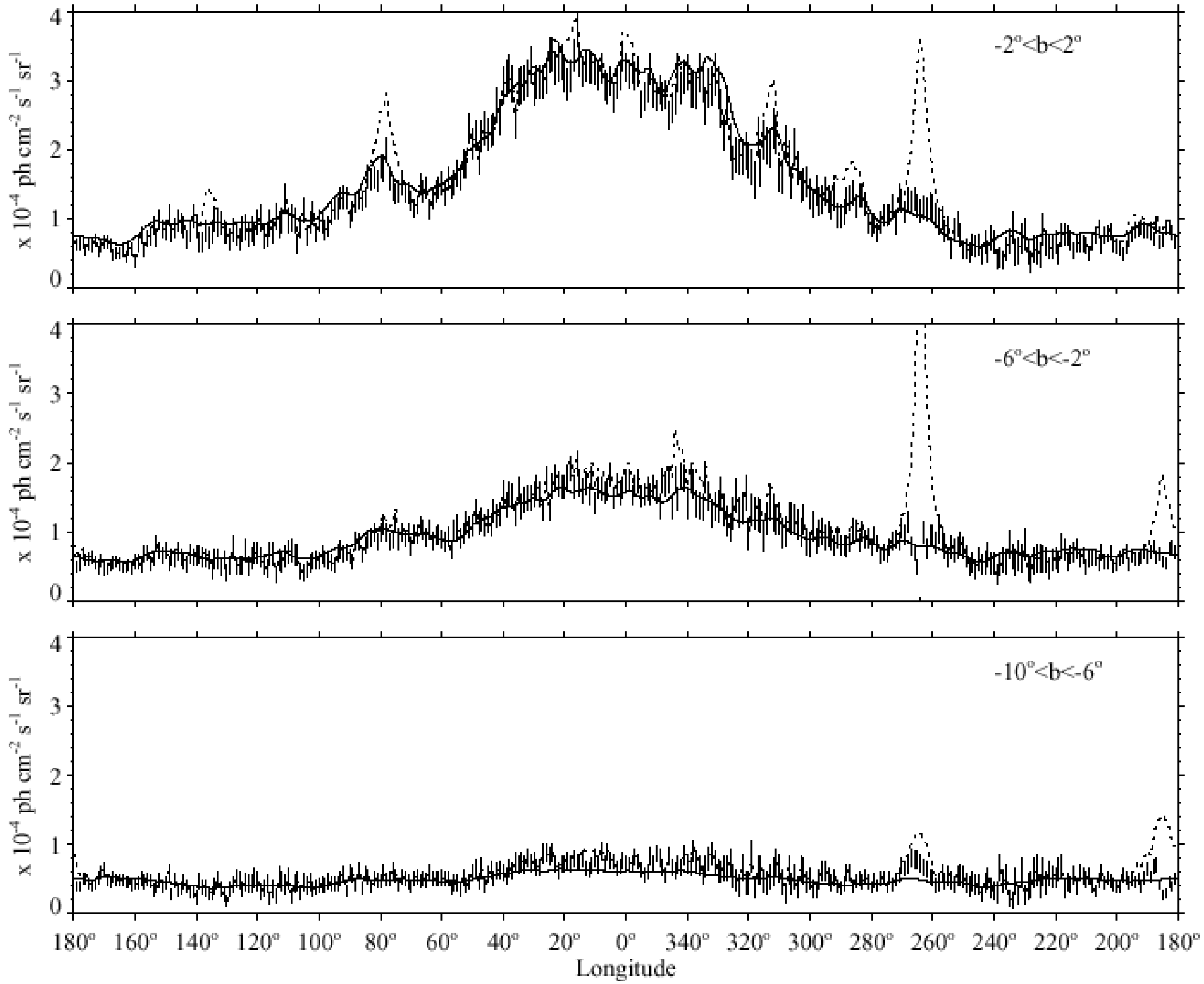

100-300 MeV

Hunter et al. ApJ 481, 205 (1997)

GALDIF: Latitude Profile

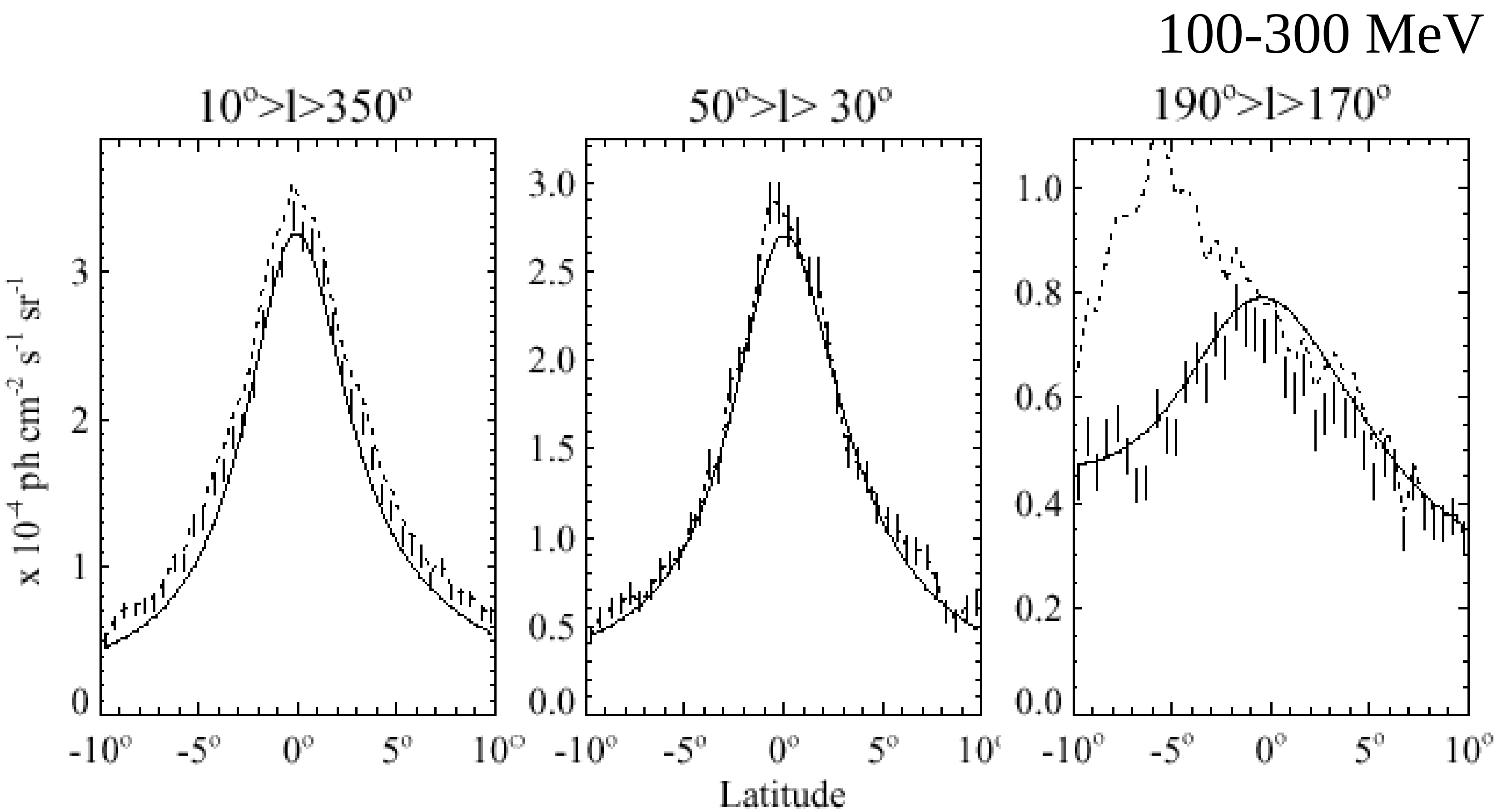

EGRET spectrum

Hunter et al. ApJ 481, 205 (1997)

FIG. 4.—Average diffuse gamma-ray spectrum of the inner Galaxy region, $300° < l < 60°$, $|b| \leq 10°$(0.73 sr). The contributions from point sources detected with more than 5 σ significance have been removed. The data are plotted as crosses where the horizontal line indicates the width of the energy interval and the vertical line the ± 1 σ statistical error. The intensity and error for the four lowest energy intervals include corrections to the EGRET effective area derived using observations of the Crab pulsar (Thompson et al. 1993b). The best-fit model calculation (see § 5) plus the isotropic diffuse emission is shown as the solid line. The individual components of this calculation, nucleon-nucleon (NN), electron bremsstrahlung (EB), and inverse Compton (IC), are shown as dashed lines. The isotropic diffuse emission (ID, Sreekumar et al. 1997) is shown as a dash-dotted line.

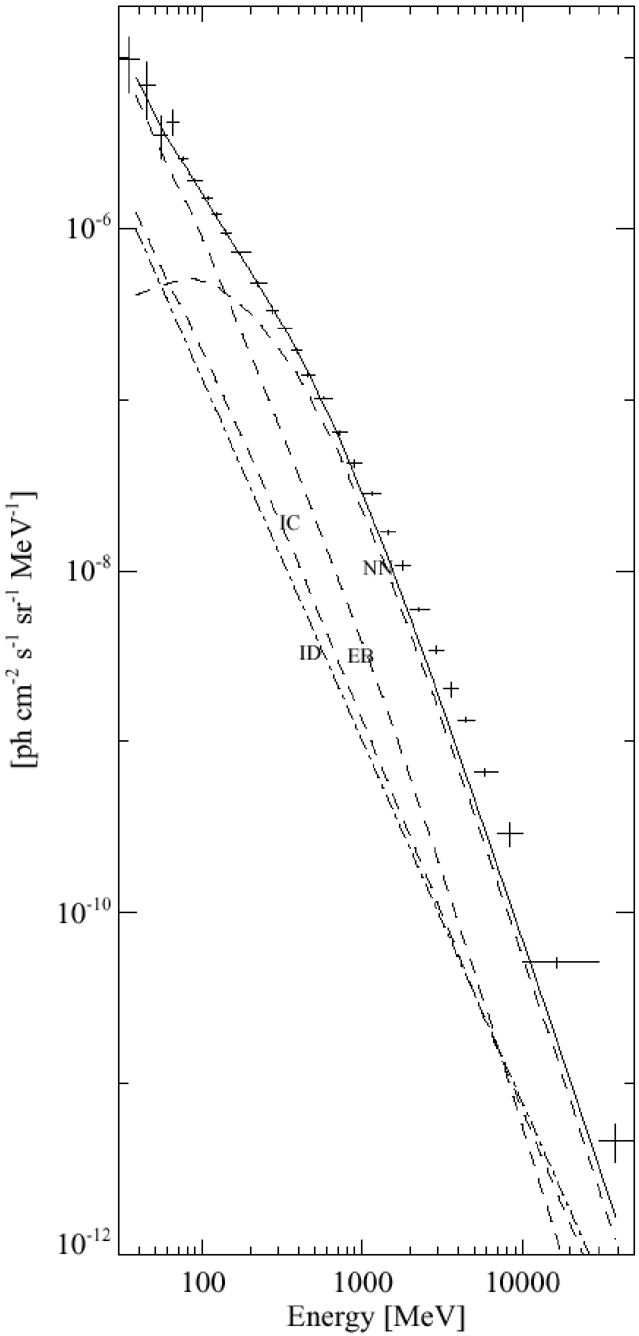

GALDIF: Contribution of each components

Hunter et al. ApJ 481, 205 (1997)

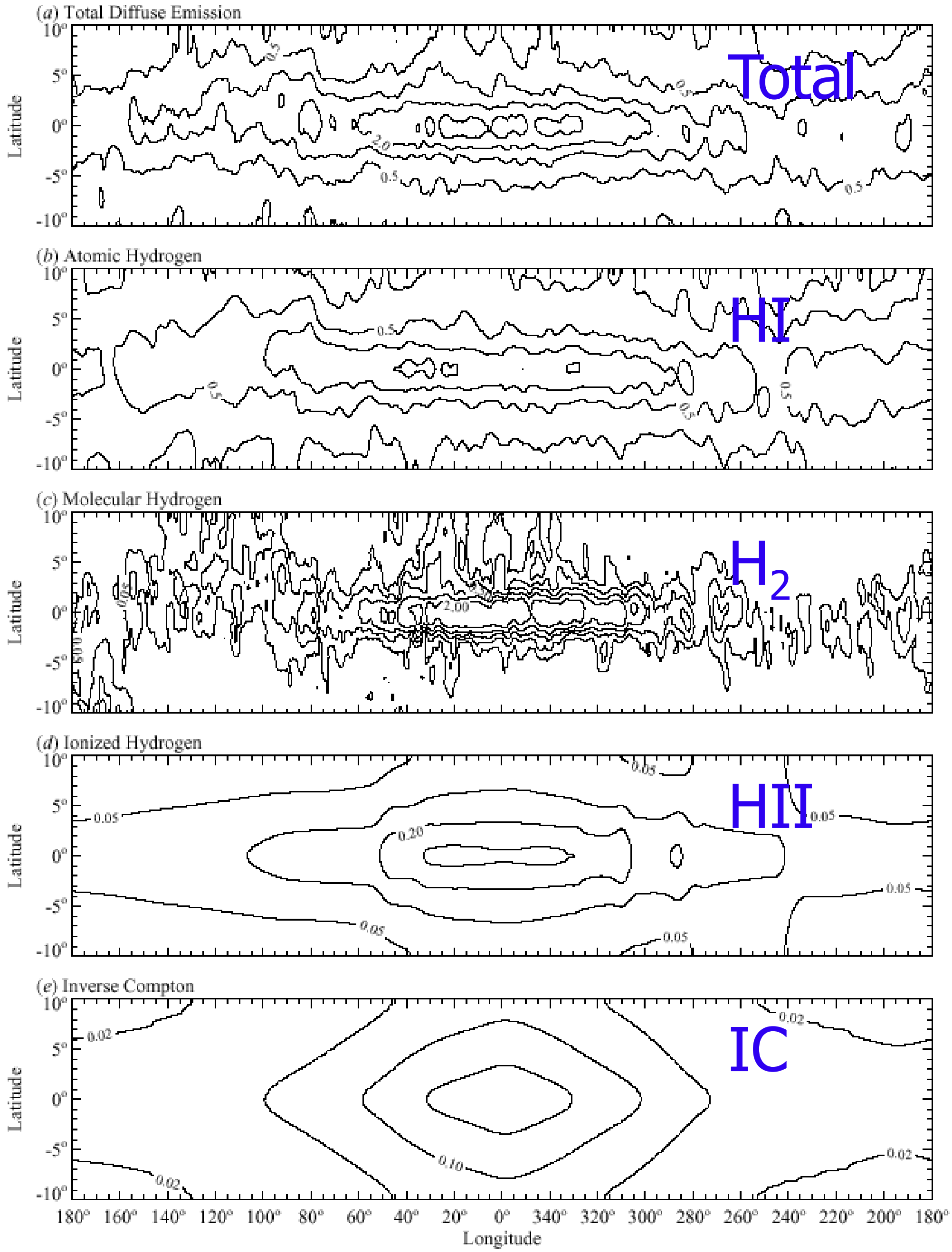

Hunter et al. ApJ 481, 205 (1997)

Observation by EGRET

○ $|b| \leq 10°$, 38 point sources ($>5\sigma$) removed

◎30MeV - 50GeV with excellent statistics (cf. COS B)

◎General agreement with model predictions in spatial profile

● 40-60% excess against model predictions above 1 GeV

$\Rightarrow$ Possible solutions:

- Instrumental calibration error?
- Unresolved sources?
- Nuclear interaction model?
- Cosmic-ray spectrum?

Interstellar radiation field (GALPROP)

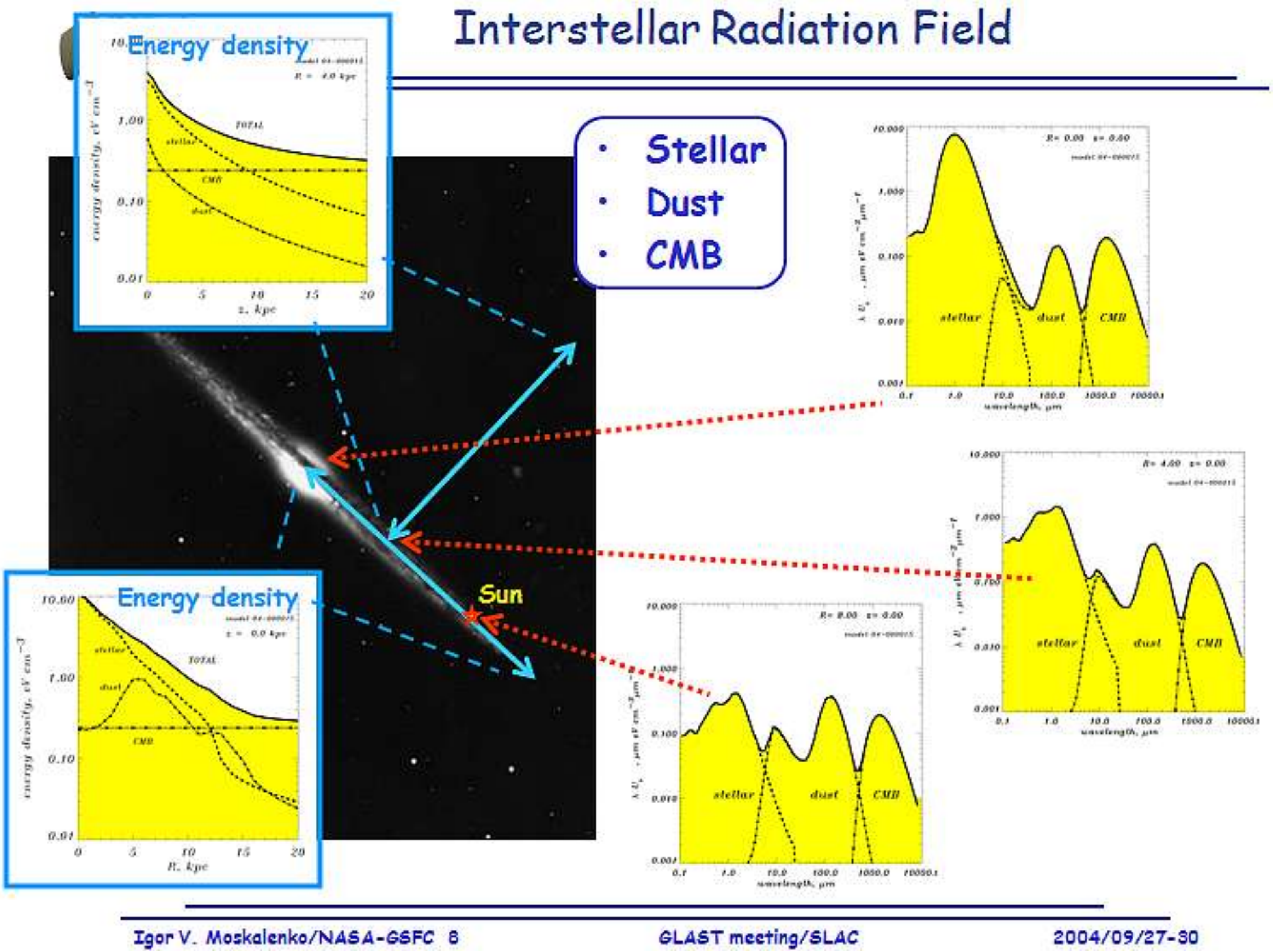

Gas distribution (GALPROP)

Gas Distribution

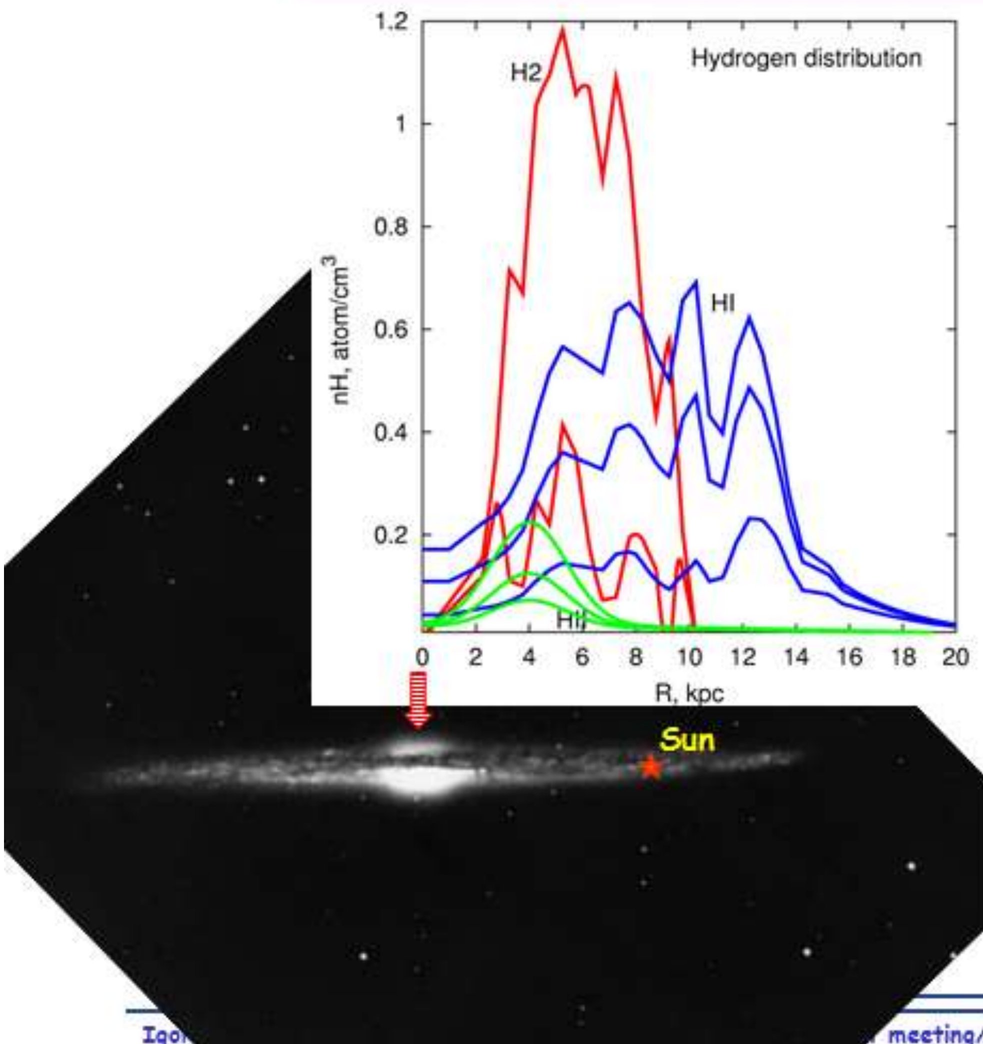

Molecular hydrogen H_2
<u>is traced using J=1-0 transition of ^{12}CO,</u> concentrated mostly in the plane
(z~70 pc, R<10 kpc)

Atomic hydrogen H I
has a wider distribution
(z~1 kpc, R~30 kpc)

Ionized hydrogen H II –
small proportion, but exists even in halo
(z~1 kpc)

Strong, Moskalenko & Reimer, ApJ 613, 962 (2004)

GALPROP：injection spectrum

PARTICLE INJECTION SPECTRA AND NORMALIZATIONS

Model	ID	Proton Spectrum: Injection Index[a]	Proton Spectrum: Break Rigidity (GV)	Proton Spectrum: Normalization at 100 GeV[b]	Electron Spectrum: Injection Index[a]	Electron Spectrum: Break Rigidity (GV)	Electron Spectrum: Normalization at 32.6 GeV[b]
Conventional.........	44_500180	1.98/2.42	9	5.0×10^{-2}	1.60/2.54	4	4.86×10^{-3}
Hard electron.........	44_500181	1.98/2.42	9	5.0×10^{-2}	1.90	...	1.23×10^{-2}
Optimized.............	44_500190	1.50/2.42	10	9.0×10^{-2}	1.50/2.42	20	2.39×10^{-2}

NOTE.—The GALPROP model IDs are given for future reference; the corresponding parameter files contain a complete specification of the models.
[a] Below/above the break rigidity.
[b] Normalization of the local spectrum (propagated). Values are in units of m^{-2} sr^{-1} s^{-1} GeV^{-1}.

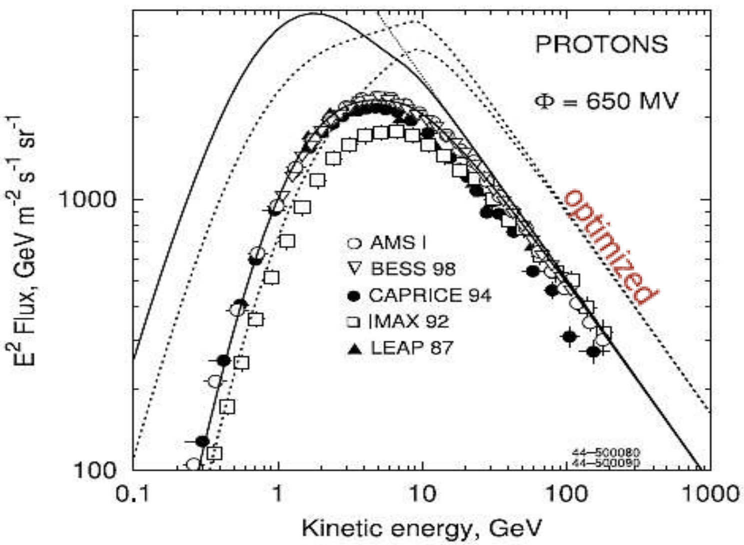

FIG. 2.—Proton spectra as calculated in conventional (*solid lines*) and optimized (*dotted lines*) models compared with the data (*upper curve*, LIS; *lower curve*, modulated to 650 MV). Thin dotted line shows the LIS spectrum best fitted to the data above 20 GeV (Moskalenko et al. 2002). Data: AMS (Alcaraz et al. 2000b), BESS 98 (Sanuki et al. 2000), CAPRICE 94 (Boezio et al. 1999), IMAX 92 (Menn et al. 2000), and LEAP 87 (Seo et al. 1991).

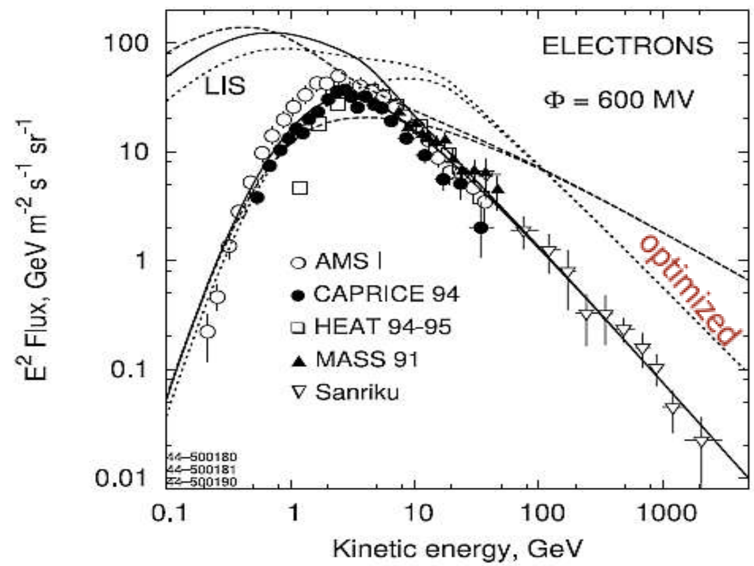

FIG. 3.—Electron spectra for conventional (*solid lines*), hard electron (*dashed lines*), and optimized models (*dotted lines*), compared with the data (*upper curve*, LIS; *lower curve*, modulated to 600 MV). Data: AMS (Alcaraz et al. 2000a), CAPRICE 94 (Boezio et al. 2000), HEAT 94-95 (DuVernois et al. 2001), MASS 91 (Grimani et al. 2002), and Sanriku (Kobayashi et al. 1999).

Strong, Moskalenko & Reimer, ApJ 613, 962 (2004)

GALPROP: Longitude profile

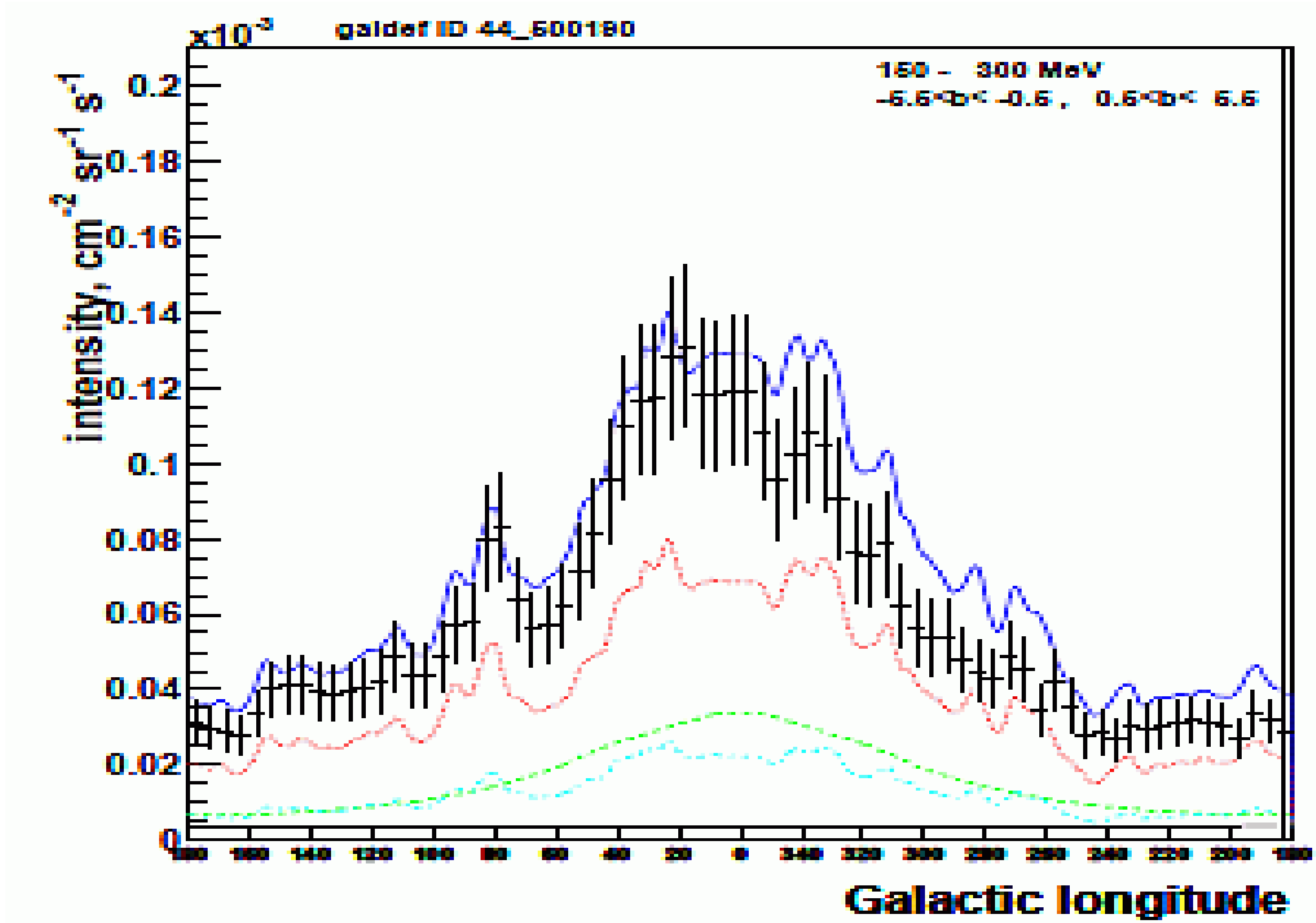

π^0-decay (dots, red), IC (dashes, green), bremsstrahlung (dash-dot, cyan), EGRB (thin solid, black), total (thick solid, blue)

Strong, Moskalenko & Reimer, ApJ 613, 962 (2004)

GALPROP: Latitude profile

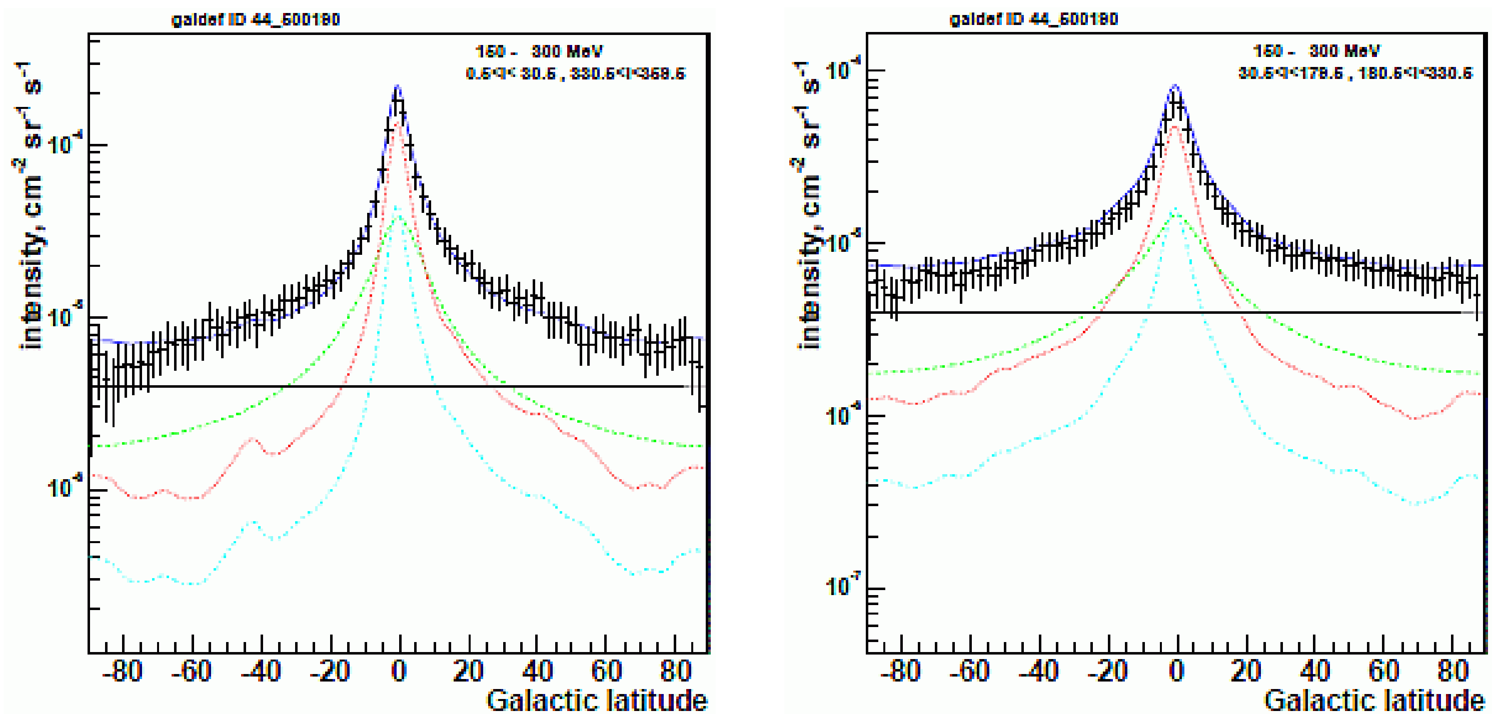

π^0-decay (dots, red), IC (dashes, green), bremsstrahlung (dash-dot, cyan), EGRB (thin solid, black), total (thick solid, blue)

Strong, Moskalenko & Reimer, ApJ 613, 962 (2004)

EGRET spectrum & optimized GALPROP

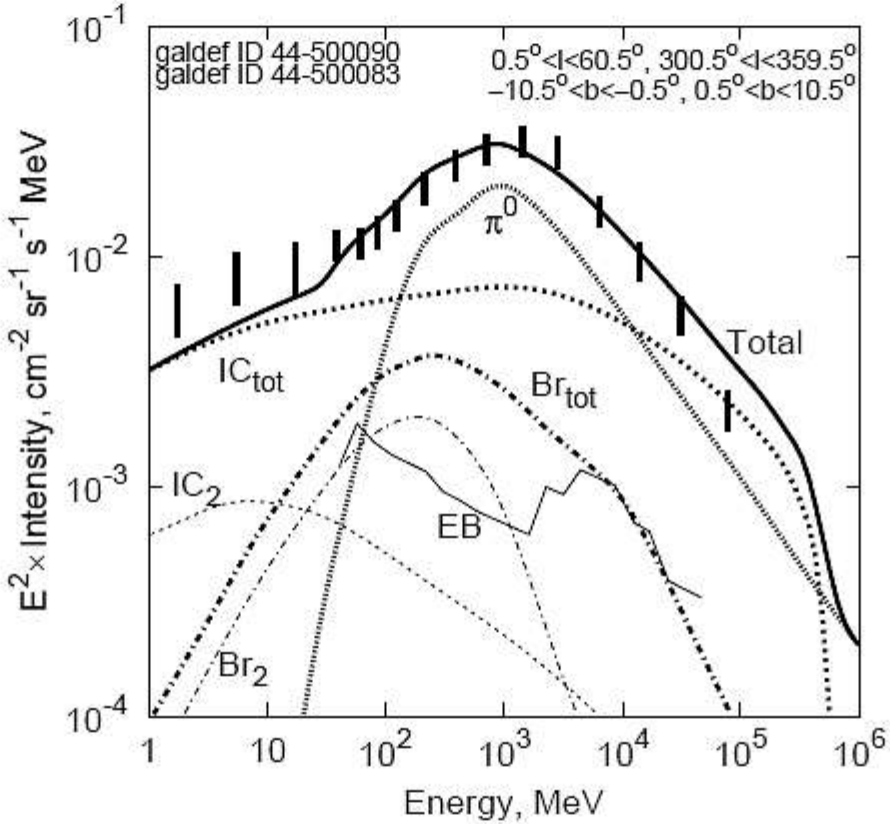

FIG. 13.— γ-ray spectrum of optimized model with (thick lines) and without (thin lines) primary electrons, to show the contribution of secondary electrons and positrons. Br_{tot} and Br_2 labels denote the total bremsstrahlung and the separate contribution from secondary leptons, correspondingly. Similarly, IC_{tot}, IC_2 indicate the total IC and the contribution from secondaries.

Flatter Proton Spectrum?　-1

Mori 1997

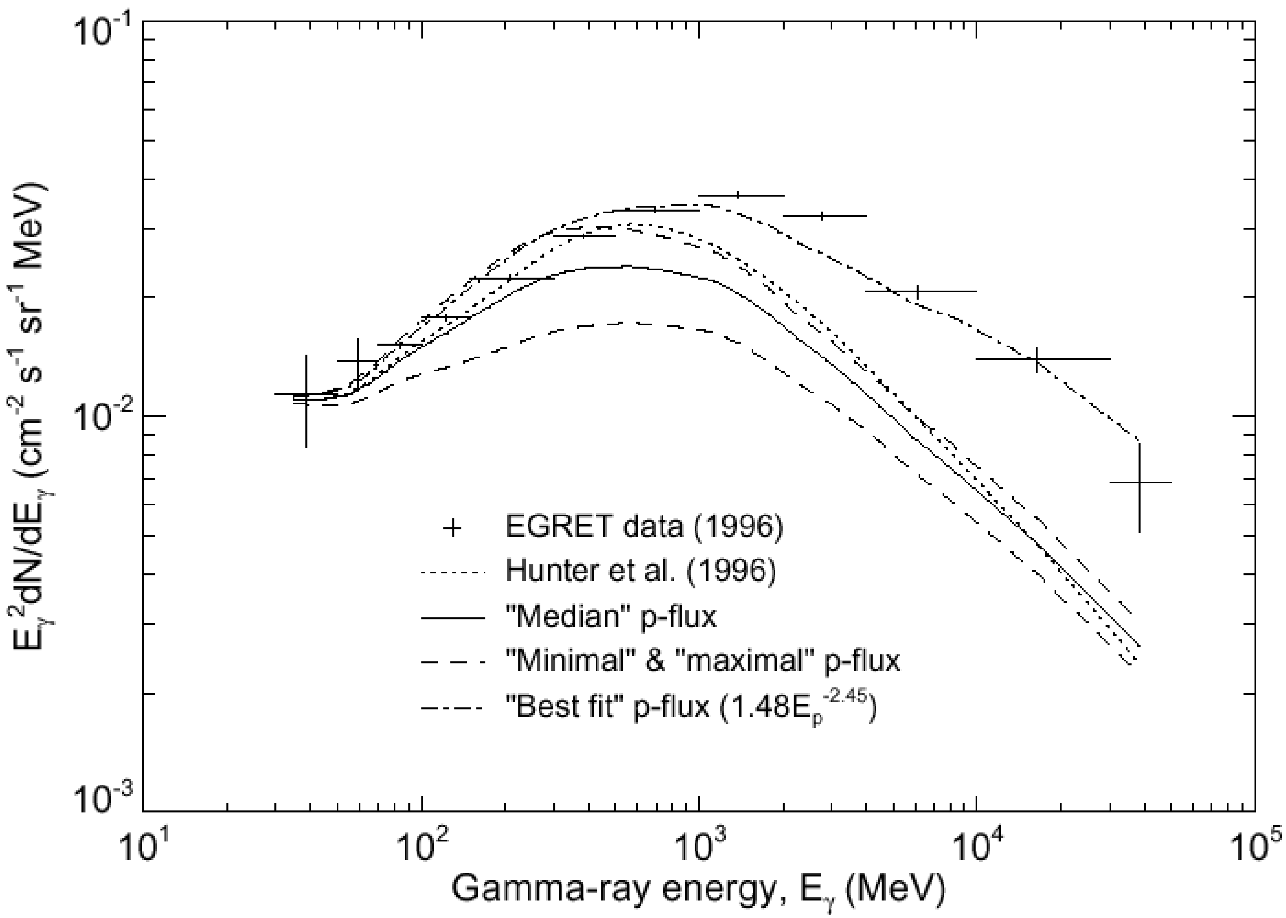

Standard:

$E^{-2.7}$

↓

$E^{-2.45}$?

Flatter Proton Spectrum? -2

Völk 2000

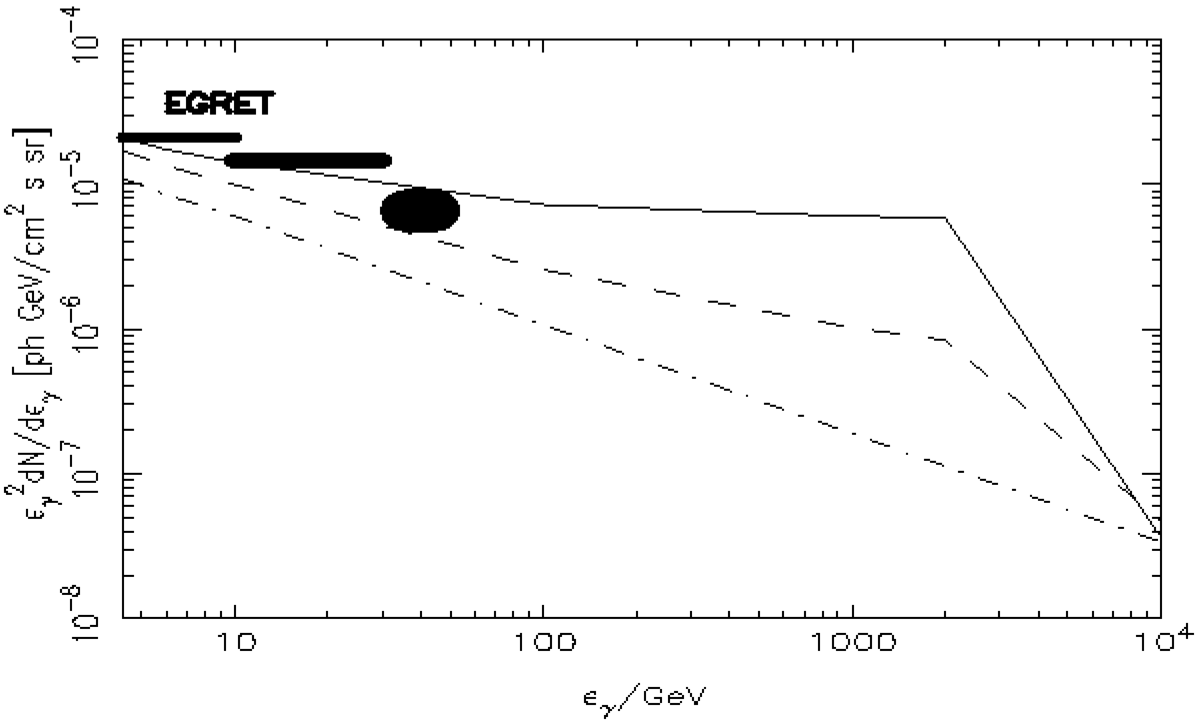

Souce: E^{-2}

↓

Transport effect

FIGURE 1. The differential diffuse γ-ray energy flux vs γ-ray energy above 4.4 GeV (cf. Berezhko & Völk, 1999). The heavy symbols are the EGRET measurements, and the dash-dot line is the model prediction of Hunter et al. (1997a). The full curve corresponds to our acceleration model with $\gamma_{SCR} = 2$, whereas the dashed curve corresponds to the Leaky Box model. Both theoretical curves incorporate energy-dependent loss from the acceleration region.

Flatter Inverse Compton? -1

Porter & Prothroe 1997

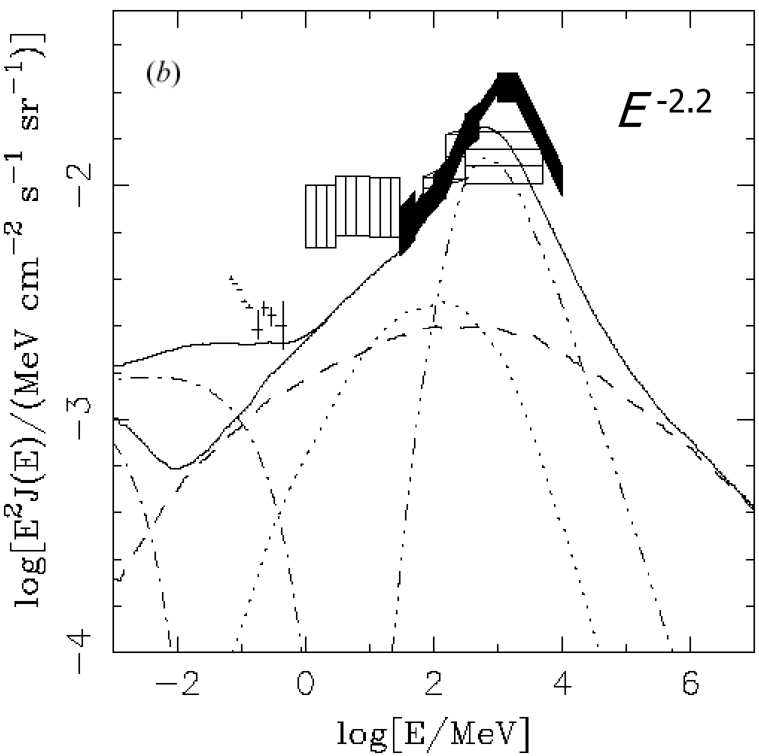

Figure 6. Average gamma-ray spectra for the inner Galaxy ($-60^\circ < l < 60^\circ$ and $|b| < 20^\circ$) for an injection spectrum of (a) $E^{-2.4}$ and (b) $E^{-2.2}$. The individual contributions to the diffuse gamma-ray spectrum are indicated: IC by the broken curve; bremsstrahlung by the dotted curve; synchrotron by the chain curve; π^0-decay by the double chain curve. The full curve is the sum of all contributions. Data are from various satellite telescopes; blocked data: EGRET [22], horizontally hatched boxes: COS-B [18], vertically hatched boxes: COMPTEL [12], and data points: OSSE [12] (original data from [20]).

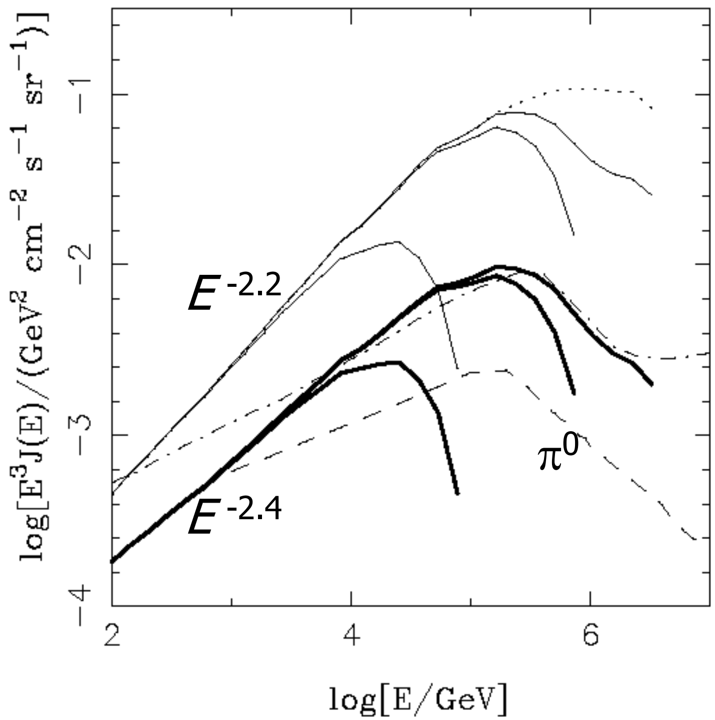

Figure 7. Diffuse gamma-ray spectra in the direction $l = 0^\circ$, $b = 0^\circ$. Heavy full curves show the IC spectrum for an $E^{-2.4}$ injection spectrum of electrons; light full curves show the IC spectrum for $E^{-2.2}$. For each injection spectrum, the lowest branch is for a cut-off at 100 TeV, the next higher branch a cut-off at 1 PeV, and the next higher no cut-off in the injection spectrum; each of these curves includes attenuation on the CMBR. The dotted curve shows the IC spectrum for an $E^{-2.2}$ spectrum with no cut-off and no attenuation on the CMBR. The chain curve shows the predicted spectrum for π^0-decay (including attenuation on the CMBR) calculated by Ingelman and Thunman [63]; the broken curve shows the predicted π^0-decay spectrum (including attenuation on the CMBR) calculated by Berezinsky *et al* [62].

Flatter Inverse Compton? -2

Pohl & Esposito 1998

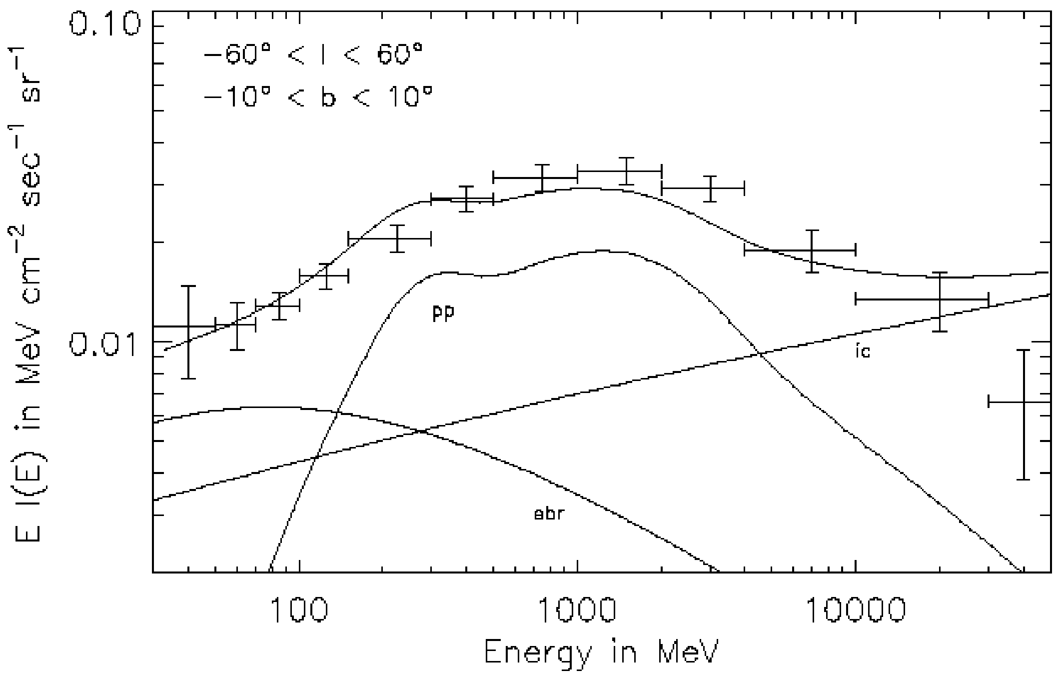

Distributed
$E^{-2.0\pm0.2}$

FIG. 5.—Gamma-ray intensity in the direction of the inner Galaxy. The data points are taken from Hunter et al. (1997). The error bars include an estimate for the systematic error of 8%, which accounts for the uncertainty in the energy-dependent correction of the spark chamber efficiency (Esposito et al. 1998). The data are compared with bremsstrahlung ("ebr") and Inverse Compton ("ic") spectra from our model, on the basis of sources with injection indexes following a normal distribution of mean 2.0 and dispersion 0.2 and the spatial distribution of SNRs in spiral arms. The π^0-component is a template and not a model.

Stecker, Hunter & Kniffen, Astropart. Phys. 29, 25 (2008)

Energy calibration?

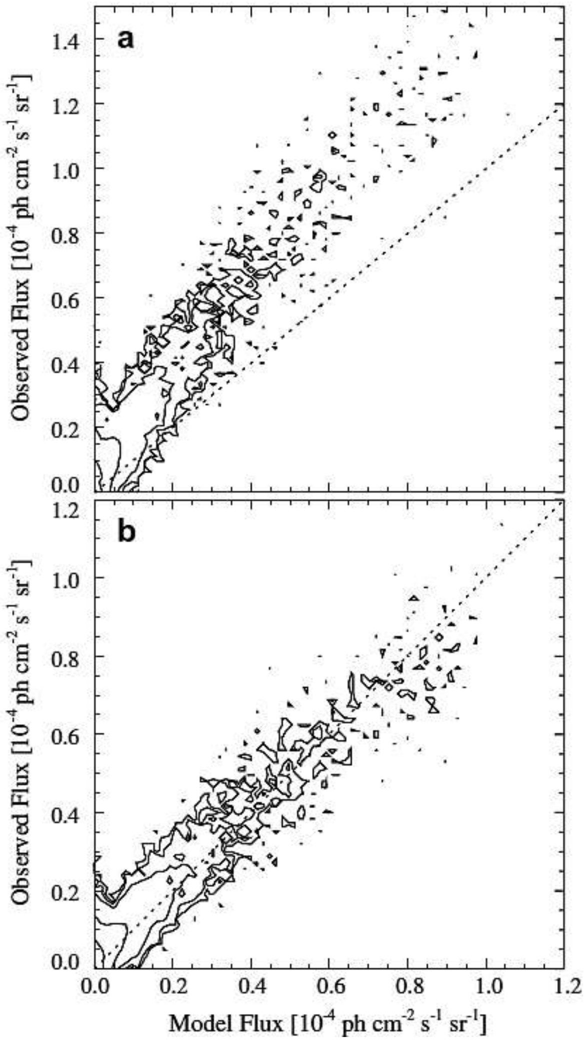

(a) Plot of integral (E > 1 GeV), all-sky diffuse model flux vs. EGRET observed flux for 335° < l < 45° , |b|< 90°. (b) A similar plot with a renormalization factor of $(1.6)^{-1}$ applied to the observed flux.

GeV anomaly exists uniformly over the whole sky and extends from high to low intensity galactic flux emission.

→Most likely traceable to the detector itself!

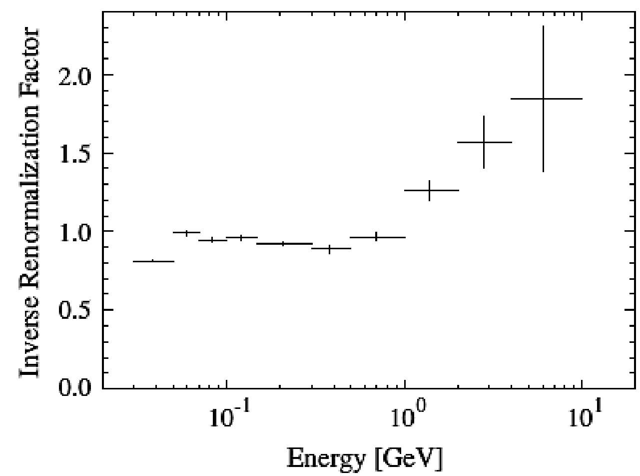

Fig. 2. Required inverse renormalization factor for different energy bins, given as the ratio of observed-to-predicted flux vs. energy.

Higher energy?

Amenomori et al. 1997

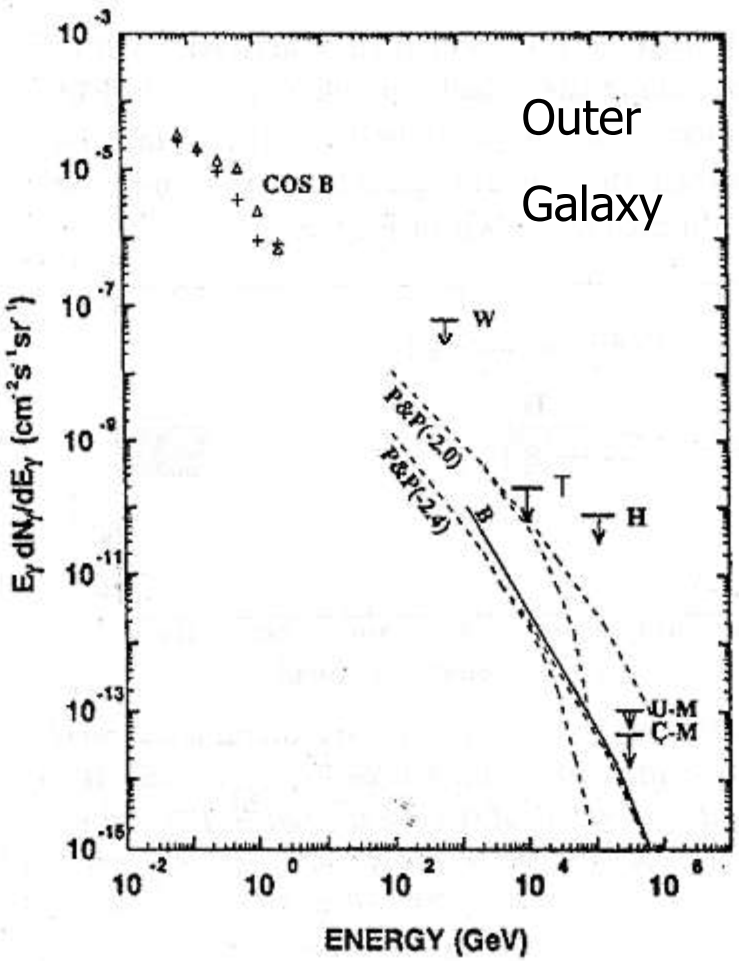

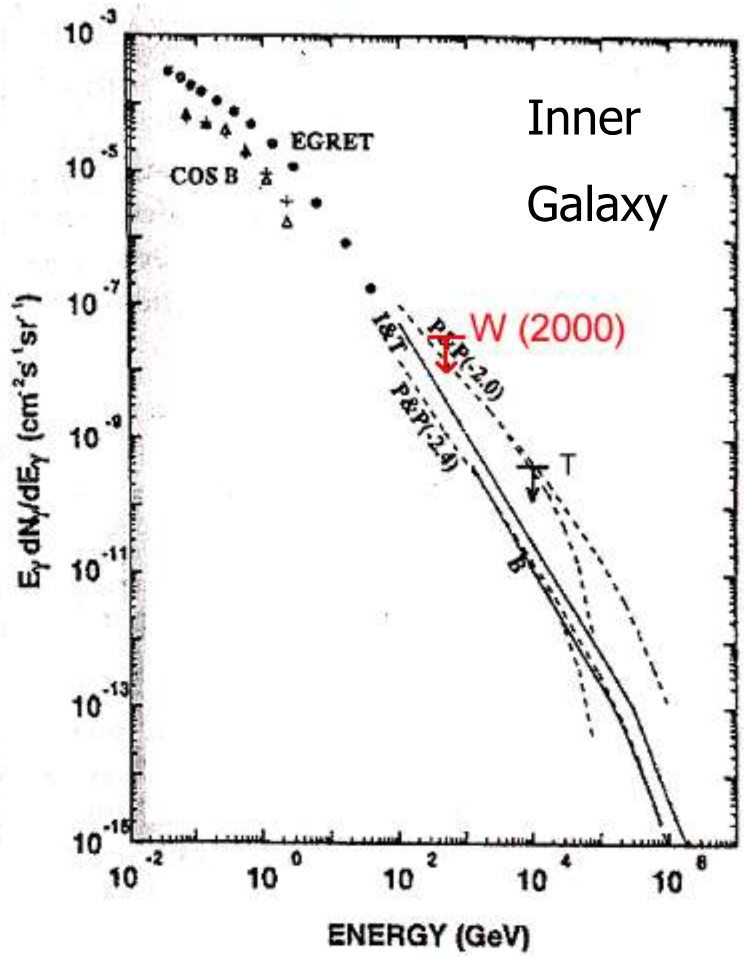

Fig. 4 *Diffuse gamma rays from the outer Galaxy. The plotted points are* **COS-B** *data (Paul et al. 1978); (△): 91° ≤ l ≤ …, | b |≤ 10°; (+): 116° ≤ l ≤ 136°, | b |≤ … Present data (*Tibet*) is given by the upper limit at 10 TeV for 140° ≤ l ≤ 225°, | b |≤ … The ground based data are shown by U-M (Utah-Michigan, Matthews et al. 1991) for 30° ≤ l ≤ 220°, | b |≤ 10° and* **C-M** *(CASA-MIA, Borione et al. 1991) for 50° ≤ l ≤ …, | b |≤ 10°. The other upper limits assigned by* **W** *(Whipple, Reynolds et al. 1993) and H (HEGRA, Karle et al. 1995) are data for sky regions apart from the galactic disk. The theoretical curves are assigned by* **B** *(Berezinsky et al. 1993) for $\pi^0 \to 2\gamma$ decay and* **P&P** *(Porter & Protheroe 1996) for the inverse Compton by electrons with injected spectral indeces -2.0 and -2.4, respectively. Lower curves of* **P&P** *are the case of energy cut at 100 TeV for the shock acceleration.*

Fig. 5 *Diffuse gamma rays from the inner Galaxy. The plotted points are* **COS-B** *data (Paul et al. 1978); (△): 16° ≤ l ≤ 36°, | b |≤ 10°; (+): 315° ≤ l ≤ 36°, | b |≤ 10°, and* **EGRET** *data (Hunter et al. 1997); (●): 300° ≤ l ≤ 60°, | b |≤ 10°. Present data (*Tibet*) is given by the upper limit at 10 TeV for 20° ≤ l ≤ 55°, | b |≤ 5°. In addition to the theoretical curves* **B** *and* **P&P** *in Fig. 4,* **I&T** *(Ingelman & Thunman 1996) for $\pi^0 \to 2\gamma$ decay is shown by a dot-dot-dashed curve.*

Ground-based observations

- CASA-MIA (Borione et al. 1998)
  $50° < l < 200°$, $-5° < b < 5°$; 310 TeV
  mu-poor showers $\Rightarrow I_\gamma/I_{CR} < 2.4\times10^{-5}$
- Tibet (Amenomori et al. 1997)
  $-5° < b < 5°$, 10 TeV, excess counts $\Rightarrow$
  $140° < l < 225°$: $< 2\times10^{-10}$ cm^{-2}s^{-1}sr^{-1}
  $20° < l < 55°$: $< 4\times10^{-10}$ cm^{-2}s^{-1}sr^{-1}
- EAS-TOP (Aglietta et al. 1996); 1 PeV
  mu-poor showers $\Rightarrow I_\gamma/I_{CR} < 7.3\times10^{-5}$
- HEGRA (Karle et al. 1995); 80 TeV
  N_e/Ch cut $\Rightarrow I_\gamma/I_{CR} < 7.8\times10^{-3}$
- MILAGRO (Abdo et al. 2008); 15 TeV
  8.6σ excess in Cygnus region: 2×10^{-13} TeV^{-1}cm^{-2}s^{-1}sr^{-1}

LeBohec et al. 2000

Whipple observation

- 4.8° FOV camera, Center: (l,b)=(40,0)
- 1998: 7 on/off pairs (28min. Each), >700GeV
  1999: 10 on/off pairs, >500GeV
- Sensitivity correction across the field

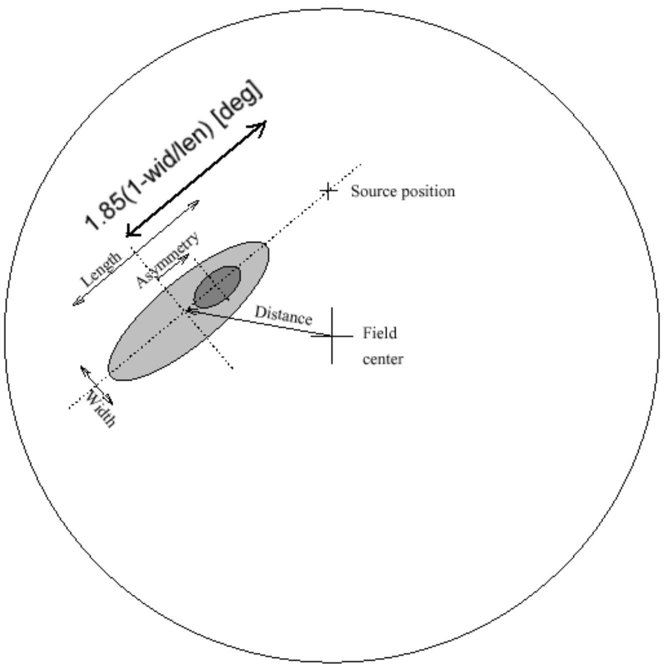

GAMMA-RAY CANDIDATE SELECTION

Parameters	Selection Criteria
Max1 (d.c.)	>78
Max2 (d.c.)	>56
Width (deg)	0°.073 < w < 0°.16
Length (deg)	0°.16 < l < 0°.43
Distance (deg)......	d < 1°.8

NOTE.—d.c. = digital counts; 1 d.c. ≃ 1 photoelectron.

Whipple results

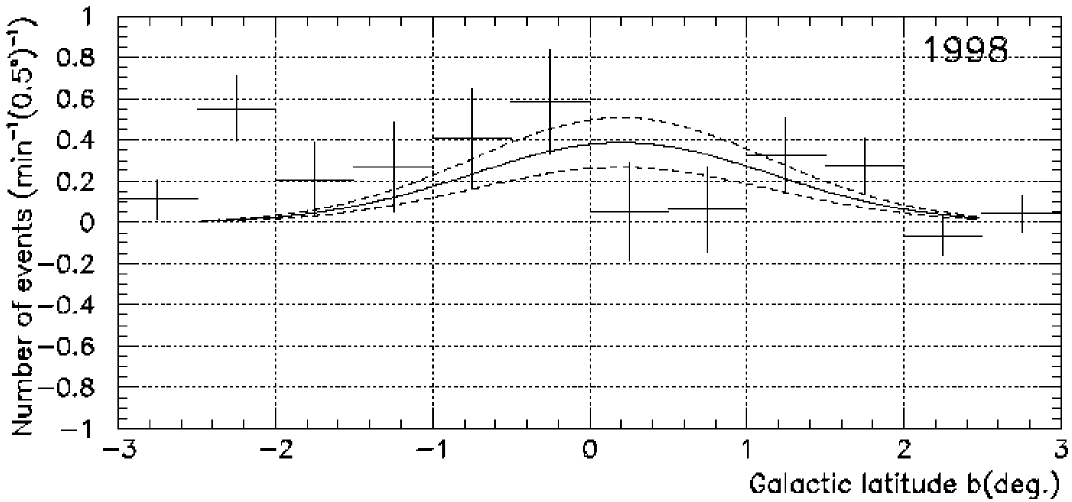

Fig. 6a

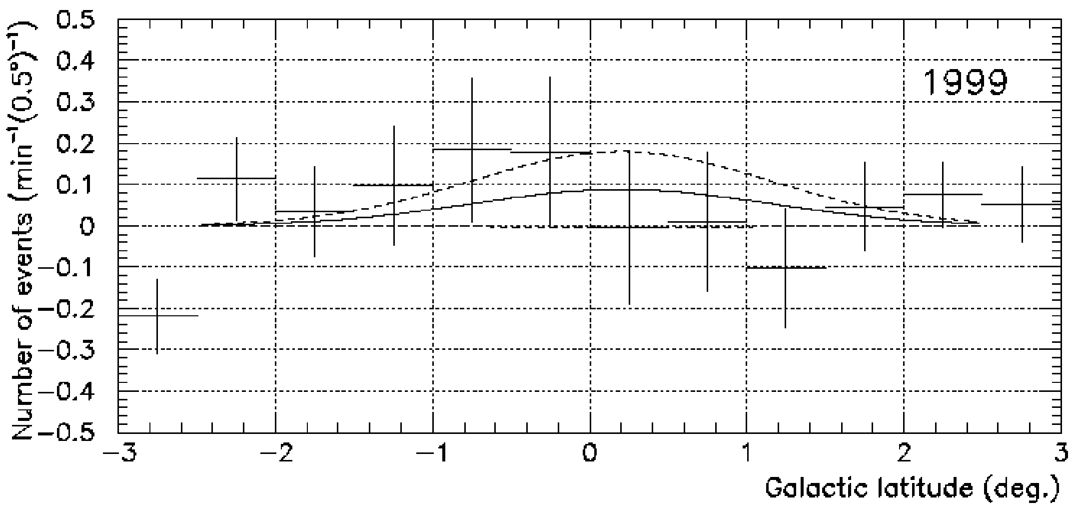

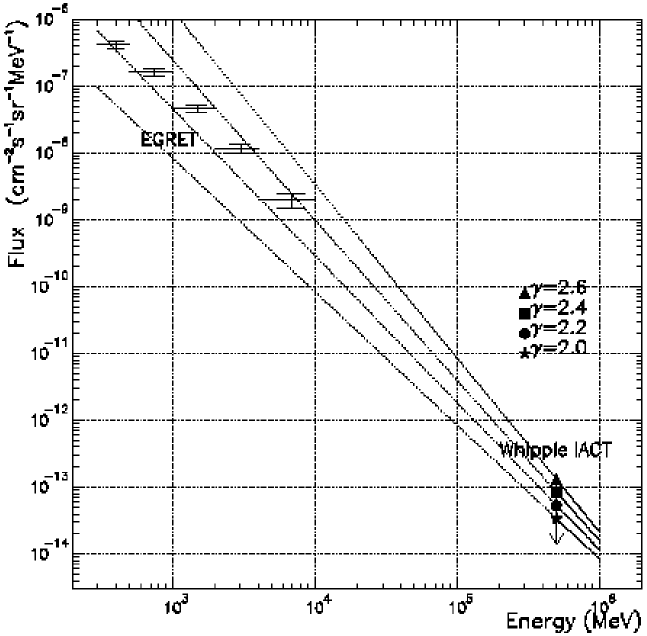

1998: 1.84±0.57/min (3.2σ!)

1999: 0.42±0.43/min

HEGRA observations

Pühlhofer et al. 1999

Lampeitl et al. 1999

- 4-telescope setup, total 105hr (1997/98)
- No source candidate above ¼ Crab
- Artificial Neural Netwo analysis for gamma/had separation in progress

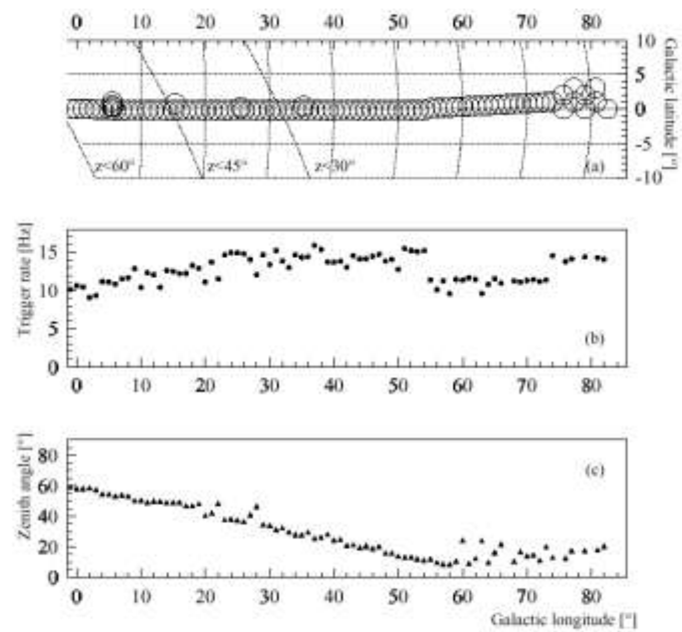

Figure 1: (a) Observed regions in Galactic coordinates. The circles indicate the field of view of the telescope system. The diagonal lines mark culmination zenith angles (from left to right) 60°, 45° and 30°. (b) Mean trigger rates. (c) Zenith angles of the observations.

Aharonian et al., Nature 439, 695 (2006)

H.E.S.S.

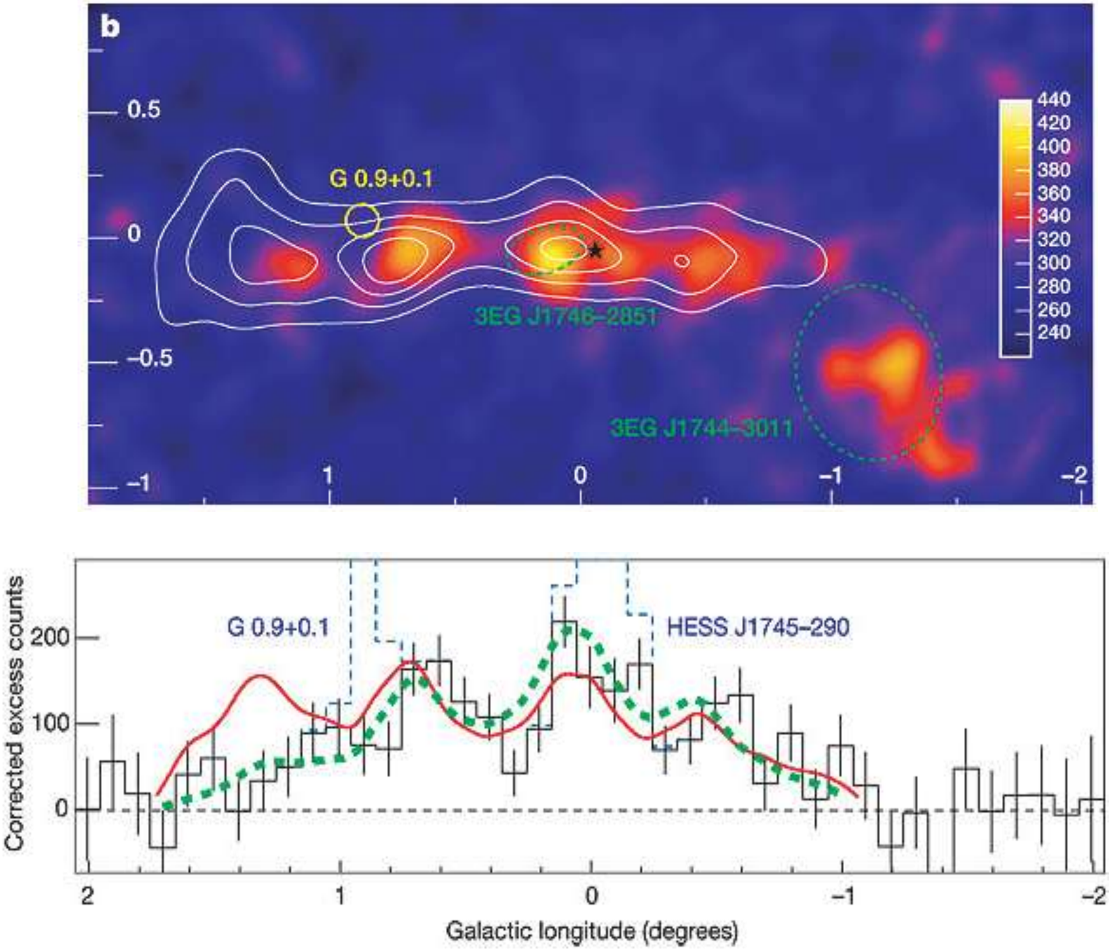

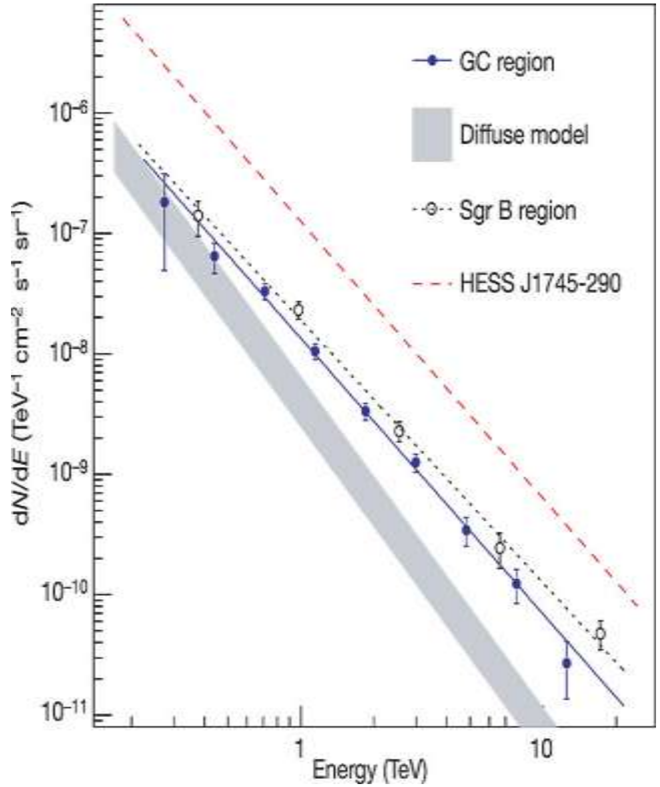

$E^{-2.29\pm0.07\pm0.02}$

Ohishi et al., Astropart.Phys. 30, 47 (2008)

CANGAROO-III results

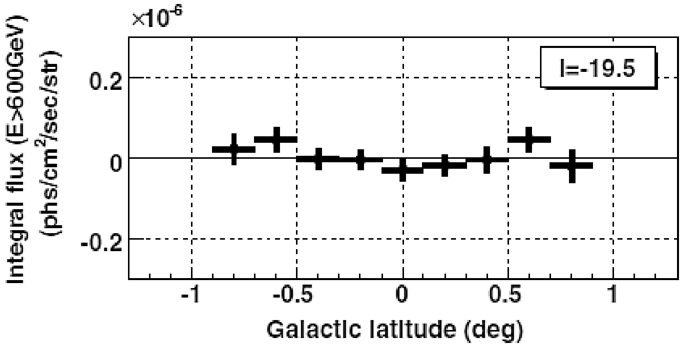

(a) $\ell = -19^{\circ}.5$

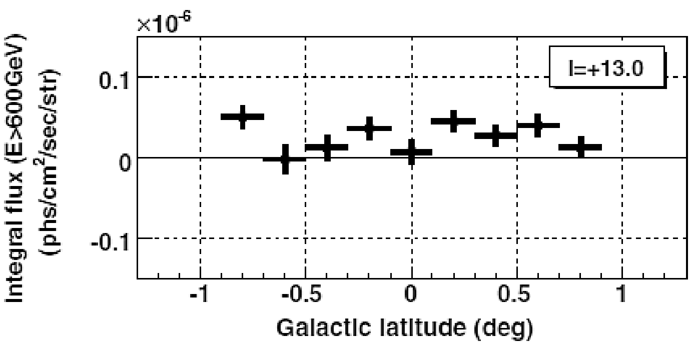

(b) $\ell = +13^{\circ}.0$

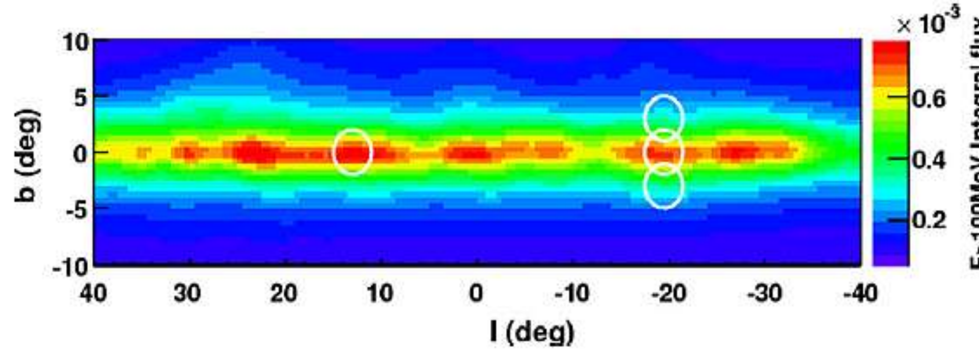

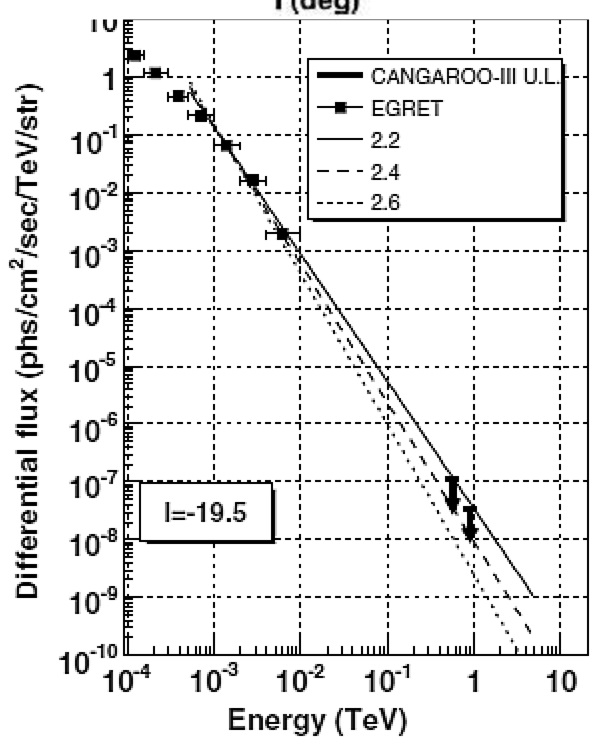

(a) $\ell = -19^{\circ}.5$

Limits from Balloon Experiments

Hunter 2000

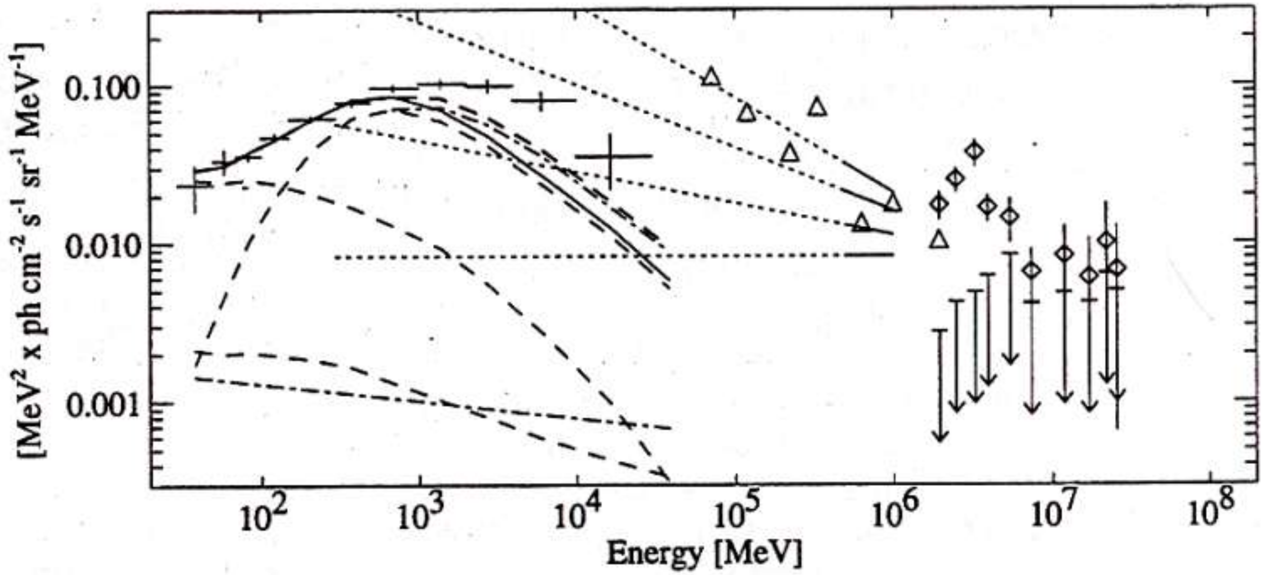

Figure 8. Measurement of the Galactic diffuse emission > 50 GeV with the Whipple telescope [29] extrapolated to the EGRET energy range on the assumption of single power-law spectral indices of 2.0, 2.2, 2.4, and 2.6. The spectral index must be ≤2.4 to be consistent with the EGRET observations, shown as ±1 σ data points. The unpointed balloon results from Nishimura et al. [28] and the JACEE experiment [27], taken at 4 gm/cm^2 and 5.5 gm/cm^2, shown as triangles and diamonds, respectively, should be treated as upper limits. The JACEE results corrected for the atmospheric contribution are shown as upper limits.

Abdo et al., ApJ 688, 1078 (2008)

Milagro

FIG. 1.—Galactic longitude profile of the γ-ray emission around 15 TeV in the Galactic plane as measured by Milagro. *Top*: Before subtraction of source contributions (*red data points with dashed error bars*) and after subtraction of source contributions (*black data points*). *Bottom*: Source-subtracted profile overlaid with prediction of the optimized GALPROP model. The red line represents the pion contribution, the green line represents the IC contribution, and the blue line represents the total flux prediction between Galactic latitude $\pm 2^\circ$. There are no data points in the region of longitude $l \in [-144^\circ, 29^\circ]$, because it is below the Milagro horizon. The region $l \in [111^\circ, 135^\circ]$ is excluded, because the analysis method is insensitive here (see text for details).

GAMMA-RAY EMISSION FROM THE GALACTIC PLANE AROUND 15 TeV

		Diffuse Flux ($\times 10^{-13}$ TeV^{-1} cm^{-2} s^{-1} sr^{-1})		
			GALPROP	
Region for $\lvert b \rvert < 2^\circ$ (l, deg)	Statistical Significance σ	Milagro[a]	Optimized	Conventional
30–65	5.1	$23.1 \pm 4.5^{+7.0}_{-8.0}$	20.0	4.9
65–85	8.6	$21.8 \pm 2.5^{+7.2}_{-7.8}$	10.2	2.7
85–110	1.3	<7.1 (95% CL)	5.8	1.3
136–216	0.8	<5.7 (95% CL)	3.1	0.9

[a] The first error represents the statistical, the second, the systematic, uncertainty. See text for details.

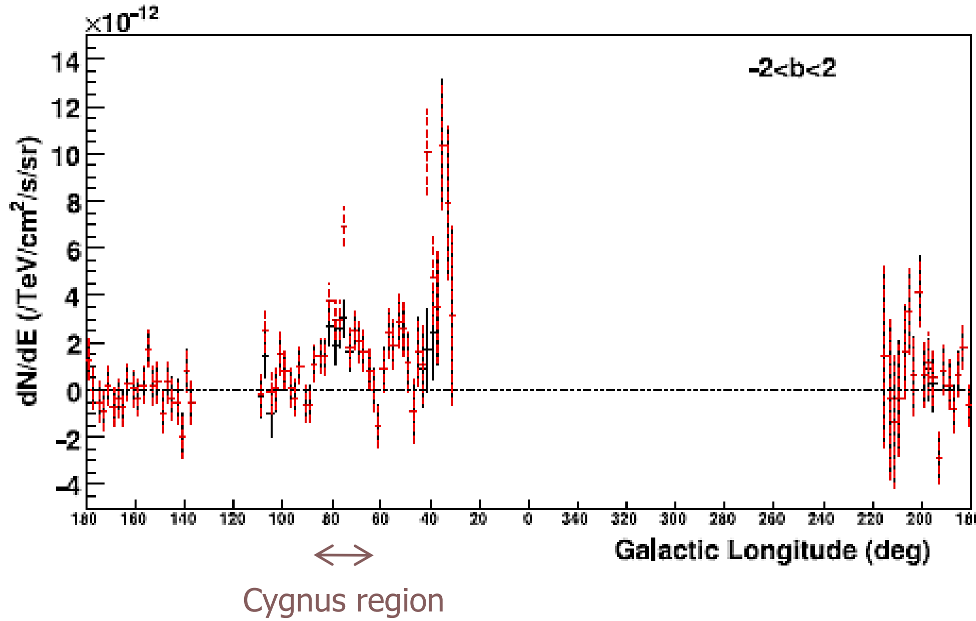

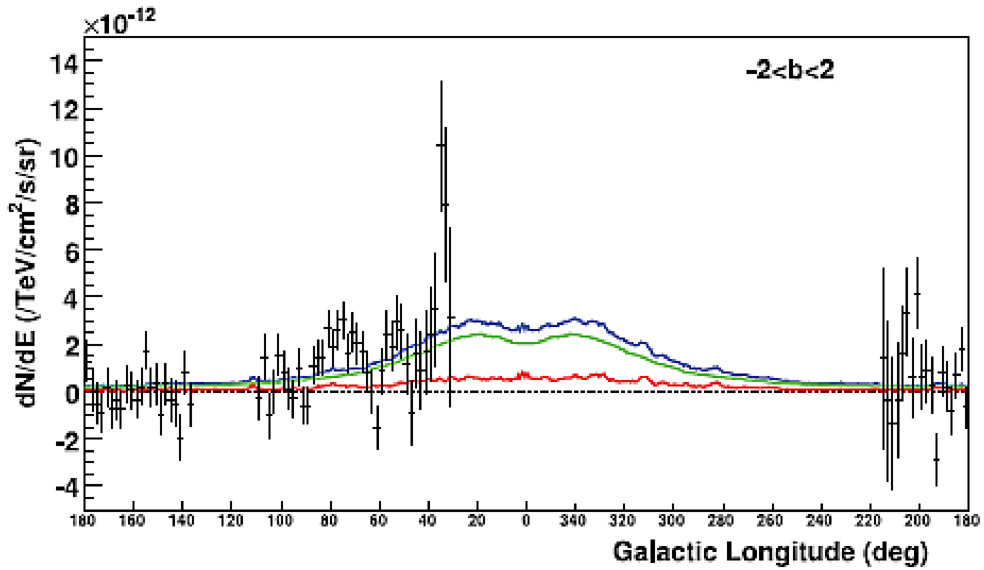

Abdo et al., ApJ 688, 1078 (2008)

Milagro: latitude profile

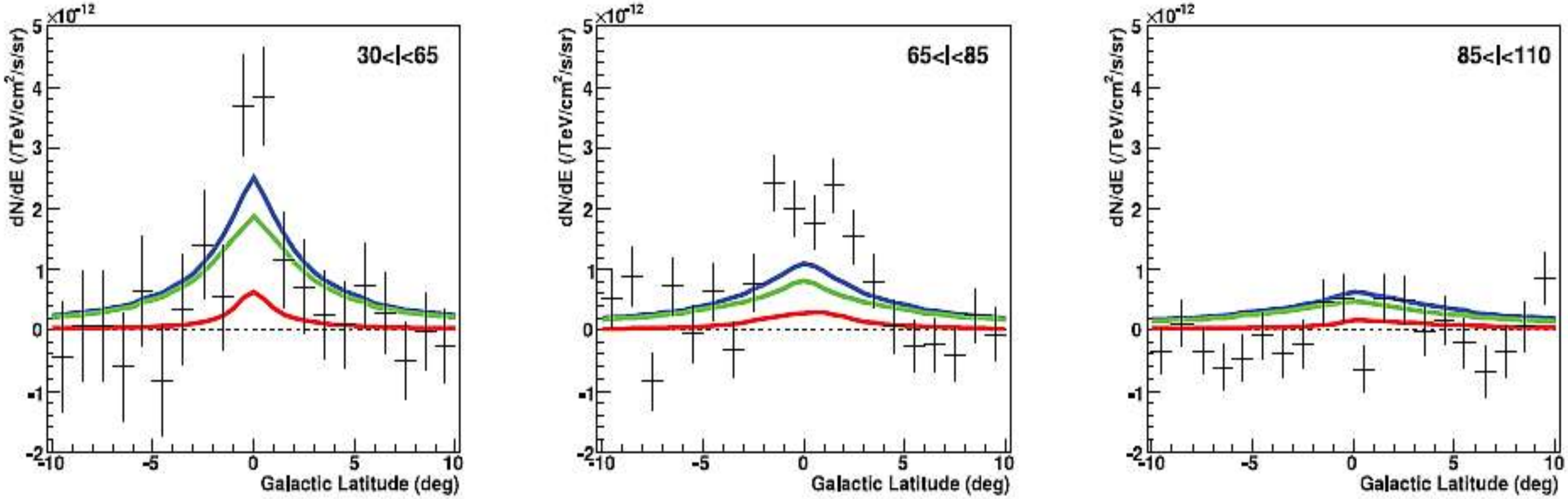

FIG. 3.—Source-subtracted Galactic latitude profile of the γ-ray emission around 15 TeV in the inner Galaxy (*left*), in the Cygnus region (*middle*), and in the region above Cygnus (*right*) as measured by Milagro (*points with errors*) and predicted by the optimized GALPROP model. The blue curve shows the total γ-ray flux, the red curve shows the pion contribution, and the green curve shows the IC contribution.

Abdo et al., ApJ 688, 1078 (2008)

Milagro: energy spectrum

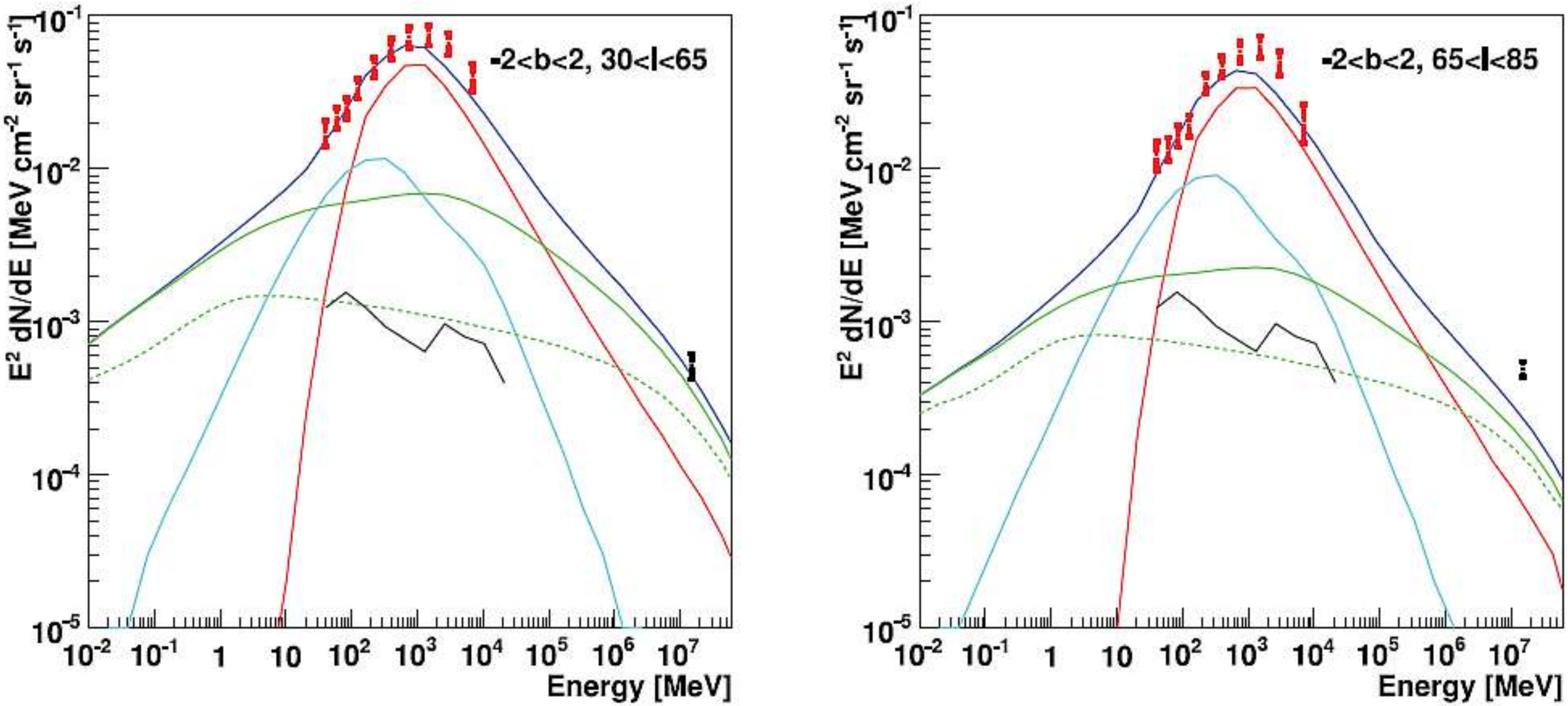

FIG. 2.—Gamma-ray spectra of the diffuse emission as predicted by the optimized GALPROP model for the Galactic plane. *Left*: Inner Galaxy ($l \in [30°, 65°]$). *Right*: Cygnus region ($l \in [65°, 85°]$). The red bars represent EGRET data, and the black bar represents the Milagro measurement, where the length of the bar represents the statistical uncertainty only. The dark blue line represents the total diffuse flux predicted by the optimized GALPROP model, the dark gray line represents the extragalactic background, and the light blue line represents the bremsstrahlung component. The two contributions at Milagro energies are shown as the red line, the pion contribution, and the green line, the total IC contribution. The green dashed line shows the dominant IC contribution from scattering of electrons off the cosmic microwave background, which amounts to about 60%–70% of the IC component at Milagro energies. Other IC contributions, which are less important, such as infrared and optical, are not shown separately.

Cherenkov2005 poster

Dark gas contribution!

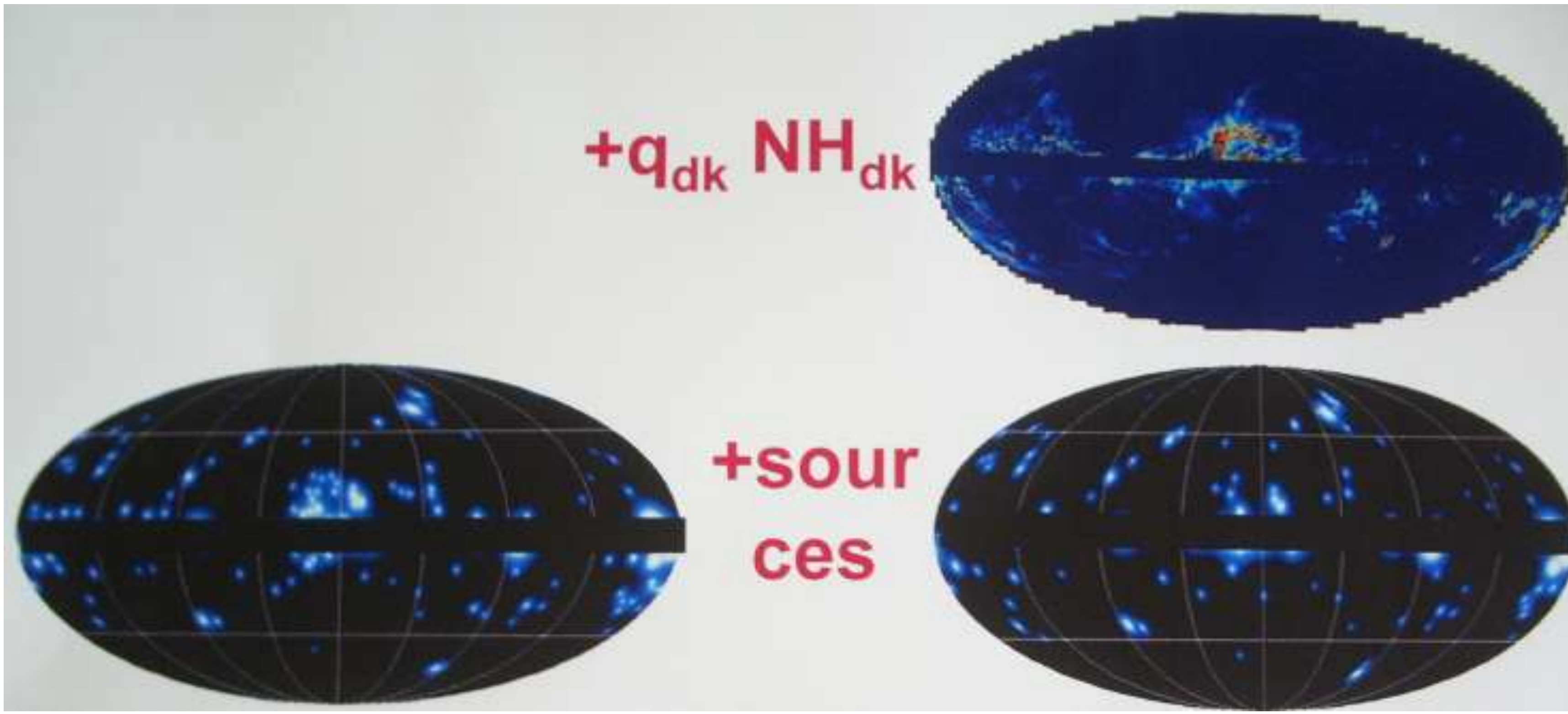

3EG catalog

"Extended" catalog

Unveiling Extensive Clouds of Dark Gas in the Solar Neighborhood

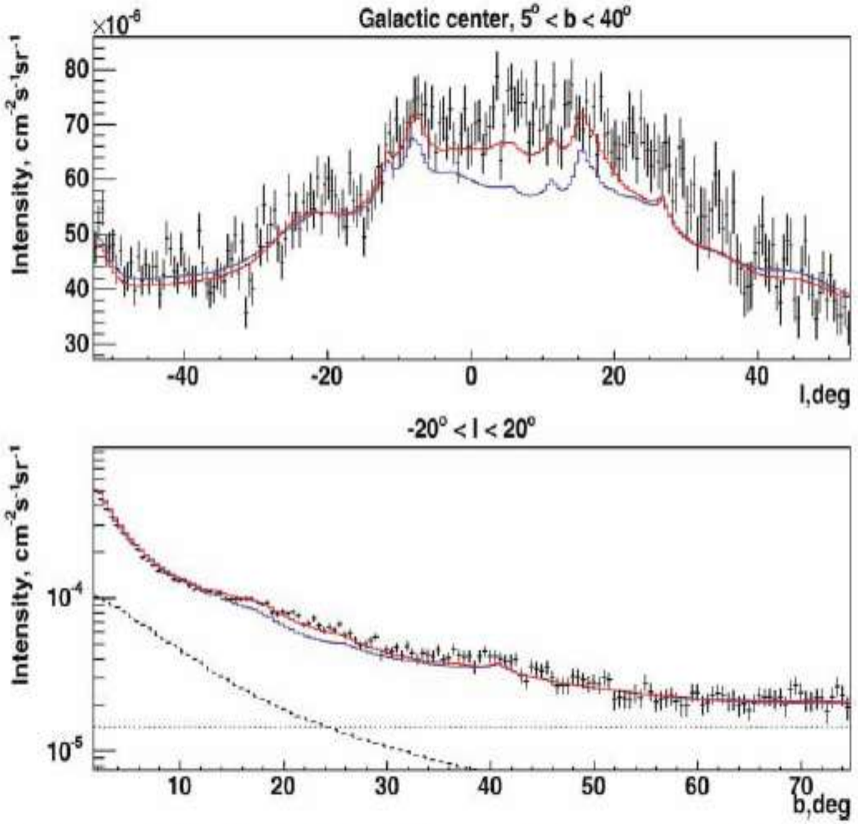

Fig. 3. Longitude (top) and latitude (bottom) profiles of the observed γ-ray intensity in the Aquila-Ophiuchus-Libra region versus the N(HI)+W(CO) gas model (blue) and the N(HI)+W(CO)+E(B-V) model (red). The dashed and dotted curves (bottom) outline the IC and extragalactic background intensities, respectively. Error bars show mean ± SD.

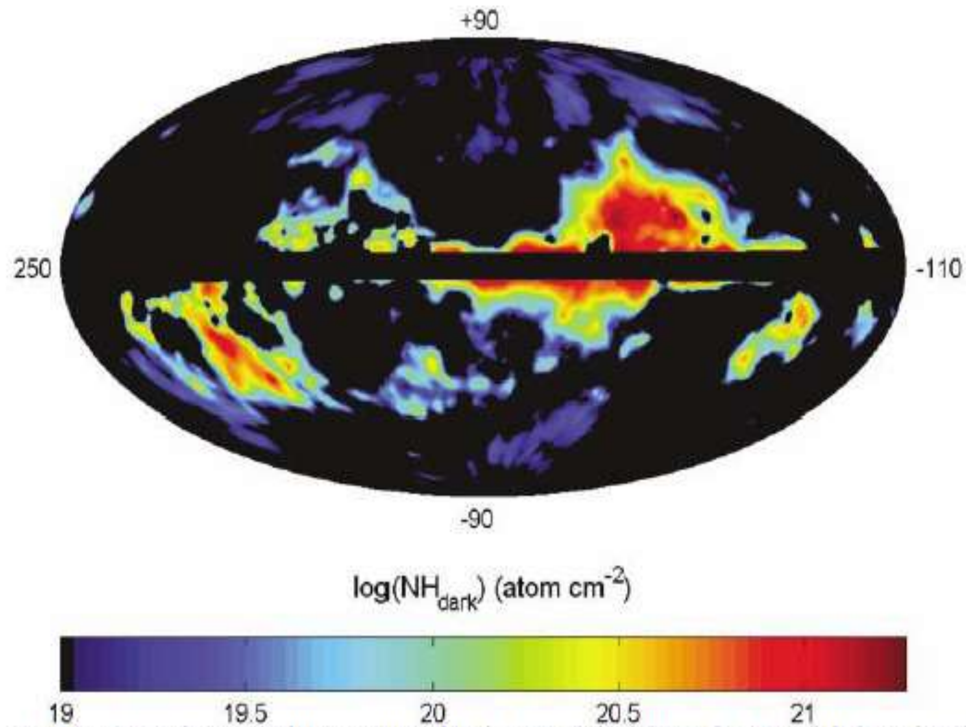

Fig. 4. Map, in Galactic coordinates centered on $l = 70°$, of the column densities of dark gas found in the dust halos, as measured from their γ-ray intensity with the reddening map. This gas complements that visible in HI and CO. The two dust tracers [E(B-V) and 94-GHz emission] yield consistent values within 30% over most regions.

Isabelle A. Grenier, Jean-Marc Casandjian, Régis Terrier, Science 307, 1292 (2005)

Casandjian & Grenier, I. A.AA 489, 849 (2008)

Skymap of 3EG and revised catalog

3EG

Hartman et al. ApJS 1999

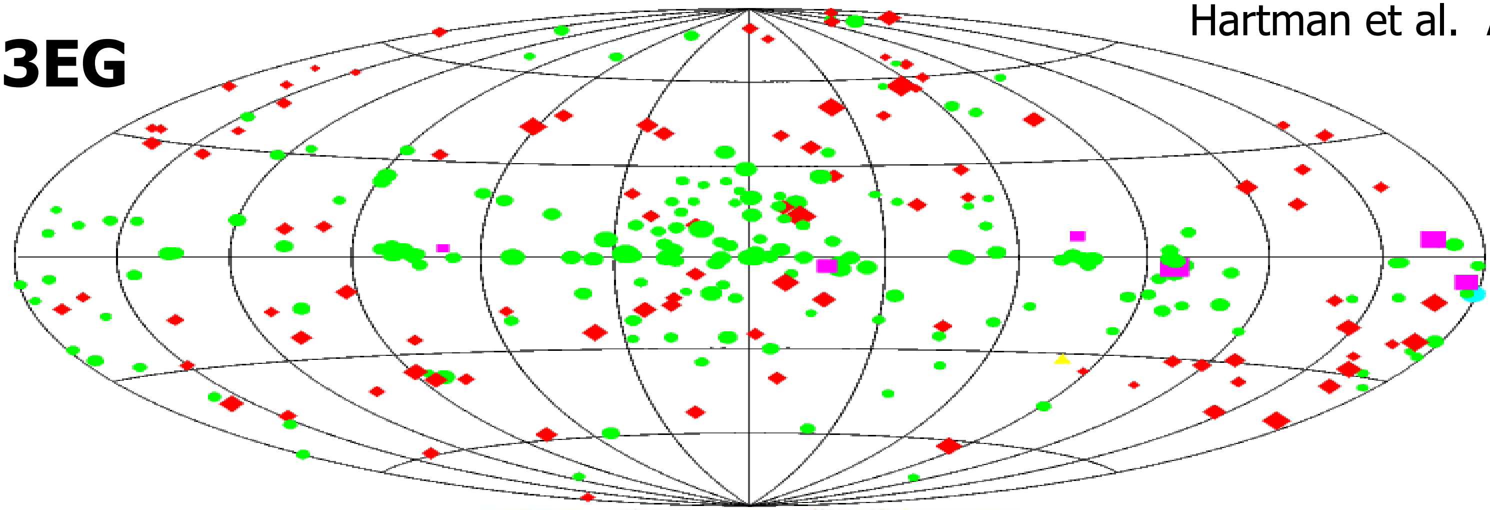

EGR

This work

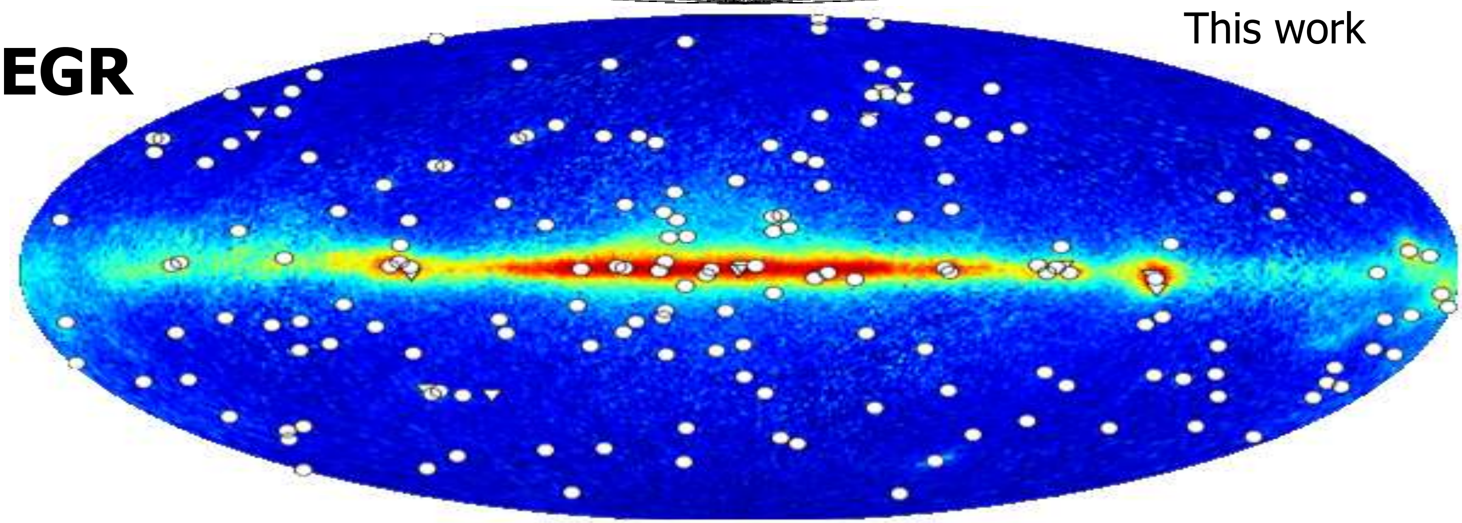

Superimposed…

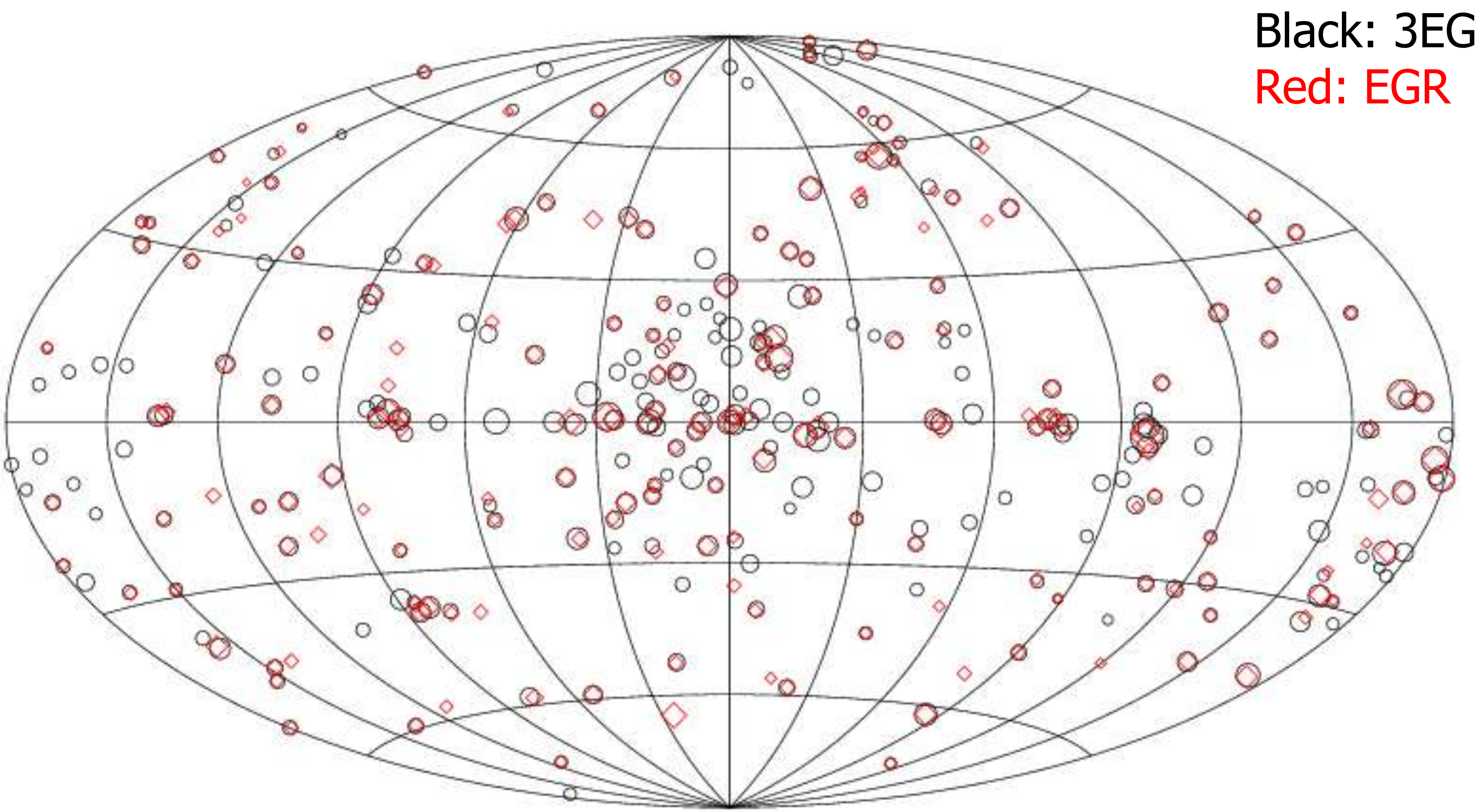

Isabelle A. Grenier, Jean-Marc Casandjian, Régis Terrier, Science 307, 1292 (2005)

Two approaches for cosmic-ray density gradient

- Ring model
  - Gas column-densities in 6 rings (boundary 3.5/7.5/9.5/11.5/13.5kpc) + IC intensity map (from GALPROP) + isotropic
- GALPROP model
  - Strong et al. 2007
  - Optimized CR spectrum to fit the GeV excess

$$N_{pred}(l,b) = [\textstyle\sum_{i=rings} q_{HI,i} N_{HI}(r_i,l,b) + \sum_{rings} q_{CO,i} W_{CO}(r_i,l,b)$$
$$+ q_{dark} NH_{dark}(l,b) + q_{IC} I_{IC}(l,b) + I_{iso}] \times \epsilon(l,b)$$
$$+ \textstyle\sum_{j=sources} \epsilon(l_j,b_j)\, f_j\, PSF(l_j,b_j)$$

$$N_{pred}(l,b) = [q_{\pi^0} I_{\pi^0}(l,b) + q_{brem} I_{brem}(l,b) + q_{dark} NH_{dark}(l,b)$$
$$+ q_{IC} I_{IC}(l,b) + I_{iso}] \times \epsilon(l,b)$$
$$+ \textstyle\sum_{j=sources} \epsilon(l_j,b_j)\, f_j\, PSF(l_j,b_j)$$

Dark gas : associated with cold and anomalous dust at the transition
Between the atomic and molecular phases (Grenier et al. 2005)

Isabelle A. Grenier, Jean-Marc Casandjian, Régis Terrier, Science 307, 1292 (2005)

Longitudinal profile

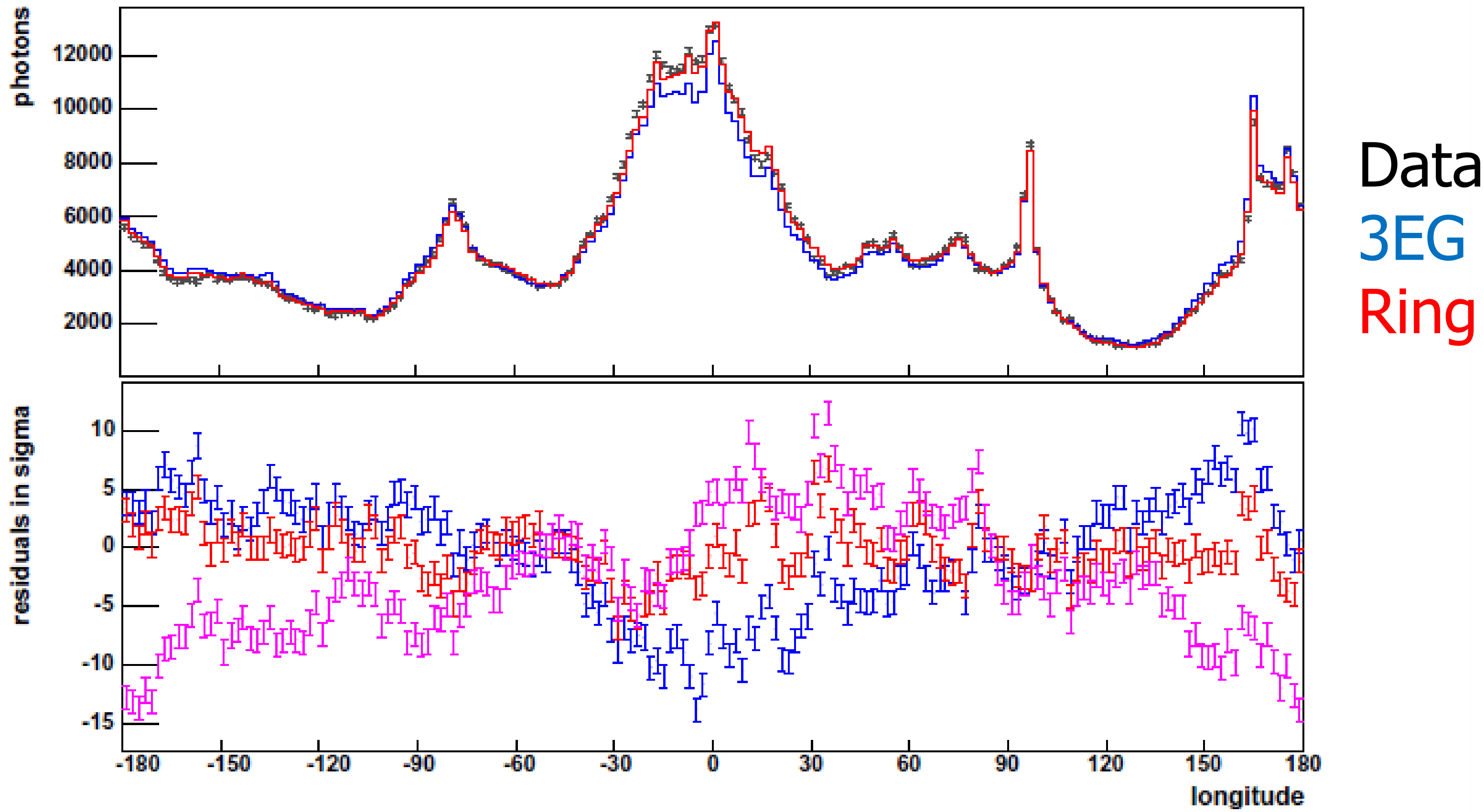

Fig. 1. The top figure is the longitude profile of all photon counts observed by EGRET above 100 MeV at all latitudes (black error bars), compared with the diffuse counts predicted by the 3EG model (blue curve) and the Ring model (red curve). The bottom figure is the residual expressed in number of standard deviation, colors are the same as above, we added the Galprop residuals in purple. Counts from bright sources have been added to the diffuse component. For more visibility the plot are presented with a binning of 4°.

Isabelle A. Grenier, Jean-Marc Casandjian, Régis Terrier, Science 307, 1292 (2005)

Map of the residuals

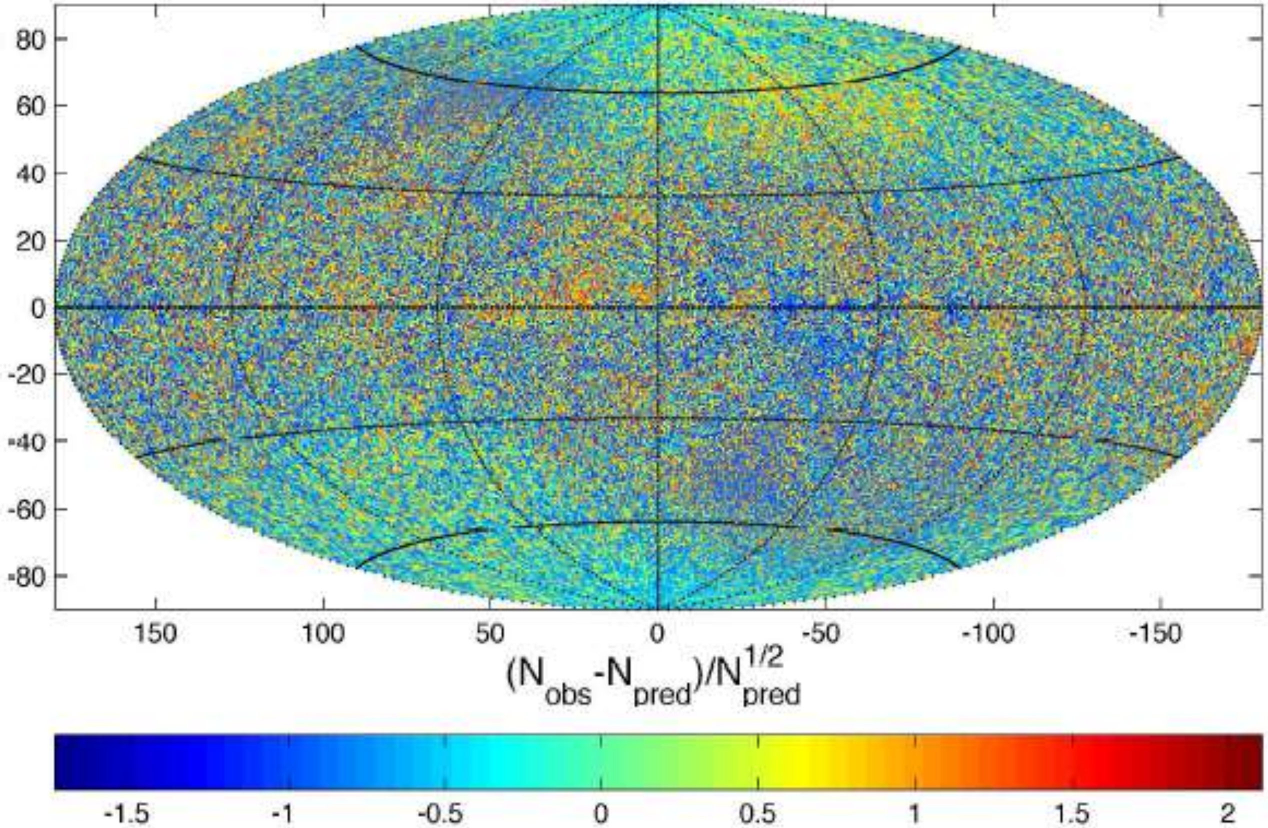

Fig. 2. Map in Galactic coordinates of the residuals (expressed in $\sigma = \sqrt{N_{pred}}$ values) between the $E > 100$ MeV photon counts (in 0.5° bin) and the best fit with the Ring model using Equation (1)

Source detection

- 3 maps: >100MeV, 0.3-1GeV, >1GeV
- 0.5°×0.5° bin both in Galactic and equatorial coordinates
- Iterative detection from high T_S to low T_S, adding detected sources to the background model until no excess ($\sqrt{T_S} > 3$) was left

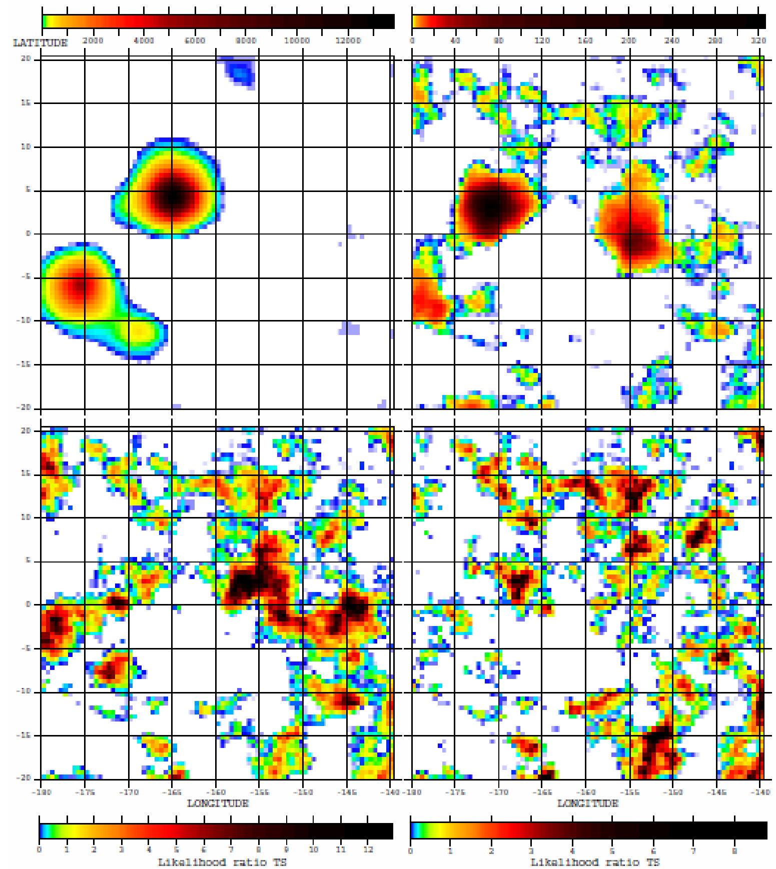

Fig. 3. An example of the iterative source detection with the 2D binned likelihood around Geminga at energies above 100 MeV. 4 consecutive TS maps are shown. Sources are detected, then are included in the background for the next step until no significant one is left. The colourbar gives TS.

P. Michelson, March 2009

Fermi Gamma-ray Space Telescope

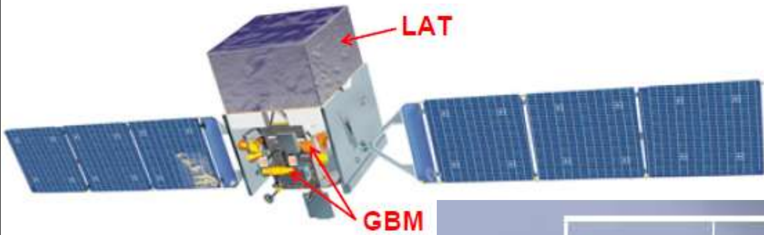

Launched in June 2008

	Years	Ang. Res. (100 MeV)	Ang. Res. (10 GeV)	Eng. Rng. (GeV)	$A_{eff}\ \Omega$ (cm^2 sr)	# γ-rays
EGRET	1991–00	5.8°	0.5°	0.03–10	750	1.4 × 10^6/yr
AGILE	2007–	4.7°	0.2°	0.03–50	1,500	4 × 10^6/yr
Fermi LAT	2008–	3.5°	0.1°	0.02–300	25,000	1 × 10^8/yr

- LAT has already surpassed EGRET and AGILE celestial gamma-ray totals
- Unlike EGRET and AGILE, LAT is an effective All-Sky Monitor
  whole sky every ~3 hours

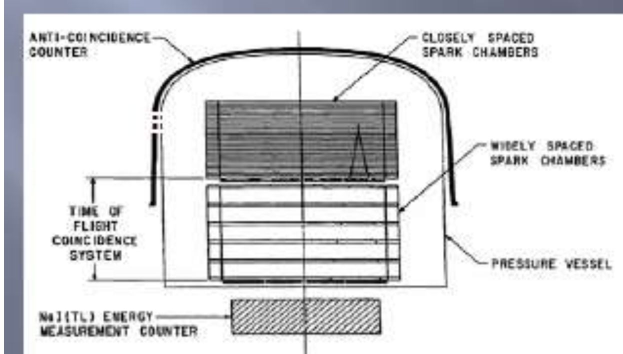

CGRO EGRET

AGILE (ASI)

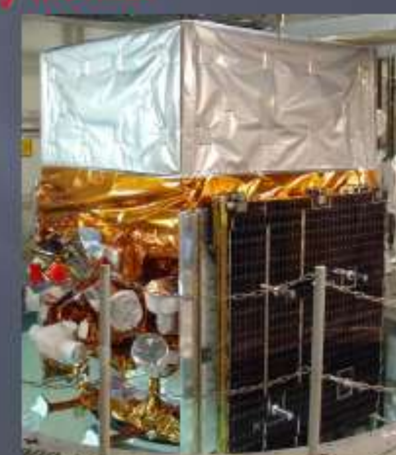

Fermi / LAT

Fermi/LAT: first 3 months

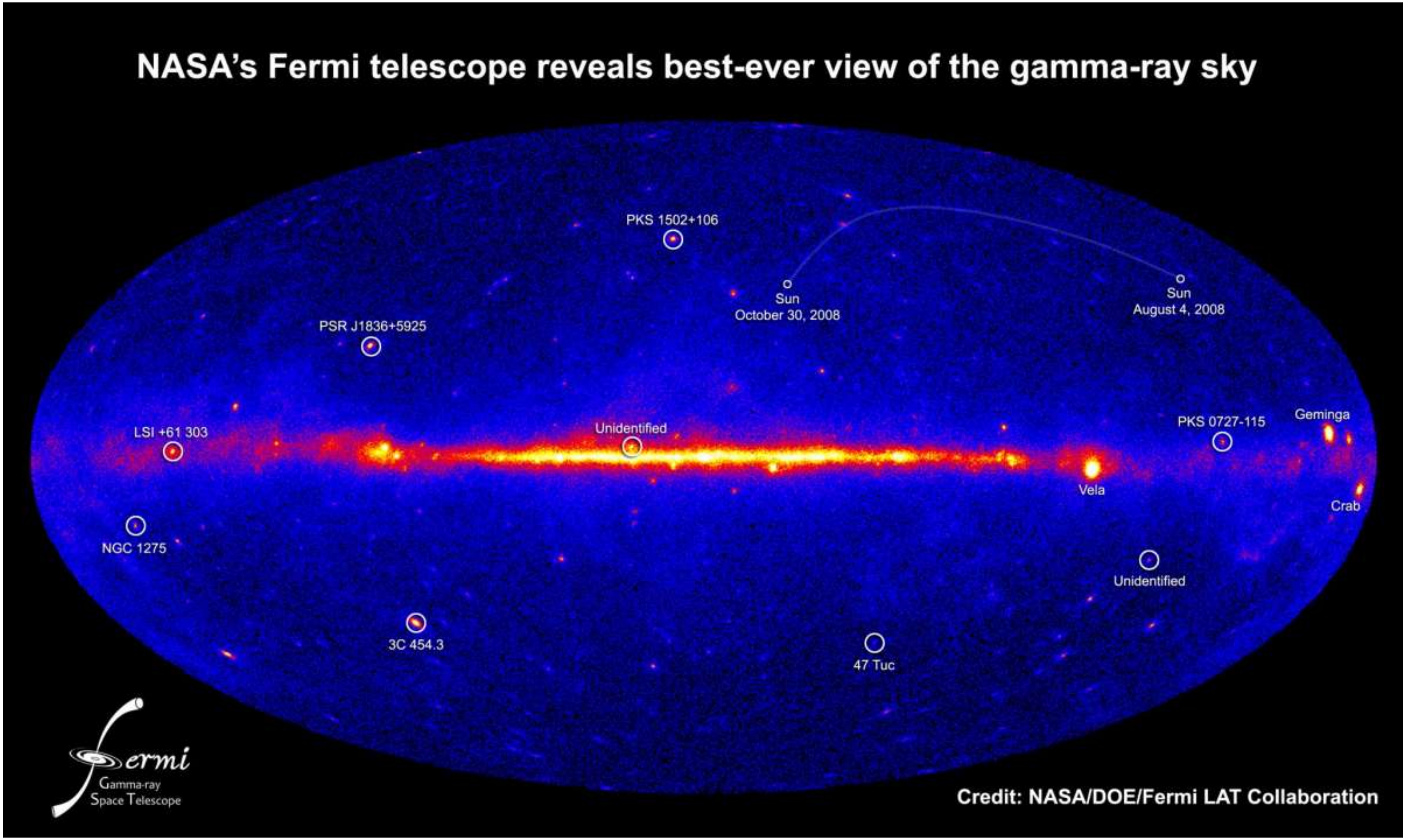

3EG / ~~EGR~~ / 0FGL sources

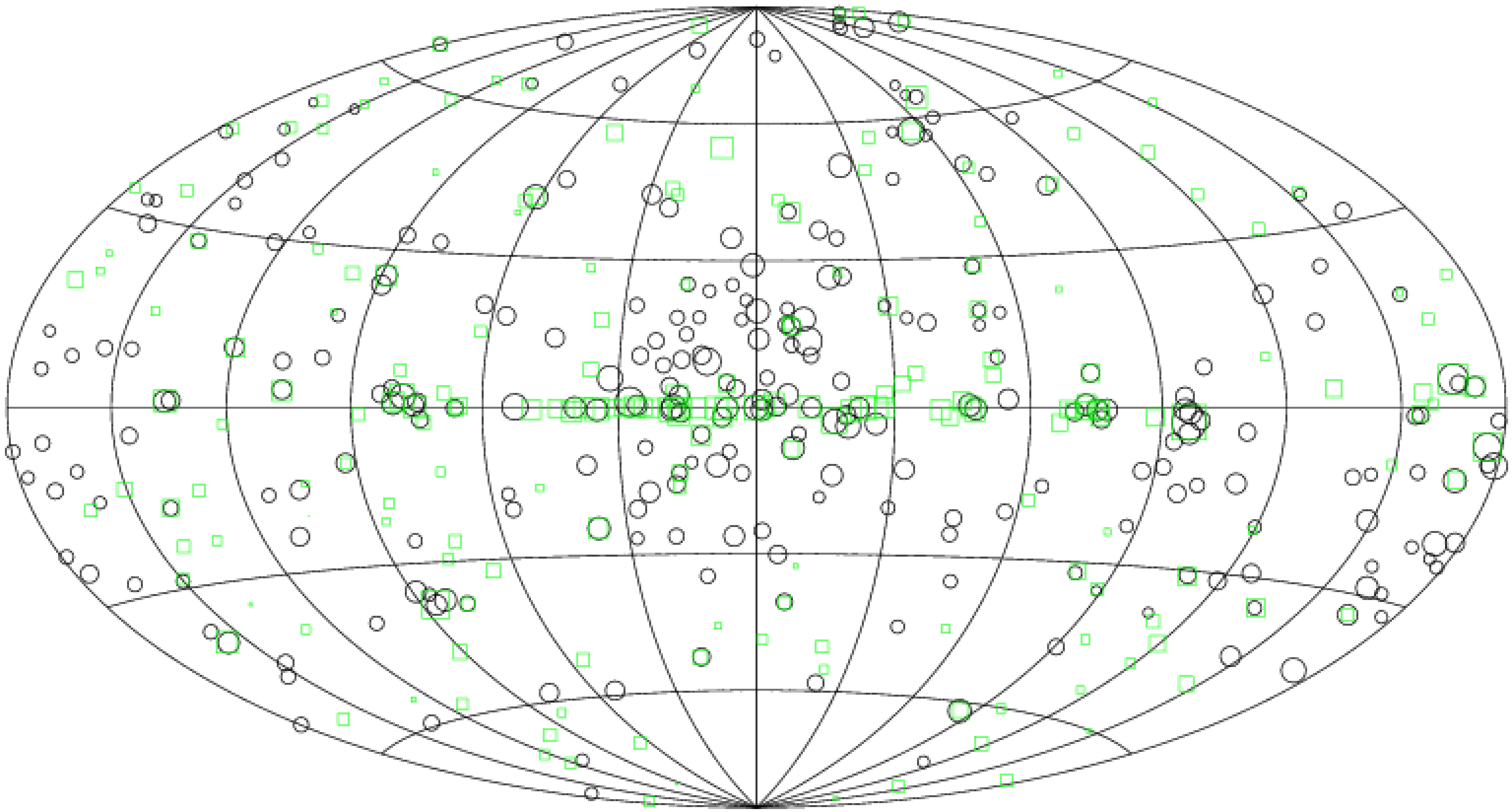

0FGL: ApJS 183, 46 (2009)

~~3EG~~ / EGR / 0FGL sources

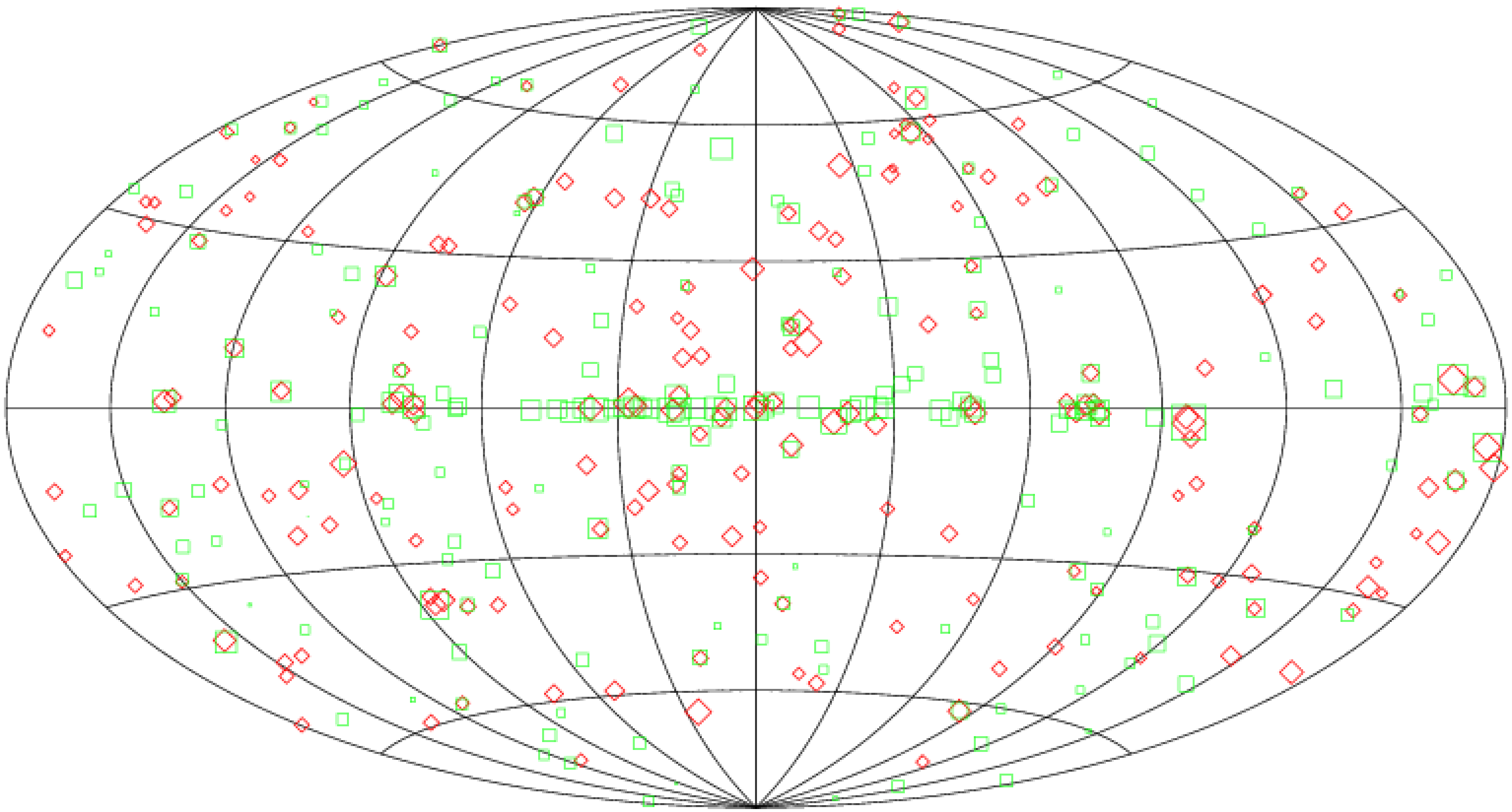

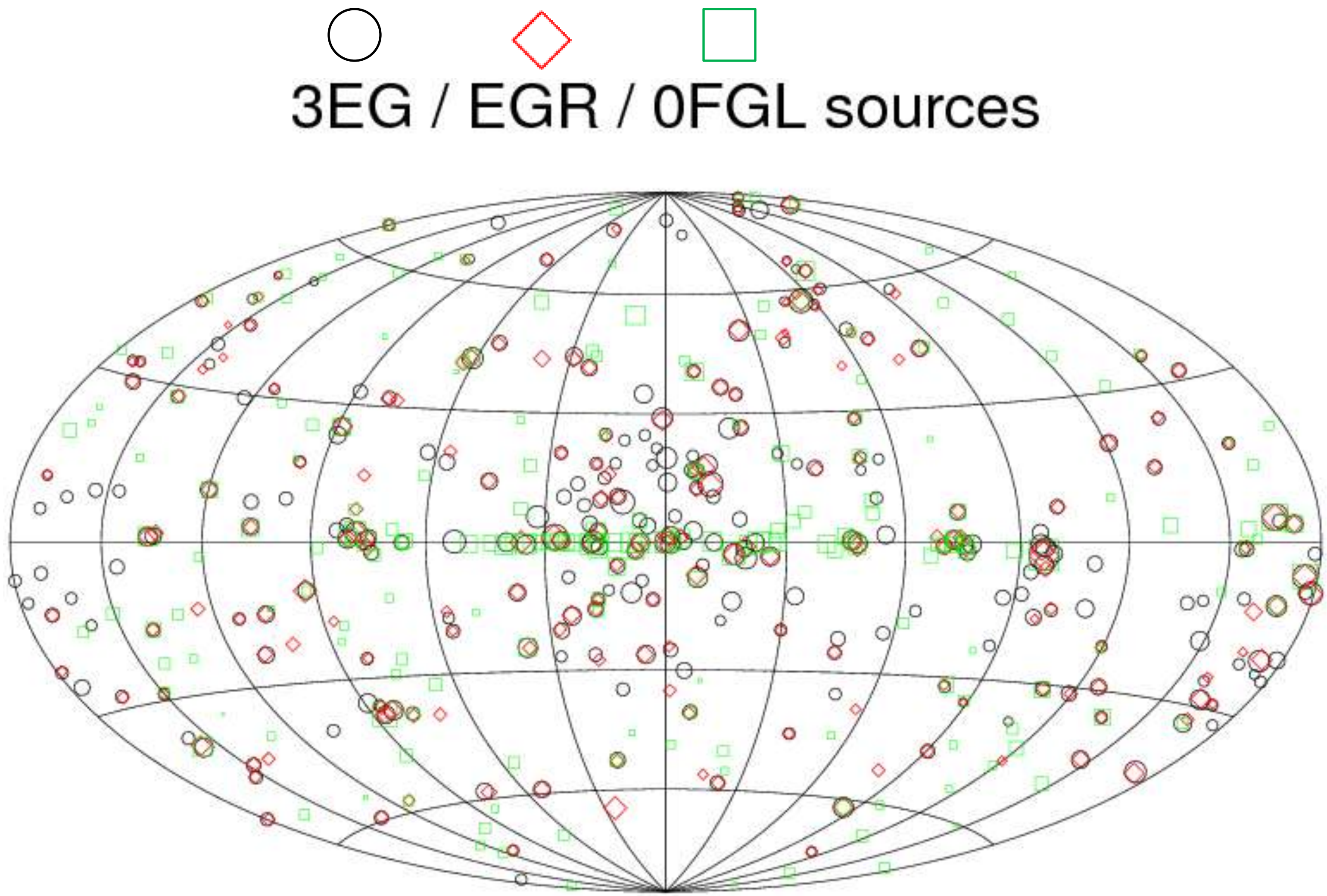
3EG / EGR / 0FGL sources

3EG / EGR / 0FGL: close up

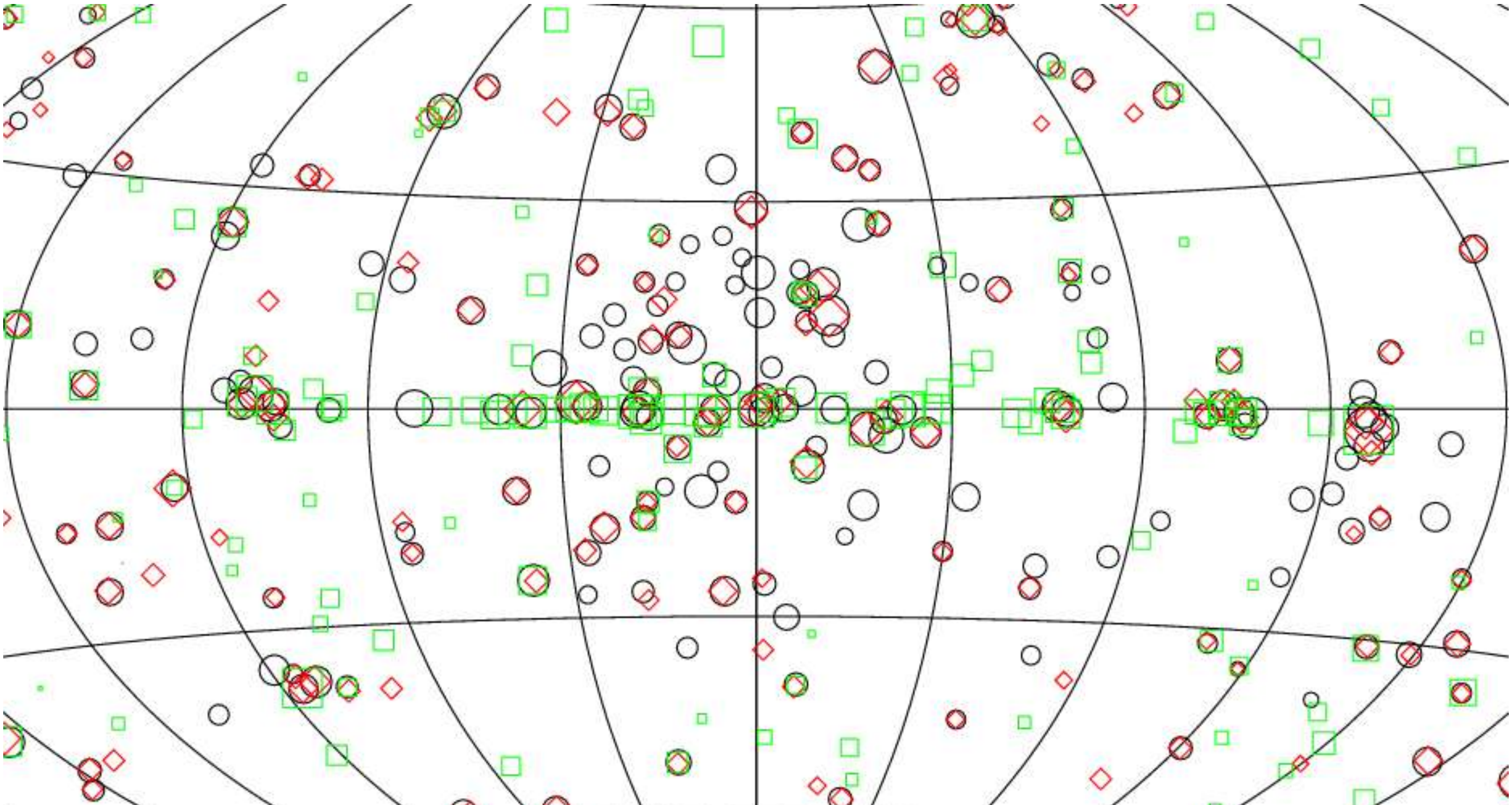

No good consistency around the Galactic center...

LAT: Galactic diffuse emission

Fermi-LAT

The Fermi LAT View

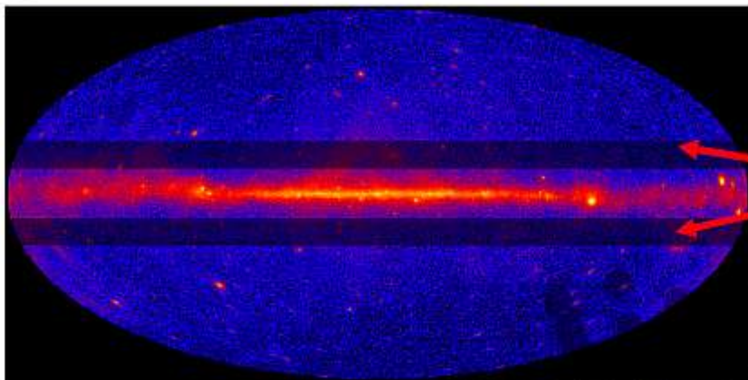

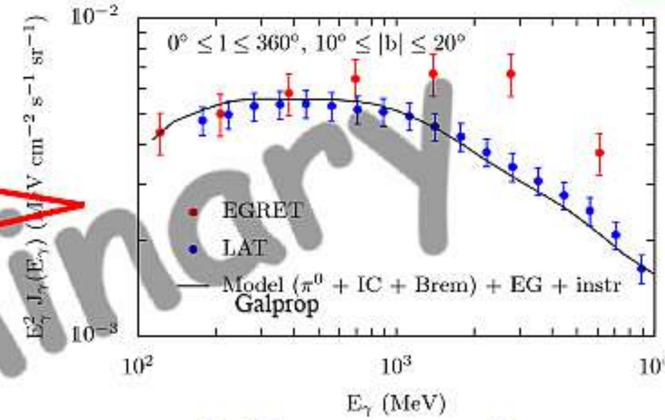

- Spectra shown for mid-latitude range → GeV excess in this region of the sky is not confirmed.
- Sources are not subtracted but are a minor component.
- LAT errors are dominated by systematic uncertainties and are currently estimated to be ~10% → this is preliminary.
- EGRET data are prepared as in Strong, et al. 2004 with a 15% systematic error assumed to dominate (Esposito, et al. 1996).
- EG + instrumental is assumed to be isotropic and determined from fitting the data at |b| > 30°.

LAT: Galactic “mid-latitude” diffuse

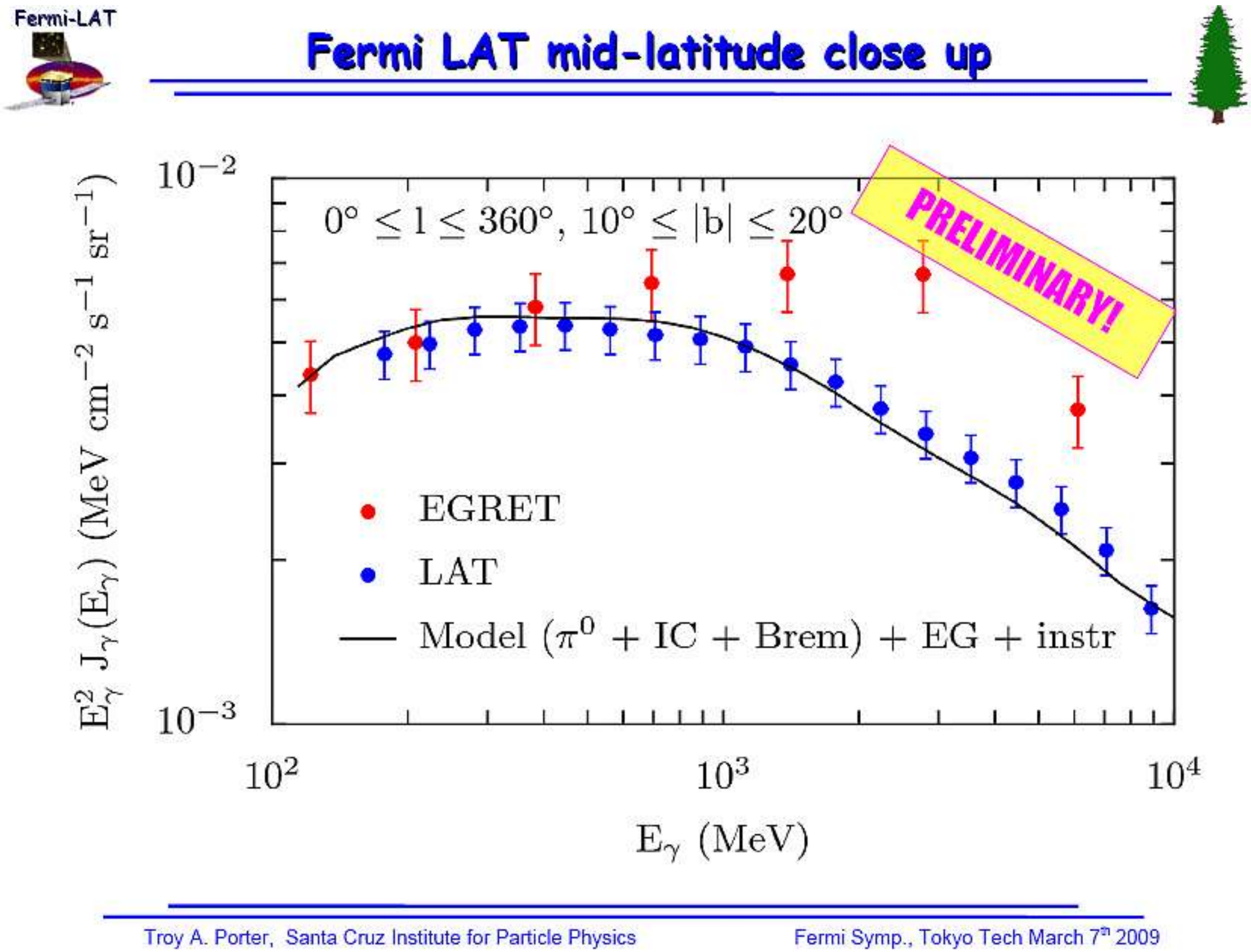

Aharonian et al. Nature 439, 695 (2006)

HESS image of the Galactic center region

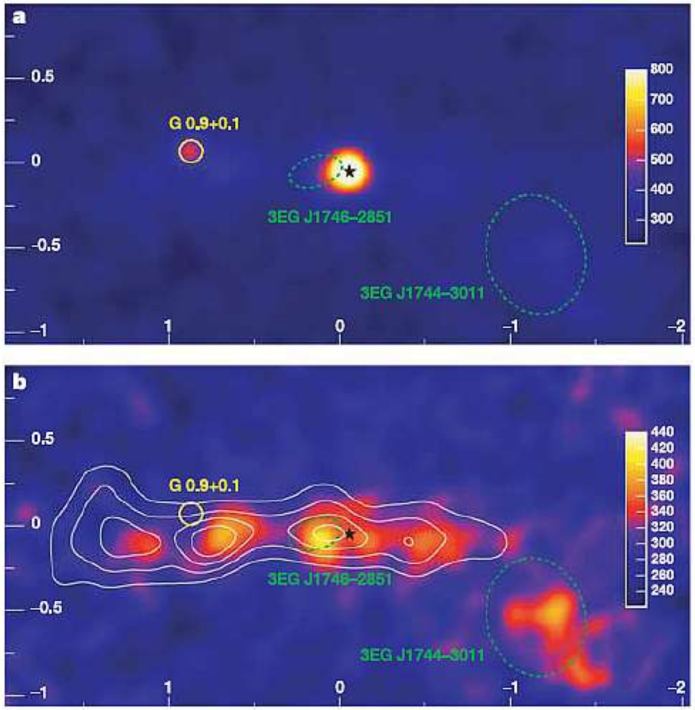

Figure 1 | VHE γ-ray images of the Galactic Centre region. a, γ-ray count map; **b**, the same map after subtraction of the two dominant point sources,

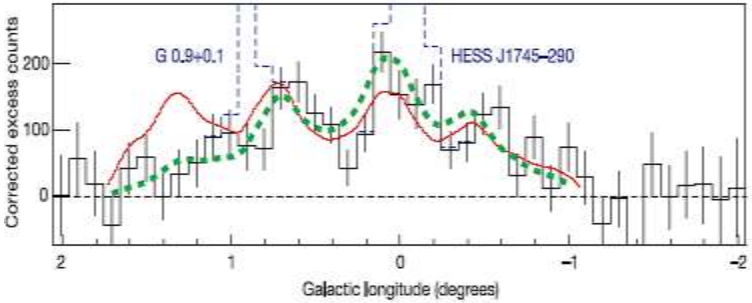

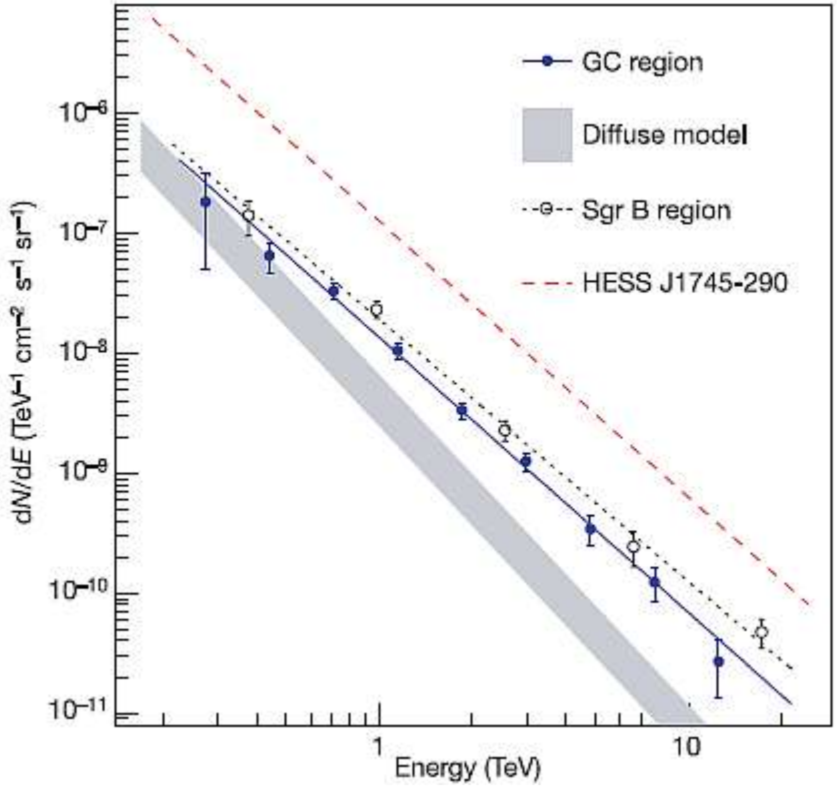

Active accelerators in the last 10^4 years?
Sgr A East (SNR) or Sgr A*?

Calculation of diffuse gamma-rays

- Input parameters:
  - Proton/electron injection spectrum
    - Local interstellar spectrum ↔ Galactic spectrum?
    - Cosmic-ray composition in the Galaxy
  - Interaction cross section for protons/nucleus
  - Matter and radiation distribution in the Galaxy (3D)
    - Gas distribution
    - Atomic abundance
      H:He:CNO:NeMgSiS:Fe=1 : 0.096 : 1.38×10^{-3} : 2.11×10^{-4} : 3.25×10^{-5}
      following the compilation by Meyer (1985)

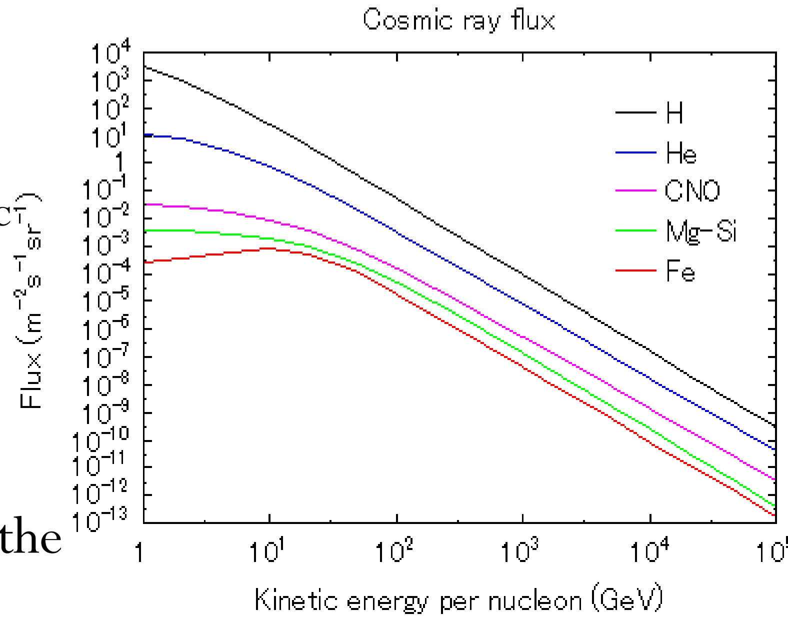

Honda et al. 2004

pp→π^0 cross section

Gammas from neutral pion decay pp→π^0

- New parameterization (Kamae+ 2005, 2006) is based on Pythia Monte Carlo event generator and includes diffraction dissociation
- New parameterization shows some improvement over the old formalism employed in GALPROP
- Galprop now has a parameter to choose a formalism

Pion decay γ-ray spectra for different regions on the sky

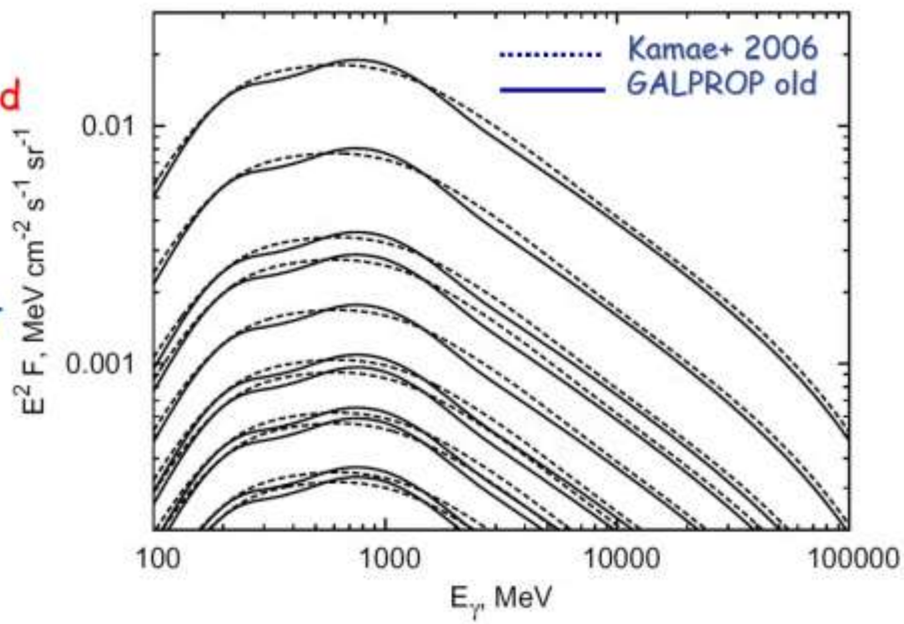

Moskalenko et al., GLAST symposium, Feb. 2007

Nuclear enhancement factor

$$\epsilon_{\mathrm{M}} = 1 + \sum_i m_{ip} \frac{\phi_i(T)}{\phi_p(T)} + \sum_i m_{i\alpha} \frac{\phi_i(T)}{\phi_p(T)} \times \frac{r}{1-r} = 1.52$$

Table 1
Multiplication factor at $T = 10$ GeV/nucleon. G&S is quoted from Ref. [9].

Nuclei	m_{ip}		$m_{i\alpha}$	
	DPMJET-3	G&S	DPMJET-3	G&S
H ($A = 1$)	(1)	(1)	3.81	3.57
He ($A = 4$)	3.68	3.57	14.2	12.6
CNO ($A = 14$)	11.7	11.4 (N)	42.5	40 (N)
Mg–Si ($A = 25$)	20.3	20 (Al)	73.2	71 (Al)
Fe ($A = 56$)	38.8	40	142	135

Mori, Astropart. Phys. 31, 341 (2009)

Nuclear enhancement factor

Table 4
Nuclear enhancement factor decomposed to each component at 10 GeV/nucleon.

	Target					Sum
	H	He	CNO	NeMgSiS	Fe	
Projectile						
H	1	0.405	0.0177	0.0047	0.0006	1.428
He	0.203	0.083	0.0036	0.0035	0.0004	0.293
CNO	0.038	0.015	0.0006	0.0018	0.0002	0.055
MgSi	0.033	0.013	0.0005	0.0026	0.0003	0.049
Fe	0.014	0.006	0.0002	0.0021	0.0002	0.022
Sum	1.288	0.520	0.023	0.0147	0.0017	1.845

Mori, Astropart. Phys. 31, 341 (2009)

Energy dependence

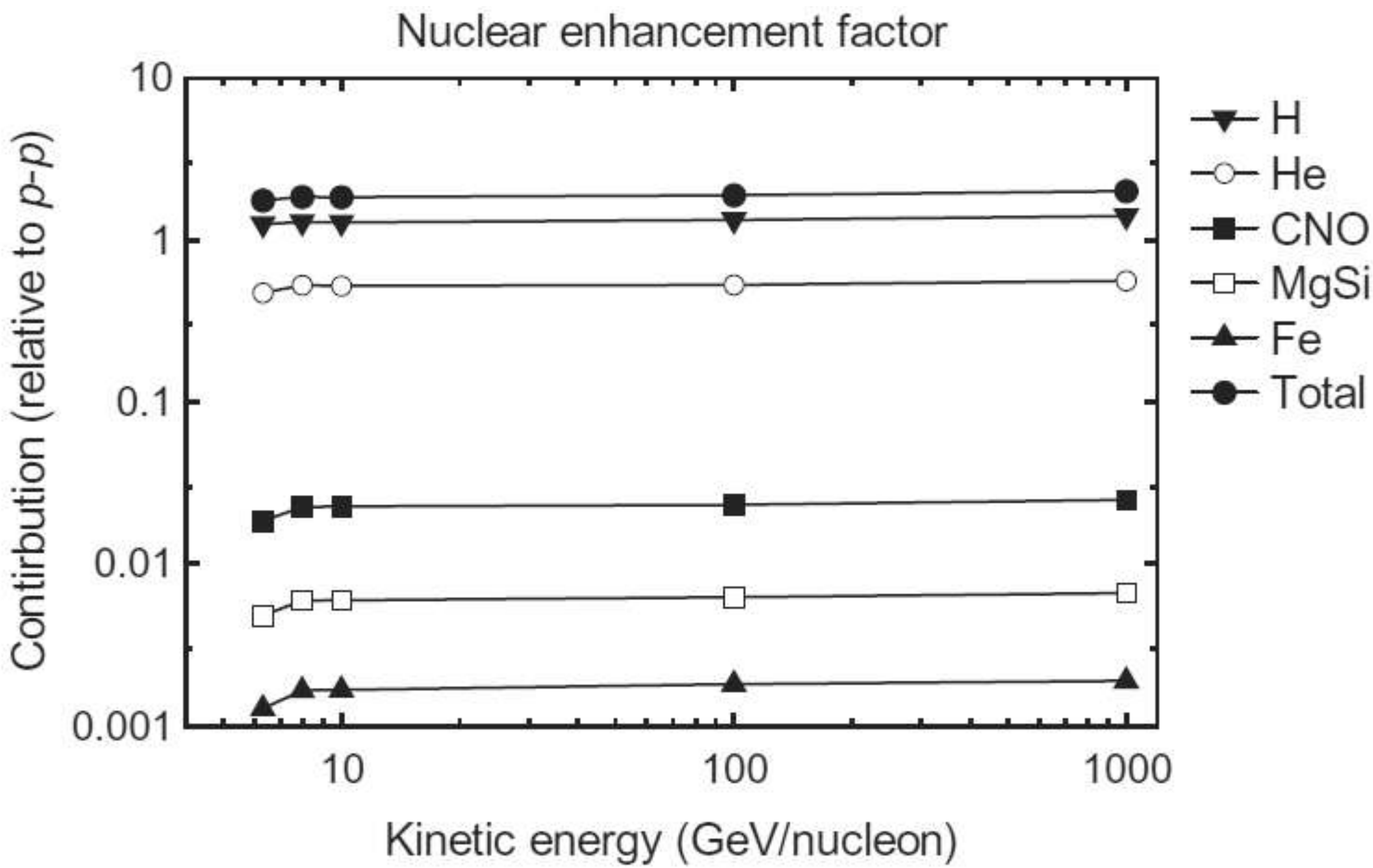

Fig. 2. Energy dependence of nuclear enhancement factor contributions from each ISM component.

Wait for details!

Fermi diffuse model

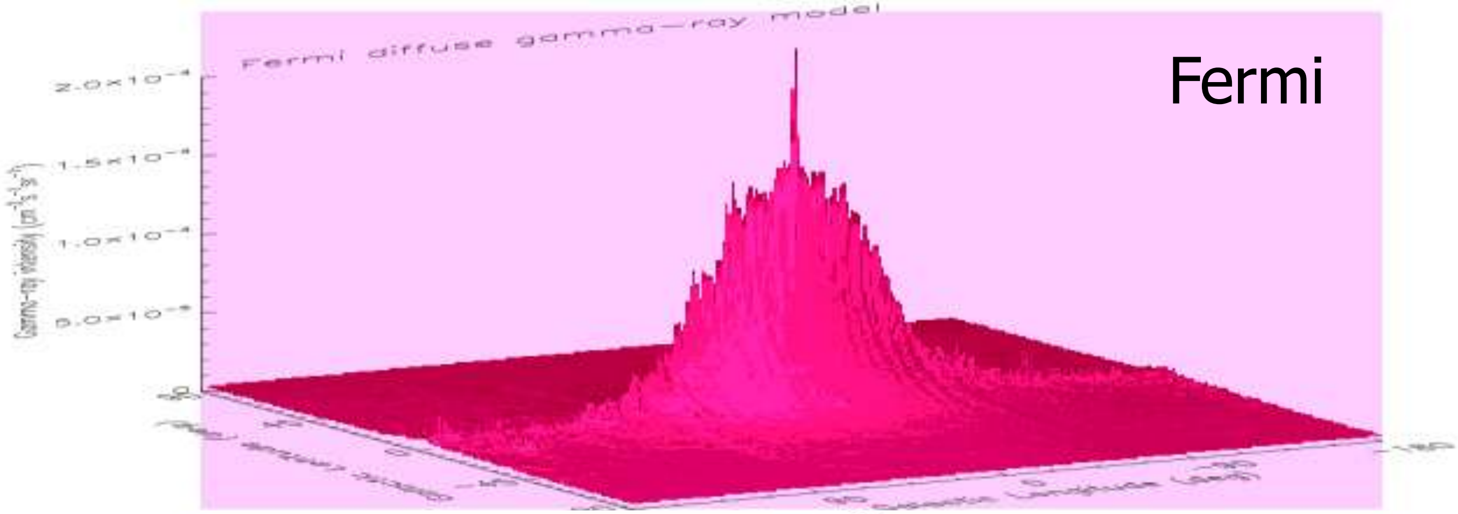

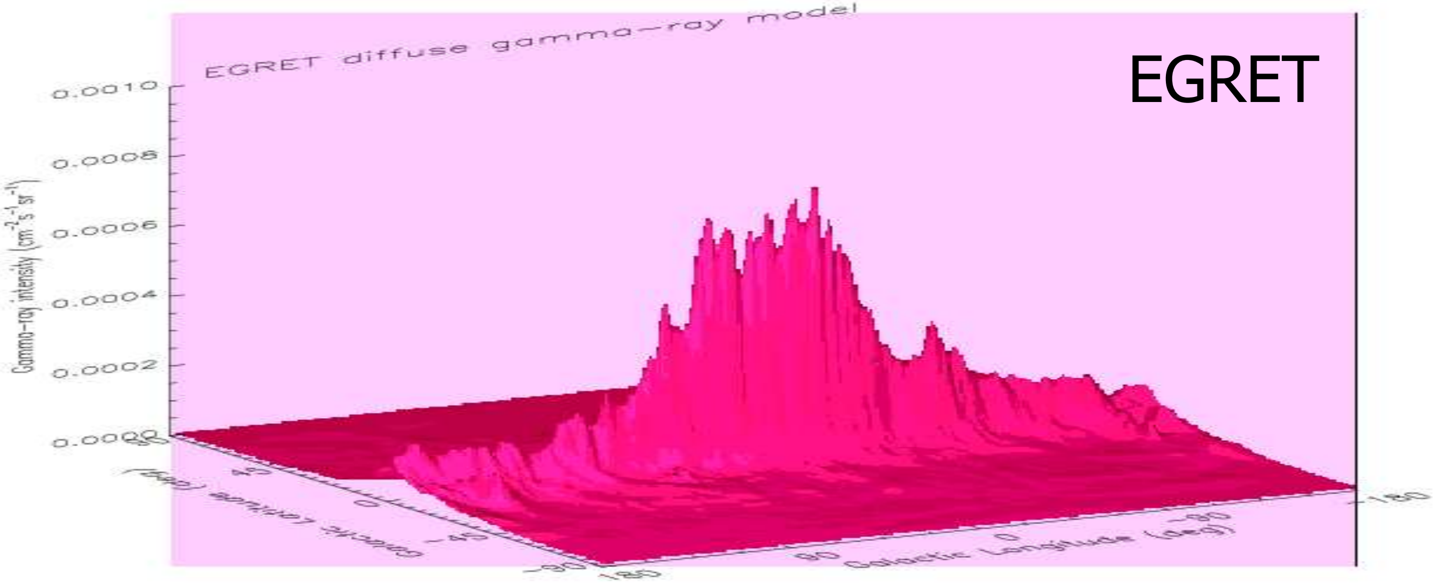

Added 01-SEP-2009

gll_iem_v02.fit (2009Aug)

Latest!

Fermi diffuse model

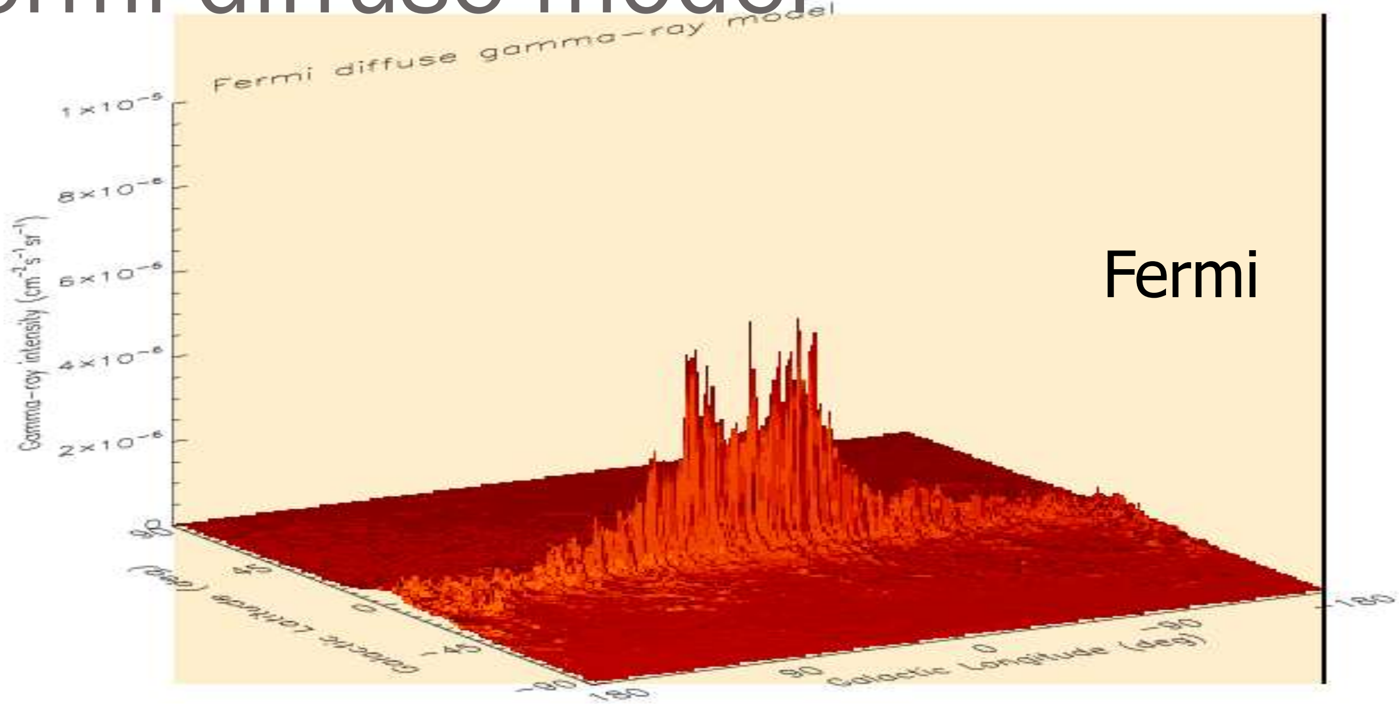

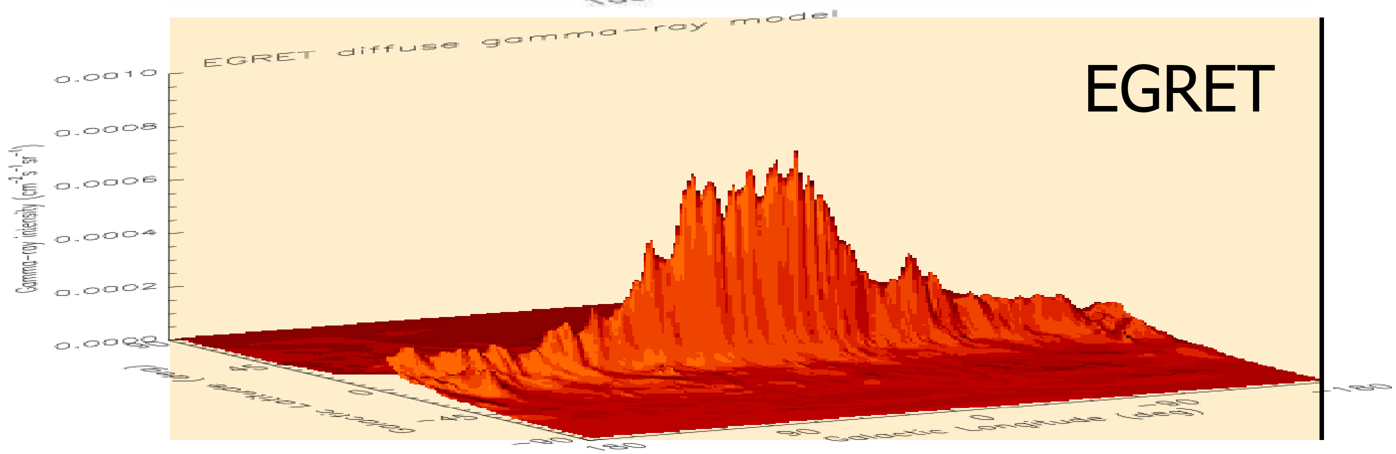

Summary

- Galactic diffuse gamma-rays are the most abundant class of gamma-rays in the GeV sky, and are the background for point source detection.
- Diffuse gamma-rays above 1 GeV observed by EGRET showed a flatter spectrum than expected.
- Fermi observations (mid-lat. range) can be accounted assuming "normal" cosmic ray spectrum. (But be patient for their results on the plane!)
- Observation of the Galactic Plane in the TeV region is difficult, but there are some indications near the Galactic center and along the plane.

Abdo et al. 2009ApJ 696,1084

Vela pulsar by Fermi

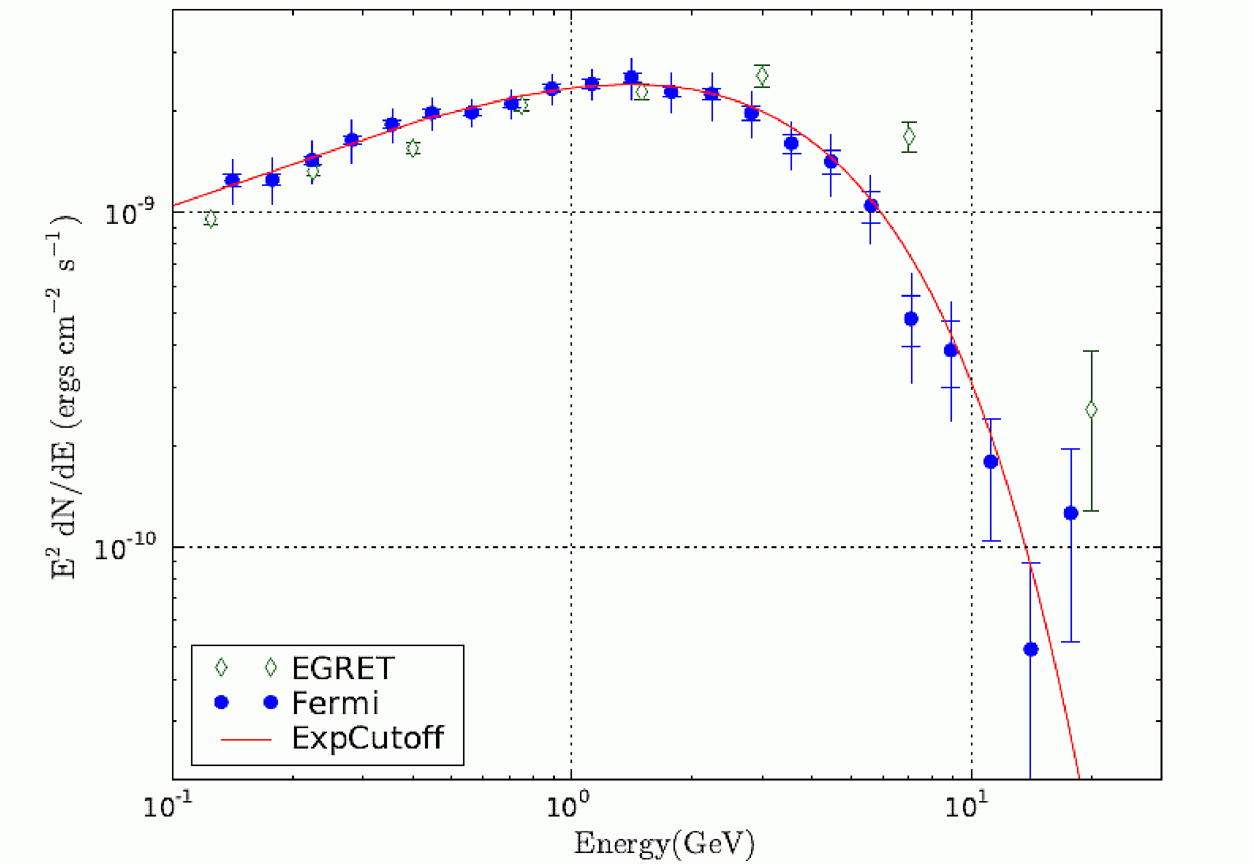

FIG. 5.— The phase-averaged Vela spectral energy distribution ($E^2 dN_\gamma/dE$). Both statistical (capped) and systematic (uncapped) errors are shown. We believe that the latter are conservative; they dominate at all energies below 7 GeV. EGRET data points (diamonds, Kanbach et al. 1994) are shown for comparison. The curve is the best-fit power law with a simple exponential cut-off.

Spectral mismatch between EGRET and Fermi!